Important Notice

UNIVERSITY OF CALGARY

STUDIES OF MULTICOMPONENT SEISMIC POLARITY AND AMPLITUDE

by

Alexandru Vant

A THESIS

SUBMITTED TO THE FACULTY OF GRADUATE STUDIES

IN PARTIAL FULFILMENT OF THE REQUIREMENTS FOR THE

DEGREE OF MASTER OF SCIENCE

DEPARTMENT OF GEOLOGY AND GEOPHYSICS

CALGARY, ALBERTA

JULY 2003

UNIVERSITY OF CALGARY

FACULTY OF GRADUATE STUDIES

The undersigned certify that they have read, and recommend to the Faculty of Graduate Studies for acceptance, a thesis entitled "Studies of multicomponent seismic polarity and amplitude" submitted by Alexandru Vant in partial fulfilment of the requirements for the degree of Master of Science.

_____

Supervisor, R. James Brown, Department of Geology and Geophysics

_____

Edward S. Krebes, Department of Geology and Geophysics

_____

Patrick Wu, Department of Geology and Geophysics

_____

R. Bart Hicks, Department of Physics and Astronomy

_____

Date

Abstract

Assuming the SEG (Society of Exploration Geophysics) polarity standard is followed, there are some cases in which reflections on the compressional (P-P) and converted-wave (P-S) sections show opposite polarities. This situation makes the correlation and interpretation processes more difficult.

To find conditions that relate polarity to elastic parameters, I derived a new approximation for the P-S reflection coefficient (R_{PS}) and also modelled seismic responses from a wide range of geologically plausible interfaces using acoustic P- and S-wave velocities and densities. In also investigate the polarity consistency with offset and how missing velocity or density well-logs used to create synthetic shot-gathers and stacks affect the interpretation process.

As a side result, I show that, with small changes, the new R_{PS} approximation is suitable for AVO (amplitude variation with offset) studies and also describe a more accurate way of computing the theoretical AVO attributes.

Opposite polarities on P-P and P-S sections were found to be associated with situations where not all the rock parameters change in the same direction (e.g. velocities increase and density decreases) across the interface.

Acknowledgements

I express my sincerest gratitude to my supervisor, Jim Brown for his encouragement and advice in matters of science and life. His approachable, laid-back attitude made me regard him not only as a professor, but also as a good friend.

I would like to thank the CREWES students and staff for their help and advice. Being a part of this great group of people was a big privilege for me. The ideas and research results shared every week during the CREWES meetings broadened my perspective on geophysics and were a great source of information, not to mention the delicious muffins...

Furthermore, I would like to thank Louise Forgues, Kelly Fries and Cathy Hubbell, whose great managerial and administrative skills made my years here a whole lot easier. A big thank-you also goes to my office-mates, Jeff Grossman and Katherine Boggs whose company and friendship made the office seem a lot larger.

Last but not least, I am grateful to the sponsors of the CREWES project for their crucial financial support and the academic interest in my research.

TABLE OF CONTENTS

List of Tables

List of Figures

CHAPTER ONE

INTRODUCTION

1.1 Objective

The main objective of this thesis is to determine a set of mathematical conditions or types of geologic interfaces that generate on the P-P and P-S sections events with opposite relative polarities. The course of the research carried out here leads also to a slight consideration of some topics in converted-wave AVO (amplitude variation with offset).

1.2 Theoretical background

I will start with a summary discussion of the physical situation analyzed in this thesis. In the seismic survey we are dealing with spherical waves generated by a source (e.g. explosion). Generally, at great distances from the source, the sphericity of the wave diminishes, and we can treat it as a *plane wave*.

When waves travel through the subsurface, part of their energy is reflected at boundaries (interfaces) created by either sedimentation (layer boundaries) or tectonic processes (faults). A reflection occurs only at interfaces between media with contrasting elastic parameters (propagation velocities and densities). The basic reflection and transmission (refraction) of plane waves at a two-layer boundary is depicted in Figure 1.1. Throughout this study, we are dealing with two types of waves:

- Compressional waves or P-waves: waves that create in the medium particles a motion that is parallel to their direction of propagation

- Shear waves or S-waves: waves that create in the medium particles a motion that is perpendicular to their direction of propagation.

  Hence, there are two types of S-waves:

  - SH waves, for which a the particle motion is perpendicular to the direction of propagation and is longitudinal.
  - SV waves, for which the motion is perpendicular to the direction of propagation and is in the vertical plane of propagation.

Although the incident wave can also be a shear-wave, I only treat here the case of incident P-waves and reflected P-P and P-SV waves, the latter being referred to as P-S throughout this study. The relationship between the propagation velocities and the incidence, reflection and transmission angles at an interface are given by Snell's law:

$$\frac{\sin i_1}{\alpha_1} = \frac{\sin j_1}{\beta_1} = \frac{\sin i_2}{\alpha_2} = \frac{\sin j_1}{\beta_2} = p \qquad (1\text{-}1)$$

where p is the horizontal slowness, usually known as 'the ray parameter'.

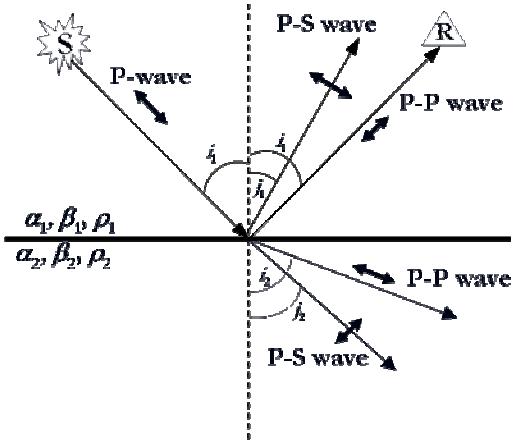

where:

- S is the source and R is the receiver
- P is the incident compressional wave
- P-P is the reflected or transmitted compressional wave
- P-S is the reflected or transmitted mode-converted shear wave
- $\alpha_1, \beta_1, \rho_1, \alpha_2, \beta_2, \rho_2$ are the P-wave velocities, SV-wave velocities and densities in the two media
- i_1 and j_1 are the incidence and reflection angles of the P, P-P and P-S waves, respectively. ; i_2 and j_2 are the transmission angles of the P-P and P-S waves.

Figure 1.1. P-P and P-S reflection and transmission for a compressional-wave source and a two-layer boundary.

In order to obtain as much information as possible about the reflector (interface), points in the subsurface are covered more than once by different source-receiver pairs (Figure 1.2). These points are named *Common Midpoints (CMP's)* when we record the reflected P-P waves (P-P surveys) and *Common Conversion Points (CCP's)* when we record the mode-converted P-S waves (P-S surveys). The source-receiver distance is commonly referred to as *offset*.

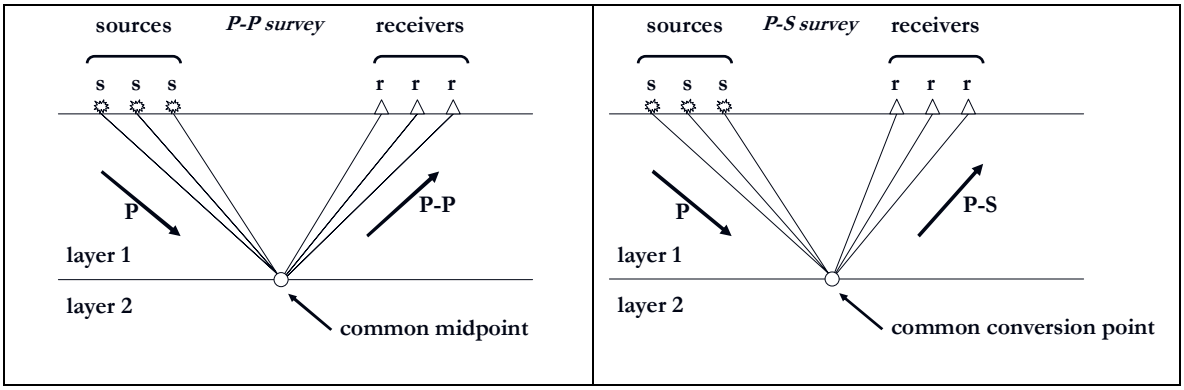

Figure 1.2. P-P and P-S recording geometries: left – the common midpoint gather; right – the common conversion point gather.

Traces belonging to the same midpoint/conversion point form a CMP gather/CCP gather. The responses of all the receivers that record information from the same CMP/CCP are summed up (stacked) to generate one single trace (Figure 1.3).

A multitude of CMP/CCP stacks form a stacked section. Usually, the polarities of a P-P and P-S reflection coming from the same reflector are the same on the P-P and P-S sections. Still, there are cases when the two polarities do not match (Figure 1.3), creating problems in the geological interpretation of our sections. The main subject of my research

is to find mathematical conditions on types of geologic interfaces that determine this "unusual" polarity situation. The following section offers a more detailed look this problem.

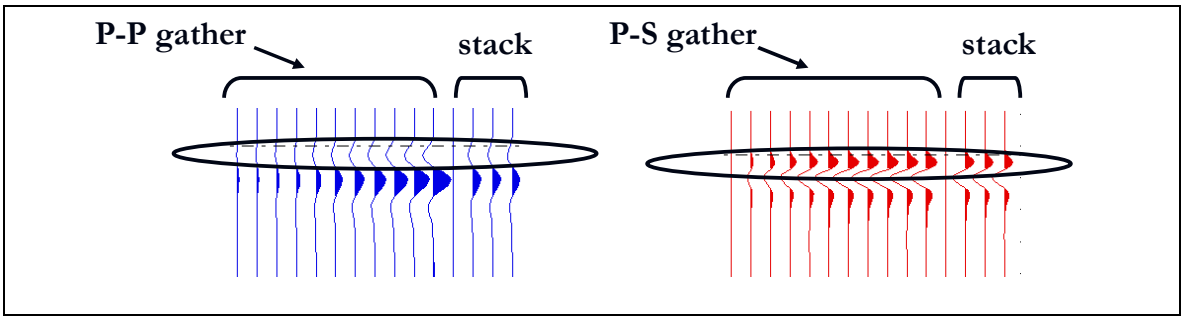

Figure 1.3. P-P and P-S gathers and stacks: left – the common midpoint gather and stack; right – the common conversion point gather and stack.

1.3 Motivation

Lately, the interest in multicomponent seismic data and, consequently, in obtaining an improved image of the subsurface has increased dramatically. Techniques like multicomponent ocean-bottom seismic have now become essential to the oil industry. Therefore, many researchers are making efforts to improve the acquisition, processing and interpretation techniques to better suit the concept of multicomponent seismology (e.g. Lawton et al., 1992; Margrave et al., 2001).

One of the issues that come into play when we try to correlate the P-P and the P-S seismic sections obtained from a multicomponent survey regards the relative polarities of the matching events from the two sections, that is, when we try to correlate the P-P and P-S seismic incidence for the same geologic interface. In most situations, for sub-critical

reflectors, there is a single sign relationship between the two reflection coefficients (R_{PP} and R_{PS}), that is $R_{PP}/R_{PS} < 0$ (Brown et al., 2002); for this conventional reflector the P-P and P-S events have the same apparent polarity on the records, assuming that recommended polarity standards (Brown et al., 2002) have been observed in the acquisition. Still, there are some reflectors for which the P-P and P-S reflections have opposite polarity on the records ($R_{PP}/R_{PS} > 0$). This unusual circumstance can make correlation of P-P and P-S sections a bit tricky (Figure 1.4). Increased knowledge of when this can happen – for what combinations of rock parameters – will be helpful in multicomponent interpretation.

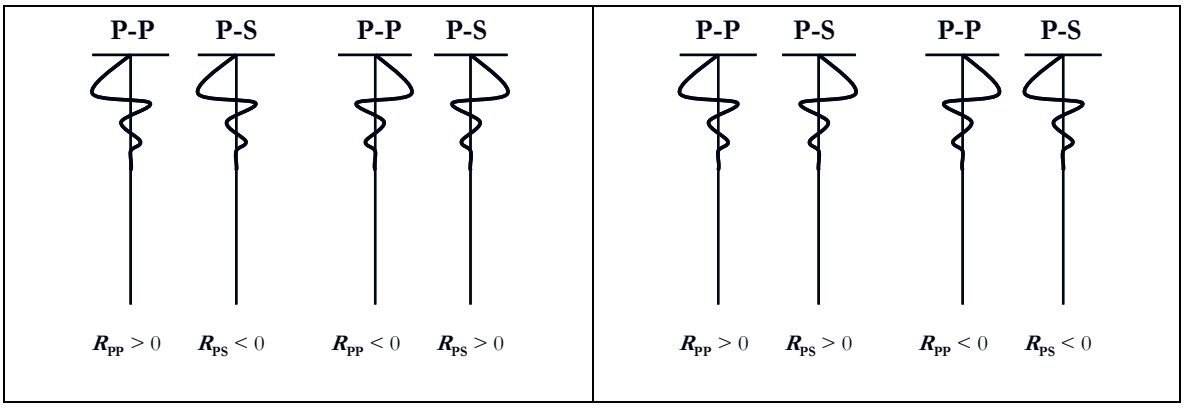

Figure 1.4. Matching events on the P-P and P-S traces: left - the "normal" polarity situation when P-P and P-S events have the same polarity; right - the "unusual" polarity situation when P-P and P-S events have opposite polarities.

1.4 Approach

A first step in trying to solve the aforementioned problem is to develop simple approximations for the reflection coefficients and to extract from them mathematical conditions that govern the polarity. I begin by looking at some of the known

approximations for R_{PS} and continue by developing a new approximation for R_{PS} and test it against other approximations and the exact Zoeppritz formula for R_{PS}. Preliminary conditions that govern the sign of the reflection coefficient are also obtained.

Since these conditions did not offer a clear relationship between the change in elastic parameters (α, β, and ρ) and the change in polarity, we pursue by creating a number of interface models for the more common sedimentary rocks, 124 of them, and creating plots of R_{PP} versus R_{PS} for each of them. These plots help us discriminate between the interfaces that produce $R_{PP}/R_{PS} < 0$ (the 'normal polarity situation') and the ones that produce $R_{PP}/R_{PS} > 0$ (the 'unusual polarity situation'). I also investigate how the depth of the interface affects the distribution of reflection coefficients generated by our interface models.

In order to investigate the polarity coherence with offset, synthetic seismograms and stacks are also generated for some of the interface models. A statistical analysis of our models was also used to pinpoint the relations between elastic parameters that are most likely to be associated with the unusual polarity situation.

Then, by combining the results obtained through modelling with conditions obtained from approximating the R_{PS} and R_{PP} expressions, we define a more precise set of conditions that define the unusual polarity situation.

In the end I show that, with only a slight modification, the already derived R_{PS} approximation becomes suitable for use in AVO studies. A method of obtaining better theoretical values for the 'gradient' and 'intercept' terms is also presented.

CHAPTER 2

A NEW APPROXIMATION FOR THE P-S REFLECTION COEFFICIENT

In this chapter, I analyze and test some of the known approximations to the Zoeppritz equations and I also derive and test an approximation of my own.. The purpose is to find an expression that is free of the usual restriction: small changes in medium parameters. In exchange it is necessary to impose other restrictions (i.e. small angles of incidence). By doing so, I try to derive mathematical relations or conditions that point exactly to where the changes in polarity occur for the P-S and P-P waves. I focus almost entirely on the behaviour of the P-S reflection coefficient from various geologic interfaces, when we vary the velocities and densities in the upper and lower medium.

The approximations discussed in this chapter are given in detail in Appendix A

2.1 A short review of the approximations to the Zoeppritz equations

A system of equations developed by Knott (1899) and Zoeppritz (1919) is used in determining the reflection coefficients of the P and SV reflected and transmitted waves. They are more commonly used in the form derived by Zoeppritz (Aki and Richards 1980). Throughout the following discussions and derivations I will stick to the notations used by Aki and Richards (1980) and shown in Figure 1.1.

Several approximate solutions for these equations have been obtained, more common being those developed by Bortfeld (1961), Aki and Richards (1980) and Shuey (1985), by assuming relatively small changes in medium properties.

These approximations, though somewhat different in detail, are really equivalent to each other (Wang, 1999; Zheng, 1991). For instance, Shuey (1985) modifies the expression developed by Aki and Richards (1980) by using σ and $\Delta\sigma$ instead of β and $\Delta\beta$, where σ is Poisson's ratio. Of course, the merit of his work is to have made his approximations more meaningful to the study of AVO by grouping the different terms in a manner that is more appropriate to this type of analysis. A shortcoming of Shuey's approach is that he only develops the formula for the P-P reflection. Actually, both reflected P-P and converted P-S waves contain information that is valuable for AVO.

The two most recent approximations of the reflection coefficients that I know of were developed by Zheng (1991) and Wang (1999).

Zheng (1991) develops eight new formulae for the reflection and transmission coefficients of compressional (PP), shear (SS) and converted (PS and SP) waves. All those formulae are based on the previous approximations developed by Aki and Richards (1980). They are developed by expanding the Aki-Richards approximation in a power series in the sine of incidence angle. Thus, these formulae are limited from the very beginning to small changes in medium elastic properties.

Wang (1999), on the other hand starts his whole approach with the exact formulae for the reflection coefficients; these formulae are also found in Aki and Richards (1980). To keep the tradition he, of course, develops his own, original, notation. Wang also chooses to use in the development of his formulae the P and S-wave vertical slownesses.

In brief, the main steps that Wang takes in developing his approximations are:

- Expanding the denominator of the exact Zoeppritz formulae using a Taylor series expansion in p (ray parameter). Then, he truncates it after the p^4 term and rewrites the

expressions. These new expressions are called the *pseudoquartic* approximations with respect to p.

- By imposing more limitations and assumptions, the coefficients of p^2 and p^4 terms from the previous step are simplified and a new pseudoquartic approximation is obtained.
- The expressions obtained above are then truncated after the p^2 term and a quadratic approximation for the P-P case is obtained.

The whole paper of Wang is focused on different approximations for the P-P reflection and transmission coefficients. For the P-S case, only the pseudoquartic formulae are shown and they are not further simplified to quadratic formulae. These are the formulae that I chose to use for comparison purposes in my investigations.

Wang also imposes some of his limitations without stating his physical or mathematical reason. The only place where he studies the effect of one of his assumptions is when he linearizes the quadratic expression for P-P reflection coefficient.

I particularly like Wang's approach, because he not only derives the approximation by using a Taylor series expansion from the *exact* formula, but also shows that by ignoring the last term of his quadratic approximation, we end up with a formula that is linear in each of the three elastic parameters (V_P, V_S and ρ) and is equivalent to the approximations obtained by his predecessors. Still, as I will show later, his pseudoquartic approximation for the P-S reflection coefficient needs to be corrected or rederived.

In order to become more acquainted with the previous approximations, after studying them I tested their accuracy. Thus, I coded a few of them in MATLAB and studied their accuracy on three interface models that entail large changes in medium parameters. As emphasized before, some of the approximations are equivalent to each

other, and thus I only chose to code the Aki-Richards approximation, Wang's pseudoquartic approximation – a pair – as well as the new approximation derived in the following section.

2.2 The simple derivation of a new approximation for R_{PS}

The first step in dealing with the unusual polarity situation was to delineate mathematical conditions on the rock parameters that govern the sign of the reflection coefficient. Choosing a simplistic approach, we can use the well known zero-offset expression for the P-P reflection coefficient (R_{PP}). Because there is no converted-wave energy recorded at zero-offset, we will use a small-offset approximation for R_{PS}.

The other approximations for R_{PS} reviewed here are either limited to small changes in elastic parameters and/or have very complicated mathematical expressions that would not lead to a simple solution for the sign of R_{PS}. I therefore decided to develop an approximation of my own that is only constrained to small angles of incidence and to test its behaviour for various ranges of elastic parameters and angles of incidence.

Following are the major steps taken for its derivation: The exact formula for the P-S reflection coefficient is given by Aki and Richards (1980):

$$R_{PS} = \frac{-2\frac{\cos i_1}{\alpha_1}\left(ab + cd\frac{\cos i_2}{\alpha_2}\frac{\cos j_2}{\beta_2}\right)p\alpha_1}{\beta_1 D} \tag{2-1}$$

where they use the following notation:

$$a = \rho_2\left(1-2\beta_2^2 p^2\right) - \rho_1\left(1-2\beta_1^2 p^2\right) \tag{2-2}$$

$$b = \rho_2\left(1-2\beta_2^2 p^2\right) + 2\rho_1\beta_1^2 p^2 \tag{2-3}$$

$$c = \rho_1\left(1-2\beta_1^2 p^2\right) + 2\rho_2\beta_2^2 p^2 \tag{2-4}$$

$$d = 2\left(\rho_2\beta_2^2 - \rho_1\beta_1^2\right) \tag{2-5}$$

and

$$E = b\frac{\cos i_1}{\alpha_1} + c\frac{\cos i_2}{\alpha_2} \qquad (2\text{-}6) \qquad F = b\frac{\cos j_1}{\beta_1} + c\frac{\cos j_2}{\beta_2} \qquad (2\text{-}7)$$

$$G = a - d\frac{\cos i_1}{\alpha_1}\frac{\cos j_2}{\beta_2} \qquad (2\text{-}8) \qquad H = a - d\frac{\cos i_2}{\alpha_2}\frac{\cos j_1}{\beta_1} \qquad (2\text{-}9)$$

$$D = EF + GHp^2 \qquad (2\text{-}10)$$

If we now limit our interest only to small angles of incidence, we can impose a few approximations that will help simplify equation (2-1).

I now expand the sine and cosine terms from the above expressions using the Taylor series:

$$\cos u \approx 1 - \frac{u^2}{2!} + \frac{u^4}{4!} + ... \qquad (2\text{-}11)$$

$$\sin u \approx \frac{u}{1!} - \frac{u^3}{3!} + \frac{u^5}{5!} - .... \qquad (2\text{-}12)$$

Keeping only the first term seems a reasonable enough approximation for sufficiently small angles of incidence, that is:

$$\begin{aligned} \cos u &\approx 1 \\ \sin u &\approx u \end{aligned} \qquad \text{for } u = i_1, i_2, j_1, j_2 \qquad (2\text{-}13)$$

The sine of the angle of incidence is also found implicitly in the formula for the ray parameter, p and thus:

$$p = \frac{\sin i_1}{\alpha_1} \approx \frac{i_1}{\alpha_1}. \qquad (2\text{-}14)$$

Since we limit our study to small angles of incidence and are only keeping terms up to first order in small quantities, we also have:

$$p^2 \approx 0 . \qquad (2\text{-}15)$$

If we now apply these approximations to equations (2-1) to (2-10), we have:

$$a \approx \rho_2 - \rho_1 \qquad (2\text{-}16) \qquad b \approx \rho_2 \qquad (2\text{-}17)$$

$$c \approx \rho_1 \qquad (2\text{-}18) \qquad d = 2\left(\rho_2 \beta_2^2 - \rho_1 \beta_1^2\right) \qquad (2\text{-}19)$$

$$E = \frac{b}{\alpha_1} + \frac{c}{\alpha_2} = \frac{\rho_2}{\alpha_1} + \frac{\rho_1}{\alpha_2} \qquad (2\text{-}20) \qquad F = \frac{b}{\beta_1} + \frac{c}{\beta_2} = \frac{\rho_2}{\beta_1} + \frac{\rho_1}{\beta_2} \qquad (2\text{-}21)$$

$$G = a - \frac{d}{\alpha_1 \beta_2} = (\rho_2 - \rho_1) - \frac{2\left(\rho_2 \beta_2^2 - \rho_1 \beta_1^2\right)}{\alpha_1 \beta_2} \qquad (2\text{-}22)$$

$$H = a - \frac{d}{\alpha_2 \beta_1} = (\rho_2 - \rho_1) - \frac{2\left(\rho_2 \beta_2^2 - \rho_1 \beta_1^2\right)}{\alpha_2 \beta_1} \qquad (2\text{-}23)$$

$$D = EF + GHp^2 \approx EF = \left(\frac{b}{\alpha_1} + \frac{c}{\alpha_2}\right)\left(\frac{b}{\beta_1} + \frac{c}{\beta_2}\right). \qquad (2\text{-}24)$$

By substituting the new expressions for the terms *a*, *b*, *c*, *d*, *E*, *F*, *G*, *H* and *D* in the initial formula for R_{PS} [expression (2-1)], we get:

$$R_{PS} = \frac{-2\dfrac{\cos i_1}{\alpha_1}\left(ab + cd\dfrac{\cos i_2}{\alpha_2}\dfrac{\cos j_2}{\beta_2}\right)p\alpha_1}{\beta_1 EF} \qquad (2\text{-}25)$$

$$R_{PS} = \frac{-2p\cos i_1\left(ab + cd\dfrac{\cos i_2}{\alpha_2}\dfrac{\cos j_2}{\beta_2}\right)}{\beta_1\left(\dfrac{\rho_2}{\alpha_1} + \dfrac{\rho_1}{\alpha_2}\right)\left(\dfrac{\rho_2}{\beta_1} + \dfrac{\rho_1}{\beta_2}\right)} \qquad (2\text{-}26)$$

$$R_{PS} = \frac{-2\frac{i_1}{\alpha_1}\left[\rho_2(\rho_2-\rho_1)+\frac{2\rho_1\left(\rho_2\beta_2^2-\rho_1\beta_1^2\right)}{\alpha_2\beta_2}\right]}{\frac{1}{\alpha_1\alpha_2\beta_2}\left[(\rho_1\alpha_1+\rho_2\alpha_2)(\rho_1\beta_1+\rho_2\beta_2)\right]} \tag{2-27}$$

$$R_{PS} = \frac{-2\frac{i_1}{\alpha_1\alpha_2\beta_2}\left[\alpha_2\beta_2\rho_2(\rho_2-\rho_1)+2\rho_1\left(\rho_2\beta_2^2-\rho_1\beta_1^2\right)\right]}{\frac{1}{\alpha_1\alpha_2\beta_2}\left[(\rho_1\alpha_1+\rho_2\alpha_2)(\rho_1\beta_1+\rho_2\beta_2)\right]} \tag{2-28}$$

$$R_{PS} = \frac{-2i_1\left[\alpha_2\beta_2\rho_2(\rho_2-\rho_1)+2\rho_1\left(\rho_2\beta_2^2-\rho_1\beta_1^2\right)\right]}{(\rho_1\alpha_1+\rho_2\alpha_2)(\rho_1\beta_1+\rho_2\beta_2)} \tag{2-29}$$

or:

$$R_{PS} = \frac{-2i_1(\alpha_2\beta_2\rho_2\Delta\rho+2\rho_1\Delta\mu)}{(\rho_1\alpha_1+\rho_2\alpha_2)(\rho_1\beta_1+\rho_2\beta_2)} \tag{2-30}$$

where $\Delta\mu$ is the contrast in shear modulus and:

$$\Delta\mu = \mu_2 - \mu_1 = \rho_2\beta_2^2 - \rho_1\beta_1^2$$

If we analyze equation (2-30), we find there are a few statements that we can make:

- For $i_1 > 0$, the sign of R_{PS} is given by the sign of the numerator of expression (2-30). This translates to the following:

$\alpha_2\beta_2\rho_2\Delta\rho+2\rho_1\Delta\mu<0$	$\Rightarrow$	$R_{PS}>0$	(2-31)
$\alpha_2\beta_2\rho_2\Delta\rho+2\rho_1\Delta\mu>0$	$\Rightarrow$	$R_{PS}<0$	(2-32)

- We observe that, at least in this approximation, the change in polarity is not influenced by the change in P-wave velocity because the parameter α_1 is not involved in expressions (2-31) or (2-32).

As stated in the introduction, one of the goals of this research was to develop a simple mathematical expression for the P-S reflection coefficient. Equation (2-30) is the

simplest formula that could be derived without compromising its accuracy or imposing more restrictions. To date, expressions (2-31) and (2-32) are the simplest conditions that I could derive for the sign of R_{PS}.

The new formula for R_{PS} developed here will later be used, in conjunction with results of the interface modelling done in Chapter 3, to obtain a more straightforward relationship between the change in polarity and the change in medium parameters over the interface.

For now I will focus on examining the accuracy of this approximation and showing that, under the imposed restrictions, it is suited to the purpose for which it was derived.

2.3 Testing the new approximation for R_{PS}

The next step is to test the new approximation against the exact Zoeppritz equation and the other approximations briefly reviewed in Section 2.1.

2.3.1 *Choosing the interface models*

In order to test the approximations, I used three models of geologic media – the same as in Brown et al. (2002). Each of them consists of a plane interface between two layers characterized by quite different elastic parameters. The models are presented below; the term "conventional reflector" refers to the most usual type of seismic reflector where all elastic parameters increase across the interface.

The greatest contrasts are in shear-wave velocity ($\Delta\beta$) and are found in the first and third model. These types of interfaces are not uncommon and are sometimes encountered in areas covered by multicomponent seismic surveys. These geologic interfaces were chosen

by Brown et al. (2002) because they produce same-sign R_{PP} and R_{PS} values and consequently, miscorrelations between P-P and P-S seismic events.

Conventional reflector:	α_1=2000 m/s, β_1=800 m/s ρ_1=1900 kg/m^3	α_2=3500 m/s β_2=1800 m/s ρ_2= 2400 kg/m^3
Clastic over salt:	α_1=3600 m/s β_1=2400m/s ρ_1=2600 kg/m^3	α_2=4500 m/s β_2=2500 m/s ρ_2= 2100 kg/m^3
Shale over gas sand:	α_1=2150 m/s β_1=860 m/s ρ_1=2200 kg/m^3	α_2=1750 m/s β_2=1250 m/s ρ_2= 1950 kg/m^3

2.3.2 *Testing the accuracy of the new approximation*

I used the MATLAB software to write the code for the exact R_{PS} expression and four different approximations, namely: the Aki-Richards approximation, two approximations developed by Wang (1999) (Appendix A) and the new one-term expression derived earlier.

Exact P-S reflection coefficients, together with the results of the four approximations, are presented in Table 2.1. The accuracy of the approximations is analyzed for incidence angles of 0, 5, 10, 20 and 30°.

In order to better illustrate the results shown in Table 2.1, and also to make it easier to compare the four approximations, I also plotted their results for different ranges of velocities, densities and angles of incidence (Figures 2.2 to 2.5). Emphasis is put on the behaviour at small angles of incidence (5°). I used the same domain of variation for both the parameters of the upper and lower medium (i.e. α_1 and α_2, β_1 and β_2, $\rho_1$and ρ_2)

Because the second pseudoquartic approximation developed by Wang turned out to be very poor, I decided to show it only in Figures 2.2 and 2.5.

The first pseudoquartic approximation is very accurate for small angles of incidence and, in the plots, its curve is impossible to tell it apart from the exact Zoeppritz curve except in Figure 2.5; in this figure the reflection coefficients are plotted against the incidence angle.

Table 2.1. Values of R_{PS} computed for a range of incidence angles (i_1) using the new approximation (R_{VB}), the Zoeppritz formula (R_{ZE}), the approximation developed by Aki and Richards (1980) (R_{AR}) and two approximations developed by Wang (1999) (R_{W1}, R_{W2}).

MODEL 1: CONVENTIONAL REFLECTOR					
α_1=2000 α_2=3500	(m/s)	β_1=800 β_2=1800	(m/s)	ρ_1=1900 ρ_2=2400	(kg/m^3)
i_1	R_{ZE}	R_{AR}	R_{W1}	R_{W2}	R_{VB}
0º	0	0	0	0	0
5º	–0.0789	–0.1129	–0.0789	–0.1297	–0.0796
10º	–0.1533	–0.2166	–0.1533	–0.2532	–0.1592
20º	–0.2684	–0.3608	–0.2681	–0.4560	–0.3183
30º	–0.2642	–0.3569	–0.2521	–0.5505	–0.4775
MODEL 2: CLASTIC OVER SALT					
α_1=3600 α_2=4500	(m/s)	β_1=2400 β_2=2500	(m/s)	ρ_1=2600 ρ_2=2100	(kg/m^3)
i_1	R_{ZE}	R_{AR}	R_{W1}	R_{W2}	R_{VB}
0º	0	0	0	0	0
5º	0.0172	0.0181	0.0172	0.0071	0.0173
10º	0.0340	0.0358	0.0340	0.0136	0.0346
20º	0.0647	0.0674	0.0647	0.0230	0.0692
30º	0.0891	0.0914	0.0891	0.0244	0.1039
MODEL 3: SHALE OVER GAS-SAND					
α_1=2150 α_2=1750	(m/s)	β_1=860 β_2=1250	(m/s)	ρ_1=2200 ρ_2=1950	(kg/m^3)
i_1	R_{ZE}	R_{AR}	R_{W1}	R_{W2}	R_{VB}
0º	0	0	0	0	0
5º	–0.0255	–0.0215	–0.0255	–0.0358	–0.0256
10º	–0.0499	–0.0418	–0.0499	–0.0703	–0.0513
20º	–0.0918	–0.0743	–0.0918	–0.1311	–0.1026
30º	–0.1190	–0.0897	–0.1190	–0.1742	–0.1539

After examining Figures 2.2, 2.3 and 2.4, we can draw the following conclusions:

The new expression derived in this chapter approximates very well the exact P-S reflection coefficient at an angle of incidence 5°, for all ranges of velocities and densities that were tested.

As we expect, the approximation of Aki and Richards (1980) gets better when the change in elastic properties across the interface between the two media become smaller.

The second pseudoquartic approximation developed by Wang (1999) gives very poor results and one is justified in saying that this expression is either a very poor approximation or erroneous.

In Figures 2-1 to 2-4 the plots resulted from varying the shear-wave velocities and the densities in the upper and lower media show symmetry when compared that is, the values of the reflection coefficient in the two cases are very close. In other words, the change in shear velocity or density ($\Delta\beta$, $\Delta\rho$) is more important than the way in which this change is manifested (increase or decrease across the interface)

The plots resulting from varying the P-wave velocities in the upper and lower media are not symmetric. In my opinion, this is because the P-wave velocity is also hidden inside the 'p' (ray-parameter) terms of the Zoeppritz equation and influences in a different manner the behaviour of the R_{PS} curves.

The plots in Figure 2.5 show the variation of the reflection coefficient with the p-wave velocity and density in the upper medium. Incidence angles of 10º, 20º and 30º were used.

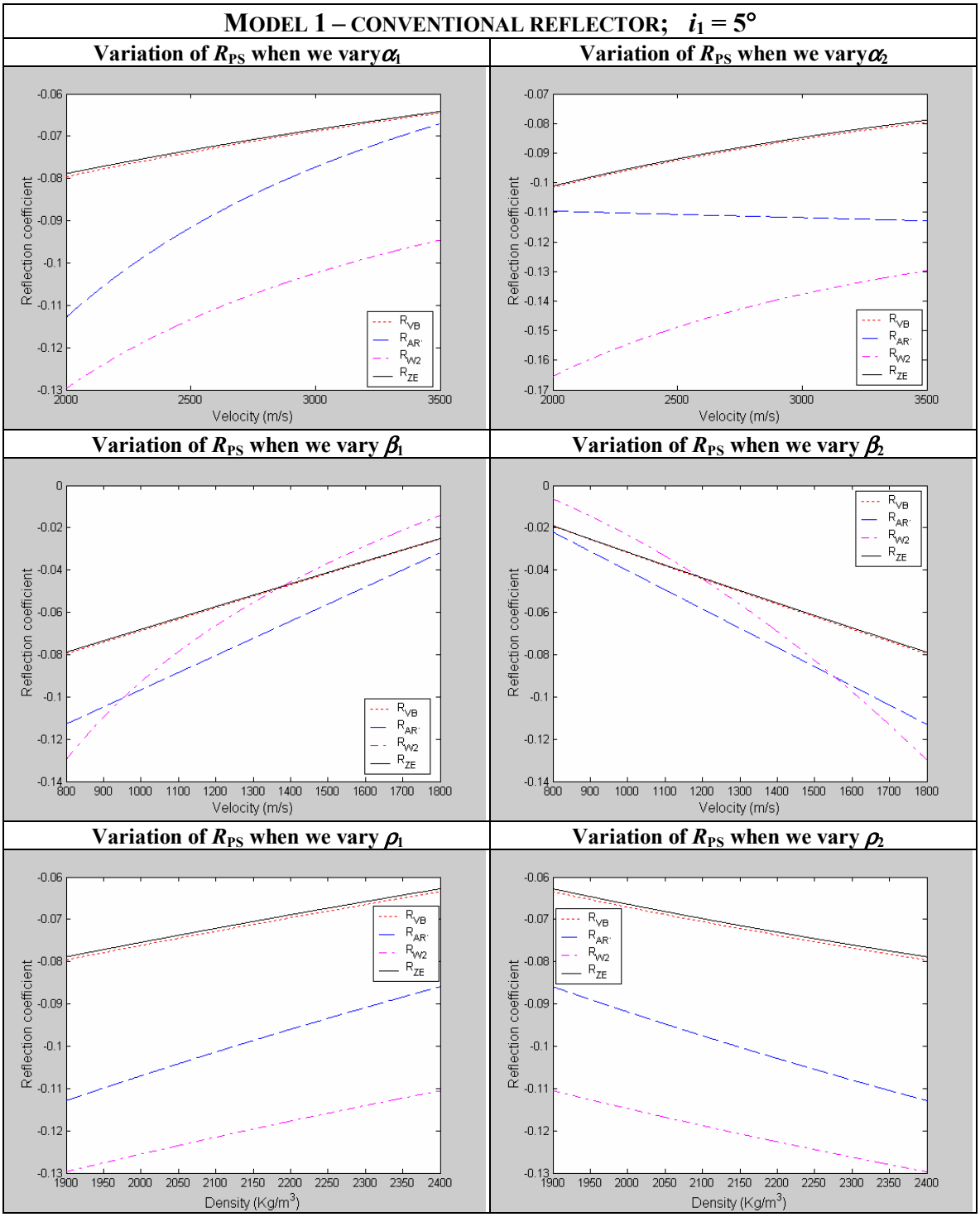

Figure 2.2. Variation of the R_{PS} with α, β and ρ for $i_1 = 5°$; the curves correspond to the exact R_{PS} (R_{ZE}) and to three of its approximations - Aki and Richards (1980) (R_{AR}), Wang (1999) (R_{W2}) and the new approximation developed here (R_{VB}). The interface model is 'model 1' from Table 2.1

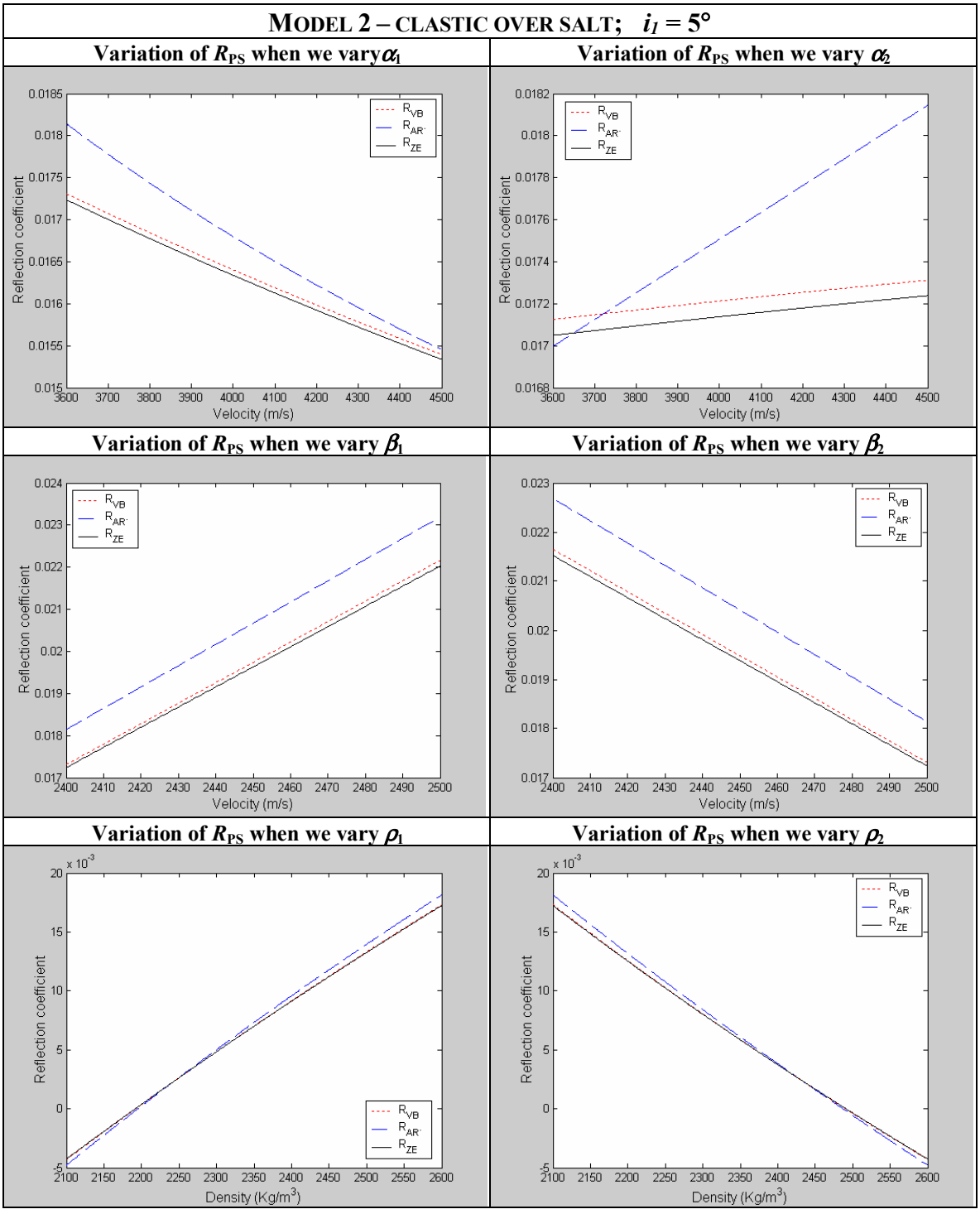

Figure 2.3. Variation of the R_{PS} with α, β and ρ for $i_1 = 5°$; the curves correspond to the exact R_{PS} (R_{ZE}) and to two of its approximations - Aki and Richards (1980) (R_{AR}) and the new approximation (R_{VB}). The interface model is 'model 2' from Table 2.1.

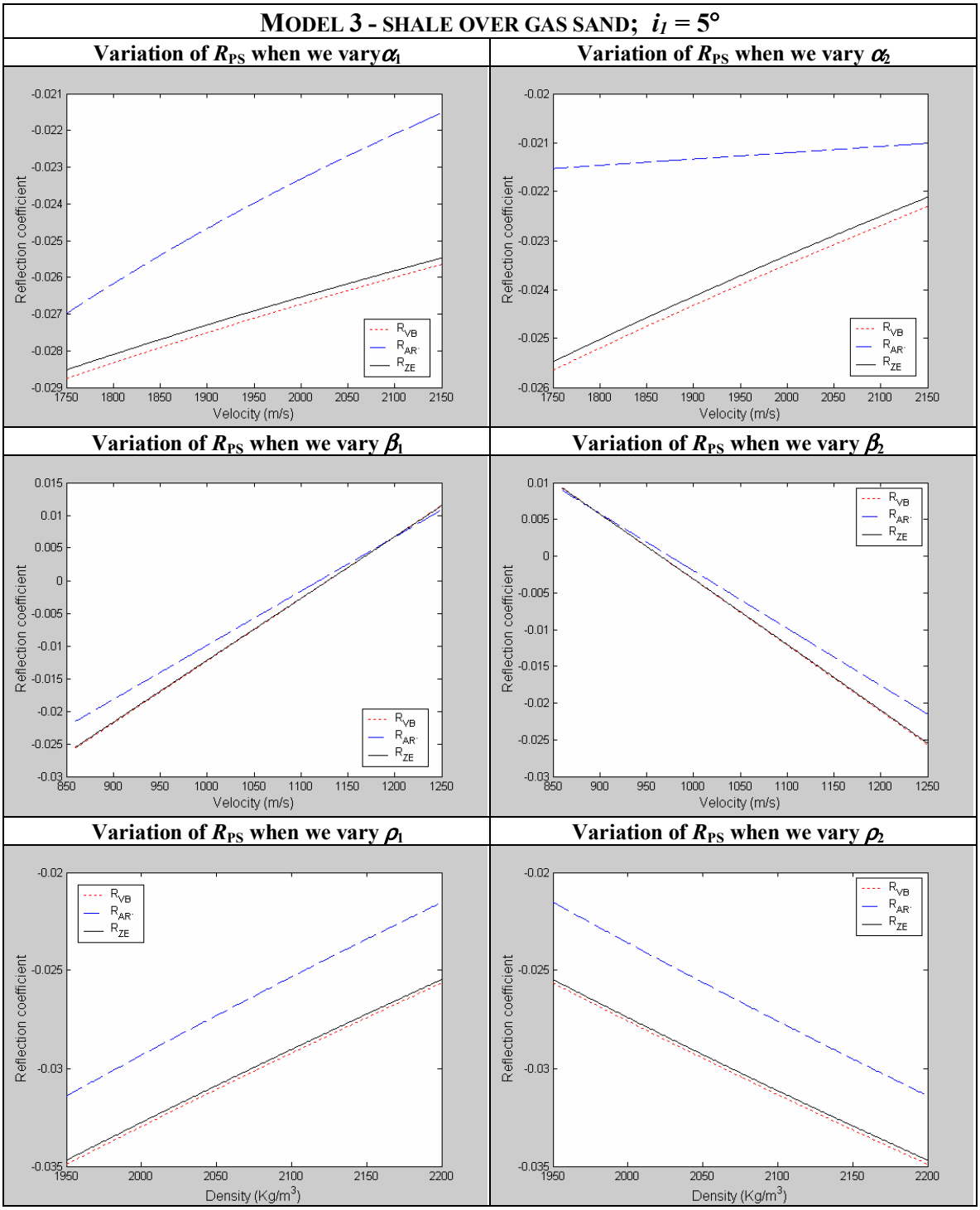

Figure 2.4. Variation of the R_{PS} with α, β and ρ for $i_1 = 5°$; the curves correspond to the exact R_{PS} (R_{ZE}) and to two of its approximations - Aki and Richards (1980) (R_{AR}) and the new approximation (R_{VB}). The interface model is 'model 3' from Table 2.1.

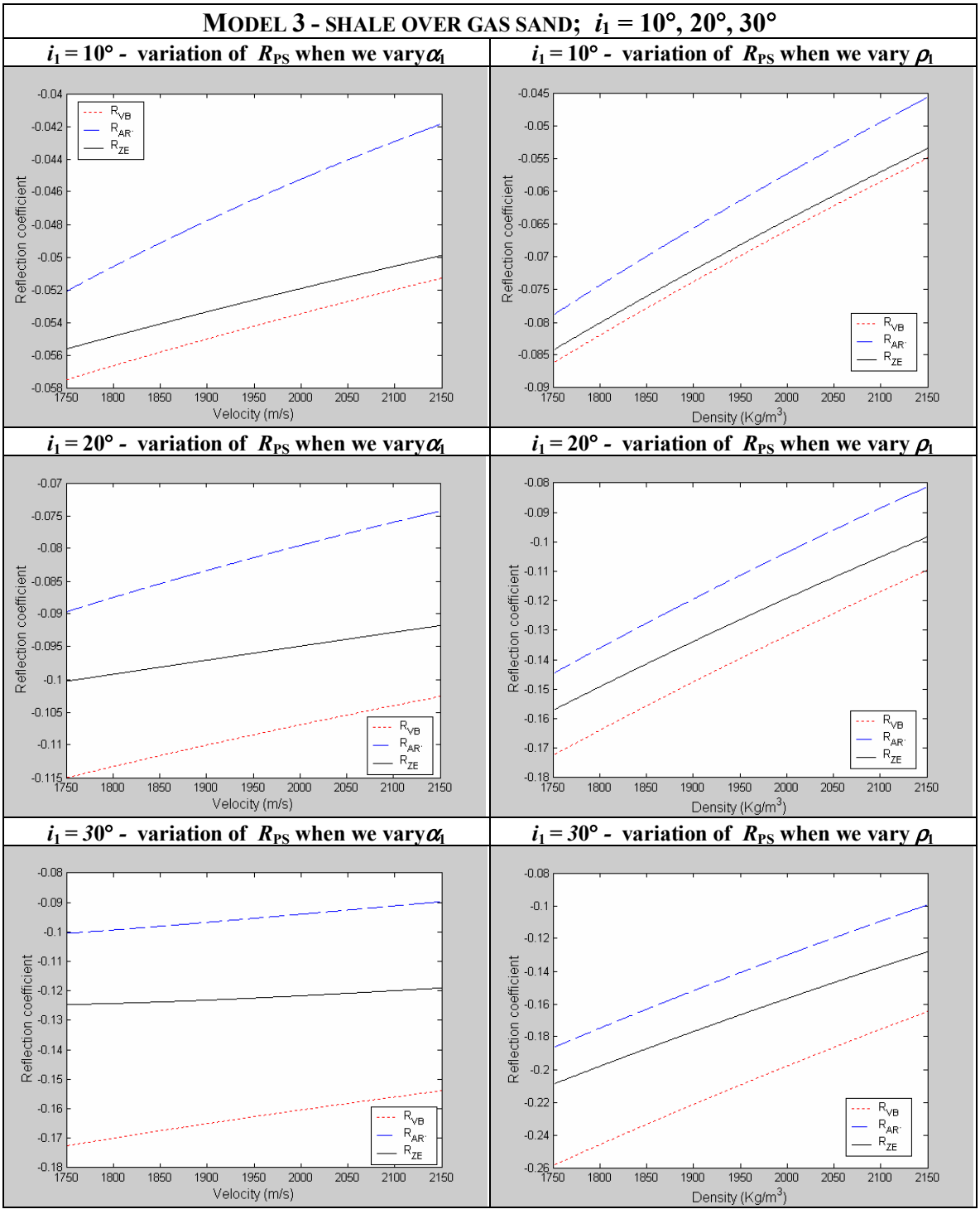

Figure 2.5. Variation of the R_{PS} with α_1 and ρ_1 for i_1 = 10°, 20°and 30°; the curves correspond to the exact R_{PS} (R_{ZE}) and to two of its approximations - Aki and Richards (1980) (R_{AR}) and the new approximation (R_{VB}). The interface model is 'model 3' from Table 2.1.

By analyzing the plots, we can conclude that for the Aki-Richards formula the accuracy of the approximation is hardly perturbed by changes in the angle of incidence. On the other hand, the error in my approximation increases at an increasing rate with incidence angle and loses its accuracy for incidence angles greater than about 25º.

This affirmation is also supported by Figures 2.6 and 2.7. Figure 2.6 shows the more familiar variation of the reflection coefficient with the incidence angle for all three models from Table 2.1 and for all approximations that were studied.

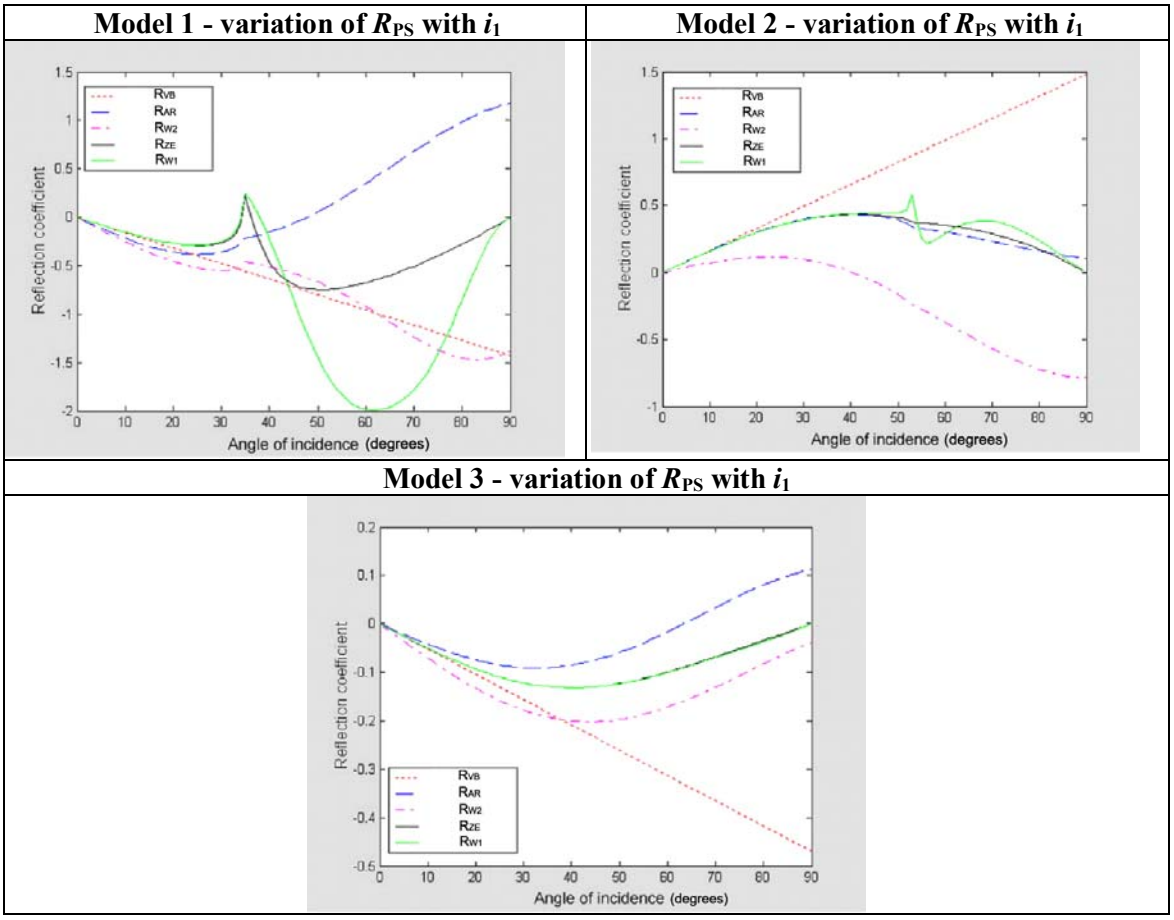

Figure 2.6. Variation of R_{PS} with the incidence angle; the curves correspond to the exact R_{PS} (R_{ZE}) and to four of its approximations - Aki and Richards (1980) (R_{AR}), Wang (1999) - two approximations (R_{W1}, R_{W2}) and the new approximation (R_{VB}). The graphs were plotted for all three models from Table 2.1.

It is obvious that the first pseudoquartic formula provides the best approximation; its wild behaviour beyond the critical angle is less important. These plots also prove the inaccuracy of the second pseudoquartic approximation.

Figure 2.7 presents error charts that were computed for my approximation and the Aki-Richards approximation. The error was computed as an absolute value of the difference between the approximated and the exact value of R_{PS}: $E = \left| R_{ZE} - R_{APPROX} \right|$

Model 1 - variation of the approximation error with the incidence angle i_1

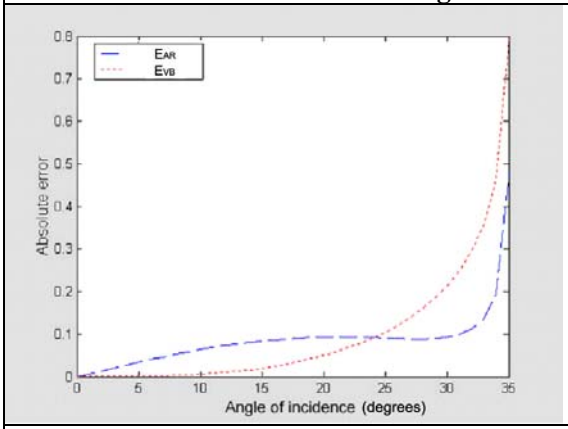

Model 2 - variation of the approximation error with the incidence angle i_1

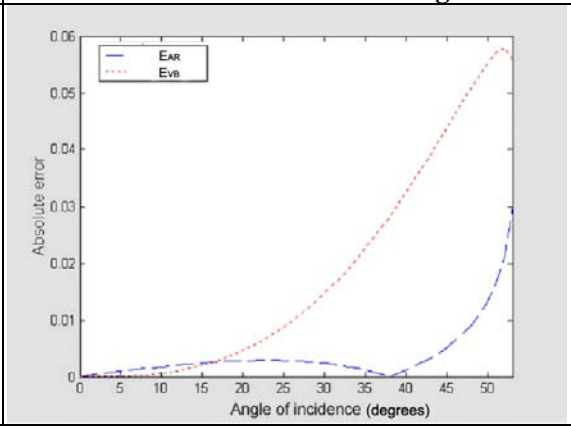

Model 3 - variation of the approximation error with the incidence angle i_1

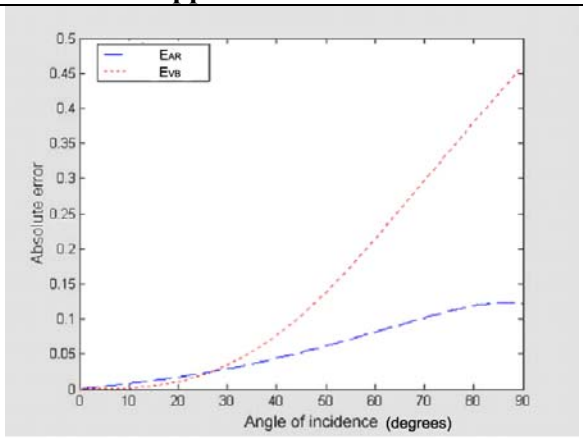

Figure 2.7. The absolute error in the estimation of the R_{PS}; the plotted curves correspond to the error in the PS reflection coefficients calculated with two approximations - Aki and Richards (1980) (E_{AR}) and the new approximation (E_{VB}). The error curves were plotted for all three models from Table 2.1.

The 'model 2' plot in Figure 2.7 shows that, in this case, my approximation can only be utilized for incidence angles that are smaller than about 20º. This is because in this example the contrast in elastic parameters across the interface is smaller and in this case the Aki-Richards formula is more accurate.

Still, if we stick to small incidence angles, the accuracies of the two approximations are comparable, even for small changes in medium parameters (Table 2.2)

Table 2.2. Examples of P-S reflection coefficient versus angle of incidence, computed considering small changes in elastic parameters using the exact Zoeppritz formula, the approximation of Aki and Richards and my new approximation.

Model 4: small changes in elastic parameters			
α_1=2150 (m/s) α_2=2160	β_1=800 (m/s) β_2=810	ρ_1=2200 (kg/m^3) ρ_2=2210	
i_1	$R_{ZOEPPRITZ}$	R_{AKI}	R_{APPROX}
5º	–0.0011	–0.0012	–0.0012
10º	–0.0022	–0.0023	–0.0023
20º	–0.0041	–0.0042	–0.0043

The testing done so far proves that the new expression for R_{PS} developed here is a very accurate approximation for small angles of incidence (near-zero offsets). The plots of the P-S reflection coefficients presented in Figures 2.2 to 2.6 and the error plots from Figure 2.7 prove that the new approximation works well under the imposed restrictions.

The new approximation together with the results of the interface modelling done in Chapter 3 will be used to relate the sign of R_{PP} and R_{PS} to the change in elastic parameters across a geologic interface. I will also show that, with only minor changes, the approximation can be used for P-S AVO.

There are also a few other remarks that are worth pursuing further. By analyzing expression (2-30), we observe that, because the only P-wave velocity found in the

numerator is α_1, the change in P-wave velocity across an interface does not influence the change in converted-wave polarity at small offsets. One might have expected this because neither does the shear-wave velocity influence the zero-offset expression for R_{PP}. This is seen from:

$$R_{PP} = \frac{\rho_2\alpha_2 - \rho_1\alpha_1}{\rho_2\alpha_2 + \rho_1\alpha_1}. \tag{2-33}$$

Also important is the observation that Wang's second pseudoquartic approximation gives poor results. Re-deriving it may prove to be useful in developing a further simplified quadratic or linear approximation for R_{PS} (by utilizing the same method that was used by Wang for the R_{PP} approximations).

A linear expression for R_{PS} – the equivalent of Shuey's R_{PP} formula – may be valuable for converted-wave AVO.

CHAPTER 3

GEOLOGIC INTERFACE MODELLING

Although the approximation for R_{PS} derived in the previous chapter provides us with formulae that determine the sign of R_{PS} [expressions (2-31) and (2-32)], we still need to find a more precise set of conditions that define the unusual situation ($R_{PP}/R_{PS} > 0$). To achieve this, I chose to model as many geologic interfaces as possible and compute the P-P and P-S reflection coefficients for a given angle of incidence. The best choice for P-P might have been normal incidence, but, because no converted-wave energy is measured at zero offset, I chose a 20° angle of incidence for all the interface models. For the most interesting interface types, the variation of P-P and P-S reflection amplitudes with offset was also studied by creating synthetic seismograms. Because most seismic surveys target oil and gas deposits in sedimentary basins, my interest was limited to sedimentary rocks.

3.1 The P-P to P-S correlation process

As a rule the correlation of P-P and P-S seismic sections is done through the use of synthetic seismograms. The process is straightforward and requires P-wave sonic, shear-wave sonic and density logs from a well drilled in the vicinity of our multicomponent seismic profile. Synthetic seismograms or synthetic stacks are then created using these logs and events from the sections and synthetics are matched. Finally, events on the P-P stacked section are matched with their counterparts from the P-S section by using the P-P and P-S

synthetic stacks. The result is usually a stretched P-S seismic section whose events match their counterparts from the P-P section.

The process is often complicated by the absence of the shear-wave sonic log and, sometimes, of the density log. When the density log is missing, Gardner's equation (Gardner et al., 1974) is usually used to calculate density; the problem is discussed in more detail in Section 3.6, page 55. If the shear wave or full-waveform sonic log is unavailable, then a user-defined V_P/V_S ratio is used to create the P-S synthetic stack (Lawton et al., 1992). The interval V_P/V_S can then be adjusted to stretch or squeeze the P-S synthetic stack in a time-variant manner in order to obtain the optimum tie between the synthetic stack and the P-S stacked section (Miller, 1996). As we will see, the absence of a shear-wave sonic log can lead to synthetic stacks whose polarities are incorrect.

The lack of information about the polarity of the matching events can cause misties of half a cycle between the events on the two sections and, consequently over-or underestimated V_P/V_S ratios for some intervals. This problem, although less vital when working at a regional scale, becomes important in local, small-scale, structures (e.g. for identification and correlation of fine stratigraphic sequences).

3.2 The SEG polarity standard

The polarity standard that is most widely used in industry is the SEG polarity standard for vertical-component geophones and hydrophones (Thigpen et al., 1975). According to Sheriff (2002), this standard says that "the onset of a compression from an explosive source is represented... by a downward deflection..." This implies that, when we use for display the unaltered (minimum-phase) wavelet, a P-wave reflection from an

interface with a positive reflection coefficient will begin with a downward deflection (negative numbers) on the recorded seismogram (Sheriff, 2002).

In the case of an upgoing converted P-S wave, the situation is a bit complicated by the fact that for the same event, the signal recorded for negative offsets has reversed phase compared with that recorded at positive offsets. In this case, the polarity standard is referring to the polarity recorded at positive offsets, the recordings from the negative offsets having their polarities switched in the preprocessing step (e.g. Brown et al., 2002).

Although there are no officially adopted SEG standards for P-S data, some recommendations (e.g. Landrum et. al., 1994) state that the onset of an upgoing mode-converted P-S wave, generated by a compressive source and coming from an interface with a negative reflection coefficient, will be negative (downward deflection) on the inline horizontal geophone. This convention agrees with the Aki & Richards convention for polarization vectors. Therefore, because for most interfaces, R_{PP} and R_{PS} have opposite signs, the events on P-P and P-S sections will display the same apparent polarity and will be easily matched. In this chapter, we analyze the situation when events on the two sections display opposite apparent polarities (the unusual situation).

3.3 Overview of the data used in modelling

A handful of papers published on AVO and topics related to rock properties (e.g. Castagna et. al., 1985; Mavko et al., 1998) analyze the relationships between various elastic or geological rock properties and the P- and S-wave velocities. In this respect, many laboratory measurements have been performed on a wide range of sedimentary rocks. From diverse public data, I selected those containing compressional- and shear-wave velocities

and densities for the rocks that are most common to sedimentary basins. A list of references for the data used in this study is shown in table B.2.

The change of velocity with pressure, and thus with depth, is mainly attributed, for consolidated rocks, to the closure of microcracks, which hardly affects the total porosity but significantly increases the elastic moduli of the rocks. Since the reflection coefficients are directly dependent on the seismic velocities, I chose to investigate reflection coefficients for shallow (500 m), intermediate (1000 m) and deep (2000 m) interfaces and determine if how they are influenced by the change in velocity with depth.

Laboratory measurements of acoustic properties of representative rock samples, simulating in-situ effective stress and fluid saturation, proved useful for our modelling.

In some geological formations the pressure differs from the lithostatic pressure, this phenomenon can be caused by either natural factors such as tectonic deformation or by hydrocarbon extraction itself or some of the techniques used in extraction, such as water or steam injection. Although the issue of over- or underpressured formations is very important and is currently considered in many recent research papers (e.g. Prasad, 2002), I chose to leave it aside because it complicates our already unclear polarity problem.

In this respect, I only used velocities that were measured at confining pressures corresponding to the lithostatic pressure at these depths (Figure 3.1).

The corresponding lithostatic pressures were calculated using the formula $P = \rho g z$, where P is the pressure, ρ is the average density of the sedimentary overburden and z is the depth. I chose ρ = 2.3 g/cm^3, which is a reasonable value for sediments. The following lithostatic pressure values were obtained: 500 m for 11.27 MPa, 1000 m for 22.54 MPa, 2000 m for 45.08 MPa.

Experimental results show that acoustic velocities in dry rock and in water- and oil-saturated rock samples usually increase nonlinearly with effective stress over the stress range from 5 to 60 MPa (Bonner et al., 1989).

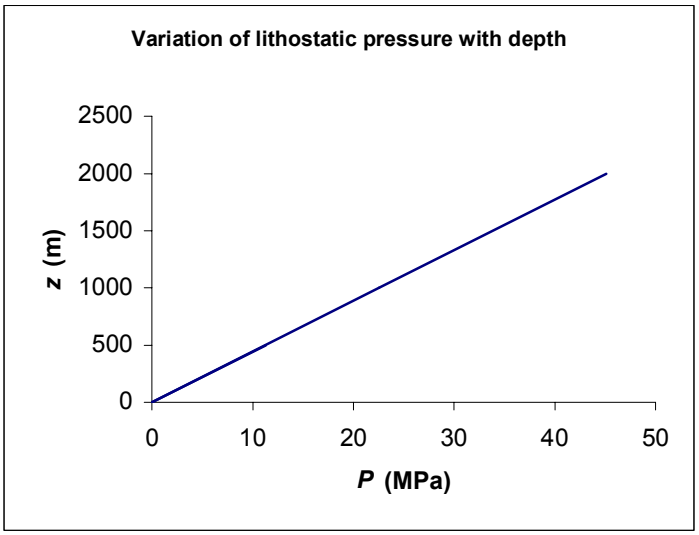

Figure 3.1 Variation of lithostatic pressure with depth for an average sediment density $\rho = 2.3$ g/cm^3.

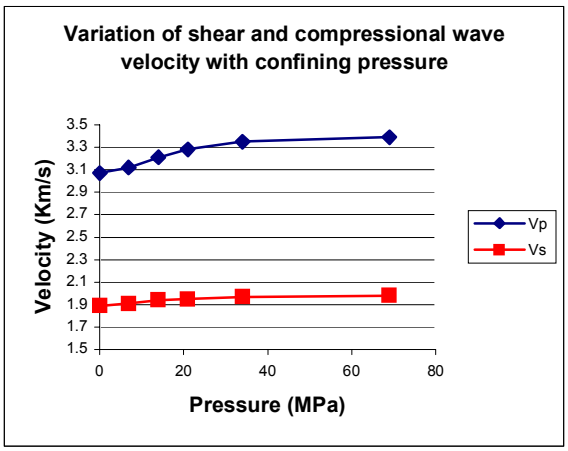

Figure 3.2. Variation of shear- and compressional-wave velocity with confining pressure. The example shown is based on data measured on a Boise sandstone sample with $\rho = 1.93$ g/cm^3 (Bonner et al., 1989).

Because the published velocities were usually measured at pressures that differ from our calculated values, I assume a linear velocity variation with pressure on the pressure intervals where the velocity measurements are not available (Figure 3.2) and calculate the velocities at the three specific pressures by means of linear interpolation (Table B.1).

3.4 Modelling the sedimentary interfaces

3.4.1 *Selecting the geologic interfaces*

Any change in rock property that causes ρ, μ or k to change will, in general, cause seismic velocities to change. For example, going from unsaturated sediment to liquid-saturated sediment will cause both the density and the bulk modulus to change. The bulk modulus changes because air-filled pores become filled with the liquid (water or oil). In this example, the change in shear modulus is insignificant when compared to the change in bulk modulus. Thus, for a change in saturant, the P-wave velocity changes a lot across the interface while the S-wave velocity changes very little.

As seen in Table 3.1 below, for modelling interfaces I had to carefully consider not only the rock type, but also the fluid that saturates its pores.

Eleven satisfactory lithological types were identified. For these rocks, the published velocity and density measurements were made at a range of confining pressures appropriate to our modelling needs. Then, in accordance with the fluid that saturates each rock type, they were further categorized into nineteen types. These final rock types whose elastic

parameters were used for the interface-modelling program are presented in Table 3.1 together with the type of pore fluid and their appropriate abbreviations.

For some of the coal and all the chalk data, no laboratory measurements were available. Well-log values were used instead. The values for chalk correspond to a depth of 3000 m (Brevik, 2002) and the values for three bituminous coal samples are from a depth of 1500 m (Margrave, 2001). For gypsum and anhydrite I used velocity and density measurements performed at room conditions (temperature and pressure) (Bonner and Schock, 1989).

Table 3.1. Rock types used in the interface-modelling program. Classification is based on lithology and pore fluid.

No.	Rock type	Pore fluid	Abbreviation
1	Sandstone	Water	SS-WS
2	Sandstone	Dry/Gas	SS-DR
3	Sandstone	Oil	SS-OS
4	Sand/Poorly consolidated sandstone	Dry/Gas	S-DR
5	Sand/Poorly consolidated sandstone	Water	S-WS
6	Tight gas sandstone	Water	SS-TG-WS
7	Tight gas shale	Water	SH-TG-WS
8	Shale	Water	SH-WS
9	Shale	Dry/Gas	SH-DR
10	Shale	Oil	SH-OS
11	Limestone	Water	LS-WS
12	Limestone	Dry/Gas	LS-DR
13	Dolostone/Dolomite	Oil	DO-OS
14	Dolostone/Dolomite	Water	DO-WS
15	Dolostone/Dolomite	Dry/Gas	DO-DR
16	Coal	Water	CO
17	Salt	-	HA
18	Chalk	Water	CH
19	Gypsum/Anhydrite	-	GY/AN

3.4.2 *Possible interfaces*

By considering all possible interface combinations for these 19 rock types (Table 3.1) we would have a total of 361 interfaces that are theoretically possible. From a geological point of view, however, more than half of them are virtually impossible (e.g. a brine sand over a gas sand). Thus, there were only 124 rock combinations that I considered likely to form an interface that would also be geologically realistic.

The following reasoning stands behind the choice of interfaces: interfaces between two different rock types whose pores are saturated with two different fluids were not considered. In nature, although possible, encountering interfaces where the oil/water, gas/oil or gas/water contact also corresponds to a significant change in lithology is very unlikely. These types of seismic interfaces where the impedance contrast is produced by change in fluid content are usually encountered inside the same formation (lithostratigraphic unit).

Still, I did not consider this second type of interface either. The decision is motivated by the fact that, although we have velocity and density measurements for the same rock type (e.g., sandstone, limestone, etc.) saturated with different fluids, the measurements were not performed on the same rock samples. For example, the laboratory measurements on water-saturated sandstone (Han, 1986) were not made on the same rock-samples as the measurements made on dry sandstone (Colorado School of Mines, 2003).

The chance of encountering dry rock in a sedimentary basin is very slim, the majority of sedimentary rocks being water-saturated and in some cases oil- or gas-saturated. Naturally, I chose not to model interfaces between two dry rocks either.

Nevertheless, many of the acoustic-velocity measurements were performed on dry rock samples. This is because the physical properties of air are very similar to those of

hydrocarbon gas and, of course, because it is handier to perform a measurement on a dry than on a gas-saturated sample. Thus, the reader should consider all the measurements made on dry samples as actually referring to gas-saturated rock.

All the possible types of interfaces are presented schematically in Table 3.2.

3.4.3 *The interface response*

As mentioned before, one purpose of this research is to model all possible types of sedimentary interfaces and calculate their P-P and P-S reflection coefficients for an angle of incidence of 20° at depths of 500, 1000 and 2000 m. Although using the same angle of incidence implies that traces are recorded at different offsets on the P-P and P-S sections, this is not crucial. That is because the same seismic reflections recorded on the two traces are generated by the same region of the subsurface (CMP or CCP) and, on the stacked trace the final spatial location of the P-P and P-S reflection points is the same.

To attain this, I created a computer program, using the MATLAB software. The program uses the *zoeppritz* function created by Gary Margrave to calculate the exact Zoeppritz P-P and P-S reflection coefficients for all the possible combinations of interfaces, and then displays the results in R_{PP} vs. R_{PS} plots.

To begin with, the results were plotted only for the case when the interface is situated at a depth of 1000 m, which is a typical target-depth for many oil and gas deposits. Reflection coefficients obtained for the other two depths (500 and 2000 m) were later analyzed in comparison with those for 1000 m only for the most interesting interface types.

	POSSIBLE INTERFACES																		
	SS-WS	SS-DR	SS-OS	S-DR	S-WS	SS-TG-WS	SH-TG-WS	SH-WS	SH-DR	SH-OS	LS-DR	LS-WS	DO-DR	DO-WS	DO-OS	Coal	Halite	Chalk	GY/AN
SS-WS					■			■				■		■		■	■	■	■
SS-DR				■					■		■		■				■		
SS-OS										■					■		■		
S-DR		■							■		■		■				■		
S-WS	■							■				■		■		■	■	■	■
SS-TG-WS							■	■									■		
SH-TG-WS						■		■									■		
SH-WS	■				■	■	■					■		■		■	■	■	■
SH-DR		■		■							■		■				■		
SH-OS			■												■		■		
LS-DR		■		■					■				■				■		
LS-WS	■				■			■						■		■	■	■	■
DO-DR		■		■					■		■						■		
DO-WS	■				■			■				■				■	■	■	■
DO-OS			■							■							■		
Coal	■				■			■				■		■			■	■	■
Halite	■	■	■	■	■	■	■	■	■	■	■	■	■	■	■	■		■	■
Chalk	■				■			■				■		■		■	■		■
GY/AN	■				■			■				■		■		■	■	■	

Table 3.2. All the possible rock combinations that can theoretically form geologic interfaces. The upper medium is shown on the first row and the lower medium on the first column.

■ → Suitable interface □ → Unsuitable interface

The R_{PP} vs. R_{PS} plots help us to discriminate between the interfaces that would have the same polarity or reversed polarity on P-P and P-S sections. For most interfaces, R_{PP} and R_{PS} have opposite signs, but sometimes, they can have the same sign, producing a 180° phase difference between the events on the P-P and P-S sections plotted using the SEG polarity standard.

The resulted plots can be divided into three basic types (Figure 3):

- Plots in which all points belong to one quadrant (either II or IV)
- Plots in which the points are diagonally spread throughout the quadrants II and IV
- Plots in which the points are diagonally spread throughout the quadrants II and/or IV, but there are some points that fall into the quadrants I and/or III.

After plotting results for all the possible interface types situated at the target-depth of 1000 m (Appendix B), the next step was to choose from them only the cases where R_{PP} and R_{PS} have matching signs as the ones shown in Figure 3.3c and d.

From these, I selected six interface types that seemed more relevant and for which both P-P and P-S reflection coefficients have reasonably high values, often close to 0.1. These interface types, which were further analyzed, are presented in Table 3.3 and Figures 3.4 to 3.6.

Table 3.3. Interface types that produce a significant number of compressional- and converted-wave reflection coefficients of the same sign.

Interface types		***Number of rock samples used in the plot***		**Figure**
Overlying rock	**Underlying rock**	**Overlying rock**	**Underlying rock**	**No.**
Coal	Chalk	13	10	Fig. 3.6
Gas Sand	Gas Limestone	6	6	Fig. 3.5
Gas Sandstone	Gas Limestone	6	6	Fig. 3.5
Water-saturated Sandstone	Chalk	10	10	Fig. 3.4
Water-saturated Sandstone	Water-saturated Dolomite	10	5	Fig.3.4
Water-saturated Sand	Coal	6	10	Fig. 3.6

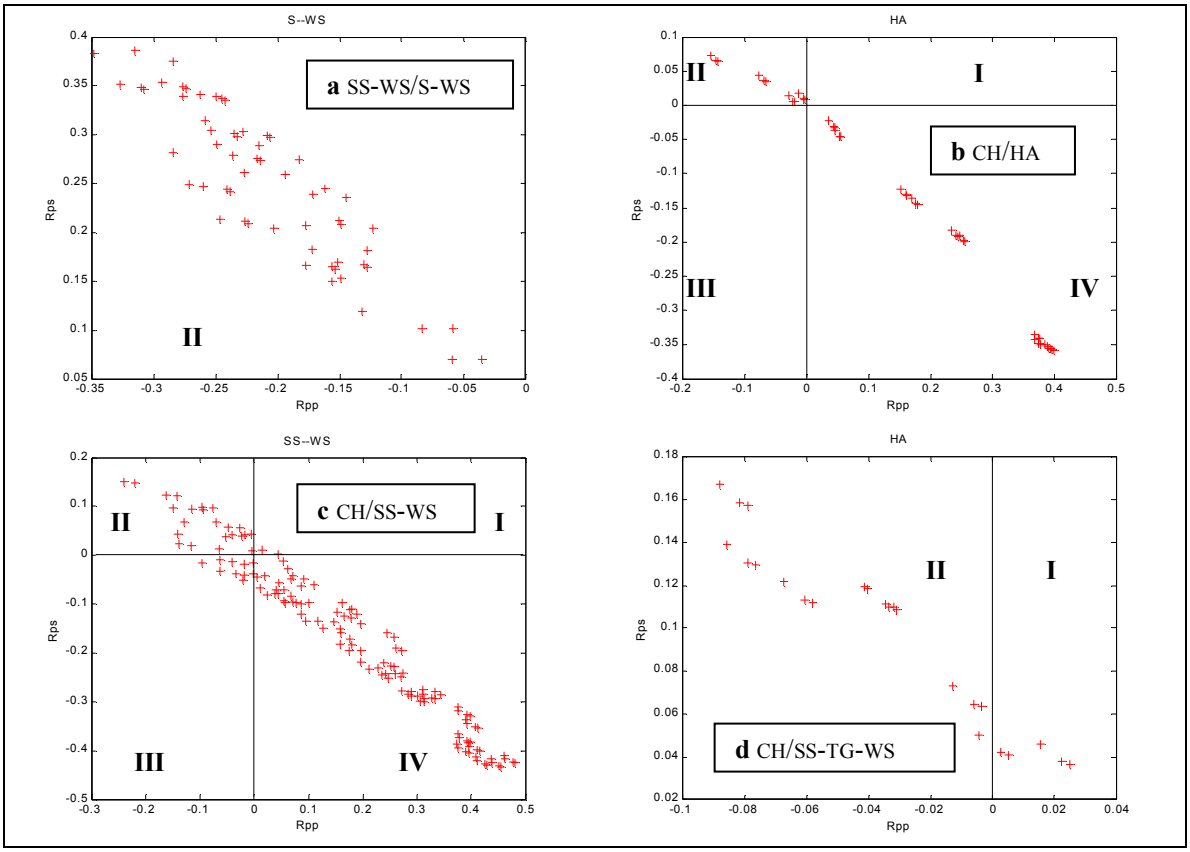

Figure 3.3. Examples of R_{PP}-vs-R_{PS} plots obtained using the Zoeppritz equations: (a) all points in one quadrant; (b) points in quadrant II and IV; (c) and (d) plots that have some points in quadrants I and/or III.

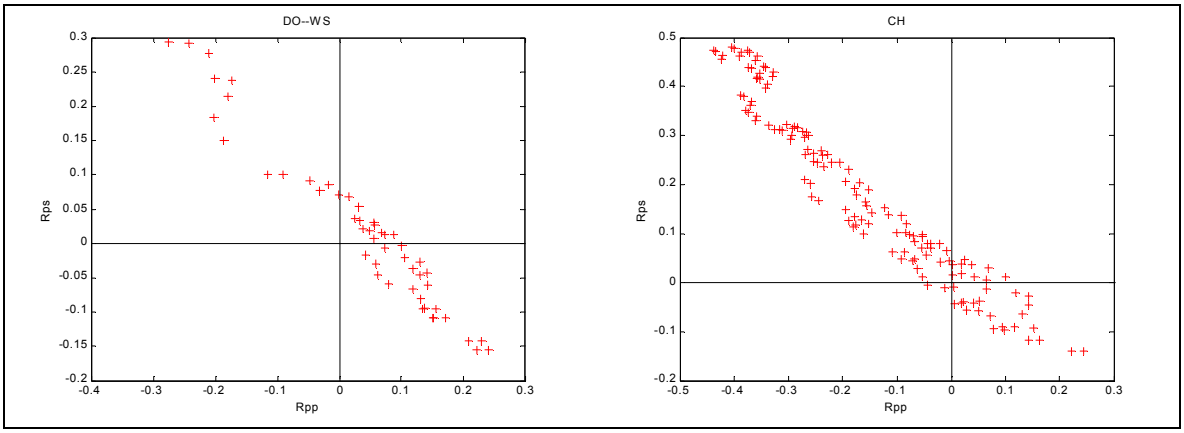

Figure 3.4. R_{PP}-vs-R_{PS} plots for the following interfaces: water-saturated-sandstone over water-saturated-dolomite (left) and water-saturated-sandstone over chalk (right).

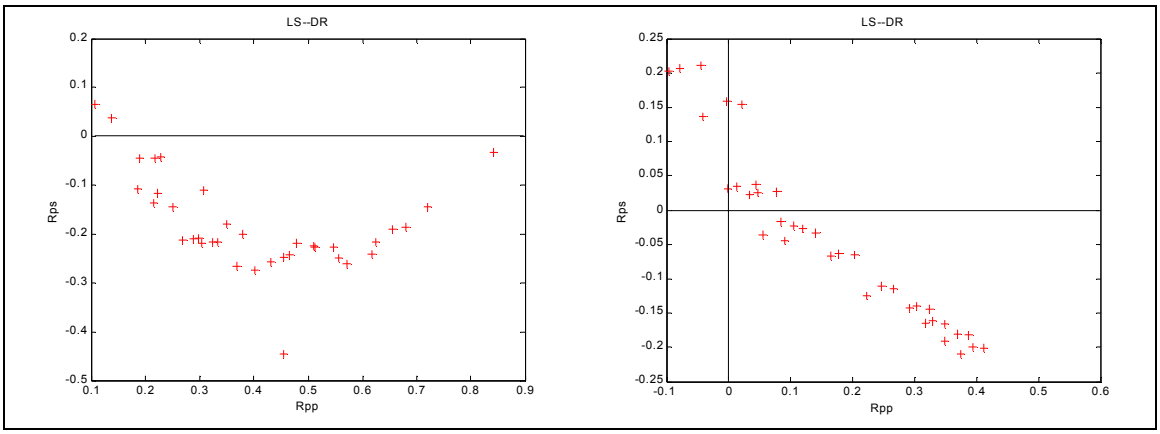

Figure 3.5. R_{PP}-vs-R_{PS} plots for the following interfaces: gas-sand over gas-limestone (left) and gas-sandstone over gas-limestone (right).

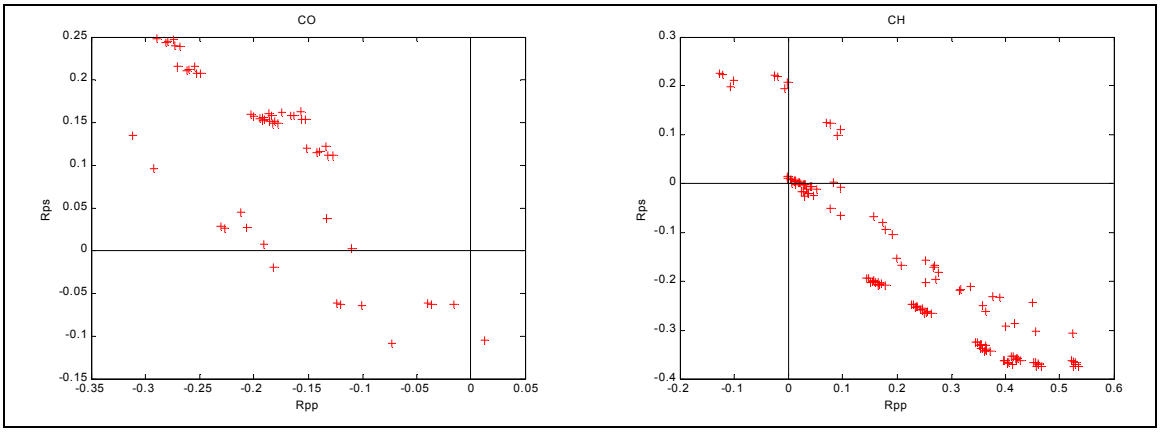

Figure 3.6. R_{PP}-vs-R_{PS} plots for the following interfaces: water-saturated-sand over coal (left) and coal over chalk (right).

3.5 Creating synthetic seismograms for the most relevant models

The aim of this study is, not only to determine the possible interfaces that create the unusual polarity situation, but also to investigate how the polarity of events produced by

these interfaces varies with offset. We have to keep in mind that, so far, the interface response was investigated only for a 20° angle of incidence.

Unfortunately, this is not enough, because the events that appear on a seismic section are the result of common-midpoint stacking in the case of P-P waves and common-conversion-point stacking for P-S waves. These incorporate gathers of traces that are recorded at different offsets and may, potentially, have different polarities.

To study if the type of polarity is consistent with offset I decided to use another MATLAB facility developed by CREWES and called "SYNTH". The SYNTH program was originally designed for creating synthetic stacks and, as an input, it uses sonic, shear-wave sonic and density logs in LAS format. The synthetic stacks are used for the P-P to P-S correlation process.

As a first step, for each of the interface-types presented in Figures 3.4 to 3.6, I chose two representative points from each of quadrants III or I. We should keep in mind that each point on the R_{PP} vs. R_{PS} plots is produced by a unique combination of rock elastic parameters for the interface type considered.

For each point chosen from the plot, I extracted the elastic parameters of the two rock samples that create the interface. These elastic parameters – namely V_P, V_S and ρ – were then used to create synthetic well logs.

The process is very straightforward: In a log from a well drilled in the Blackfoot area, I replaced well-log values of V_P, V_S and ρ with the values corresponding to the two rocks that are forming the modeled interface. To make the data manipulation easier, the log sampling interval was also increased from 0.3 m to 5 m.

Through this process were obtained twelve synthetic well logs files, two for each interface type. These logs were then used as an input for the synthetic seismogram program whose brief description is presented below.

3.5.1 *Choosing the parameters for the SYNTH package*

SYNTH is a package developed by Gary Margrave and Don Lawton that can be run using the MATLAB program. SYNTH creates primaries-only synthetic seismograms for P-P and P-S reflections. The synthetic seismograms are trace gathers for a horizontally layered subsurface model.

The final display shows the variation of amplitude with offset, as well as the stacked response for the chosen receiver type (horizontal or vertical) and reflection type (P-P or P-S). Each plot also displays the logs that were used as input for the modelling.

The reflection amplitudes are calculated by using the exact Zoeppritz equations. The traveltimes and incidence angles are calculated by raytracing.

Besides the well logs in LAS (ASCII) format, the program also requires a wavelet as input. The wavelet can be created by using the wavelet editor incorporated in the SYNTH package.

In order to obtain a minimum-phase earth response, I chose a minimum-phase Ricker wavelet with a 40-Hz dominant frequency and a length of 0.2 seconds. The wavelet, together with its frequency and phase spectra are shown in Figure 3.7.

There are three types of section to choose from:

- Normal moveout
- NMO removed

- Pseudo-zero-offset (reflections on all traces plotted at the same two-way traveltime as the one on the zero-offset trace for the P-P case or a pseudo-zero-offset trace for the P-S case).

The best choice for our study is the pseudo-zero-offset section. It bypasses the visual and stacking inconvenience created by the moveout-related event misalignment by plotting all the arrivals from a certain depth at the time corresponding to the zero-offset reflection or a virtual zero-offset mode conversion.

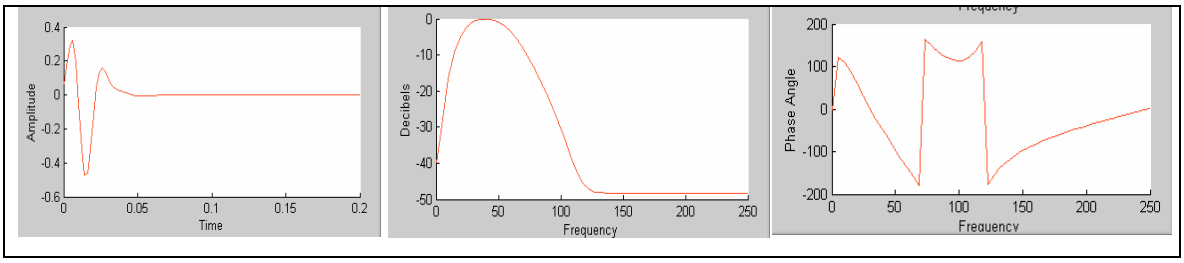

Figure 3.7. The Ricker wavelet used for creating the synthetic seismograms, together with its frequency and phase spectra.

For the polarity convention, the program presents us with two choices:

- The SEG polarity convention
- The Zoeppritz-equations polarity convention – as given in Aki and Richards (1980) – predicts opposite polarity behaviour for reflected PP and PS coming from the same interface.

I chose the SEG polarity standard because it is widely used in industry and because our definition of the unusual polarity situation is based on it. In contrast, were we to choose the Zoeppritz polarity convention, we would have events with opposite polarity when R_{PP} and R_{PS} have opposite signs.

The log editing was done using Microsoft Excel and another MATLAB log-editing package called LOGEDIT.

3.5.2 *The earth response from the chosen interface models*

In the following section are presented twelve images showing the AVO response and the synthetic stacks obtained from the well logs corresponding to the models presented in Figures 3.4, 3.5 and 3.6 (two synthetic stacks for each interface model).

For each of the studied models, the P- and S-wave velocities, together with densities and the corresponding P-P and P-S reflection coefficients are shown in Table 3.4.

Table 3.4. V_P, V_S, ρ and the corresponding R_{PP} and R_{PS} for the studied models; i_1=20º

Interface	V_P (m/s)	V_S (m/s)	ρ (g/cm^3)	R_{PP}	R_{PS}	Fig. No.
Coal	2564	1739	1.37	0.0770	0.1228	Fig. 3.8
Chalk	2581.87	1170.36	1.38			
Coal	2564	1739	1.37	0.0961	0.1106	
Chalk	2695.45	1210.6	1.38			
Gas Sandstone	3785.67	2591.4	2.0935	0.0420	0.0370	Fig. 3.9
Gas Limestone	3736.35	2232.54	2.197			
Gas Sandstone	3785.67	2591.4	2.0935	0.0765	0.0264	
Gas Limestone	3345.14	1913.02	2.62			
Gas Sand	2533.876	1701.43	1.9425	0.1377	0.0370	Fig. 3.10
Gas Limestone	2816.35	1365.08	2.13			
Gas Sand	2659.512	1795.954	2.00431	0.1073	0.0667	
Gas Limestone	2816.35	1365.08	2.13			
Water-sat. Sandstone	4407.62	2815.08	2.32	0.0780	0.0362	Fig. 3.11
Chalk	4080.48	2426.37	2.436			
Water-sat. Sandstone	5103.97	3100.16	2.53	0.0373	0.0364	
Chalk	5224.92	2746.17	2.5565			
Water-sat. Sandstone	4883.81	3082.54	2.5	0.0554	0.0306	Fig. 3.12
Water-sat. Dolomite	5168.58	2780.257	2.53			
Water-sat. Sandstone	4766.35	3065.08	2.39	0.0315	0.0537	
Water-sat. Dolomite	4795.694	2623.595	2.39			
Water-sat. Sand	2398.938	1176.192	1.99918	-0.0730	-0.1087	Fig. 3.13.
Coal	2702	1851	1.68			
Water-sat. Sand	2588.7	1283.002	2.09746	-0.1240	-0.0617	
Coal	2702	1851	1.68			

In all the models, the maximum offset-to-depth ratio was set to 1. This ratio covers well the near-offset situation or the short-spread survey. In the case of marine surveys, larger ratios may be reached. In this case, a greater consideration should be given to situations when polarity reversals that appear when the incidence angle exceeds the critical angle. Normally, most of these situations are avoided by a careful selection of the source/receiver ranges considered for stacking. All plots in figures 3-8 to 3-15 show the three synthetic well logs in the far left followed by the AVO response; each of the last three traces (far right) represents the stacking (summation) of all traces forming the AVO response.

For all but one of the interface models and combinations of elastic parameters taken into consideration, the reflections show phase continuity for both the P-P and P-S gathers.

The first example that was considered for the water-saturated-sandstone over chalk interface shows a polarity reversal on the P-P gather (Figure 3.11). Even though the example is singular, it is possible that this type of amplitude variation might be encountered significantly often.

In this unfortunate situation, stacking produces a very weak event, which in our case is still showing the same polarity as its P-S counterpart. This might not have been so, had the polarity reversal appeared on the P-P event at a smaller offset.

This ambiguous situation, associated with a chalk interface, is also encountered in the Alba field from the North Sea, where the top of the chalk formation is producing a strong event on the P-S section and a very weak one on the P-P section (Bale, 2003).

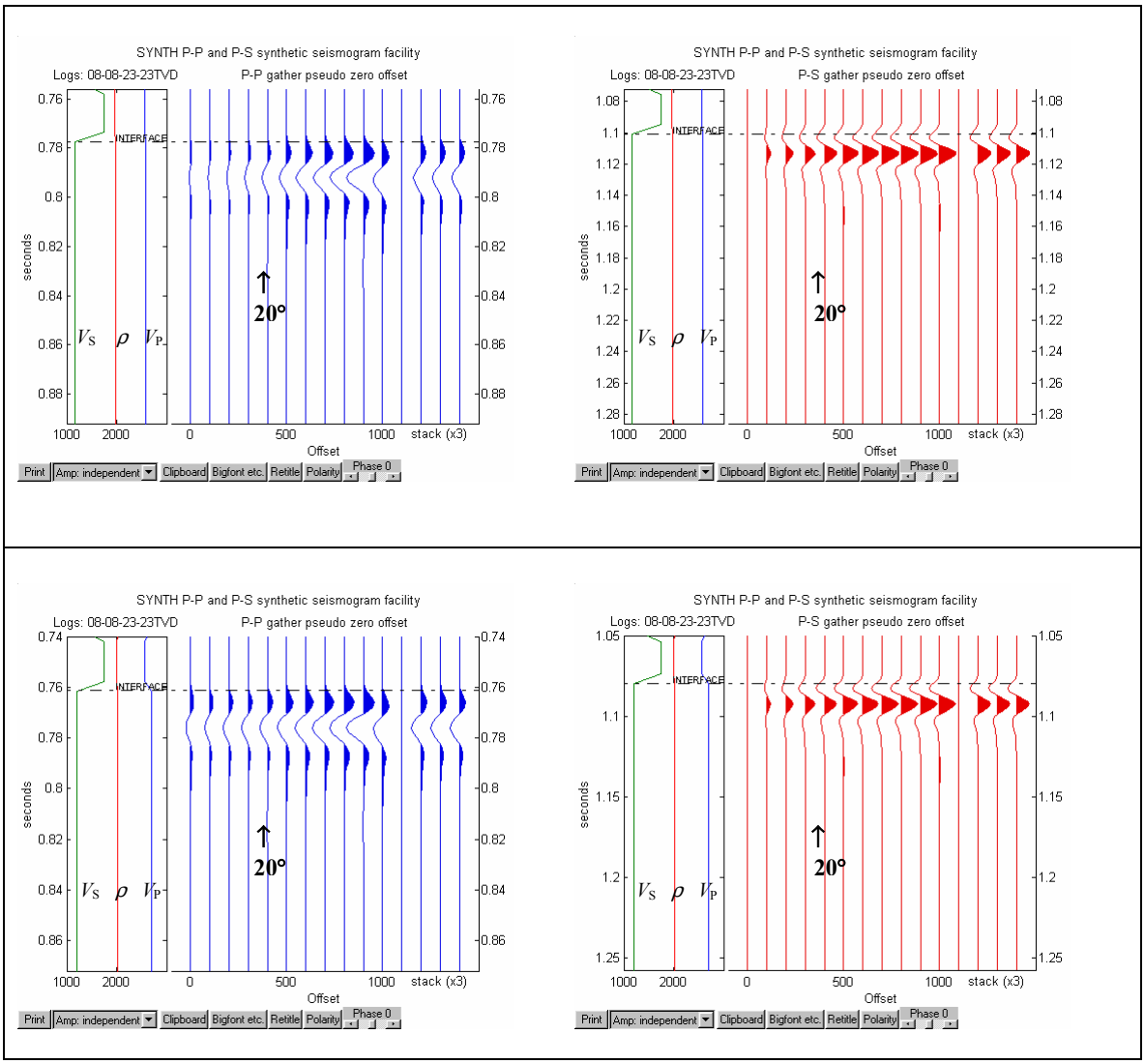

Figure 3.8. AVO responses and synthetic stacks for two combinations of elastic parameters (Table 3.4) of the coal-over-chalk model buried at a depth of 1000 m. The model assumes the upper medium starts from the surface and the lower medium extends down infinitely, i.e., a two-layer half-space.

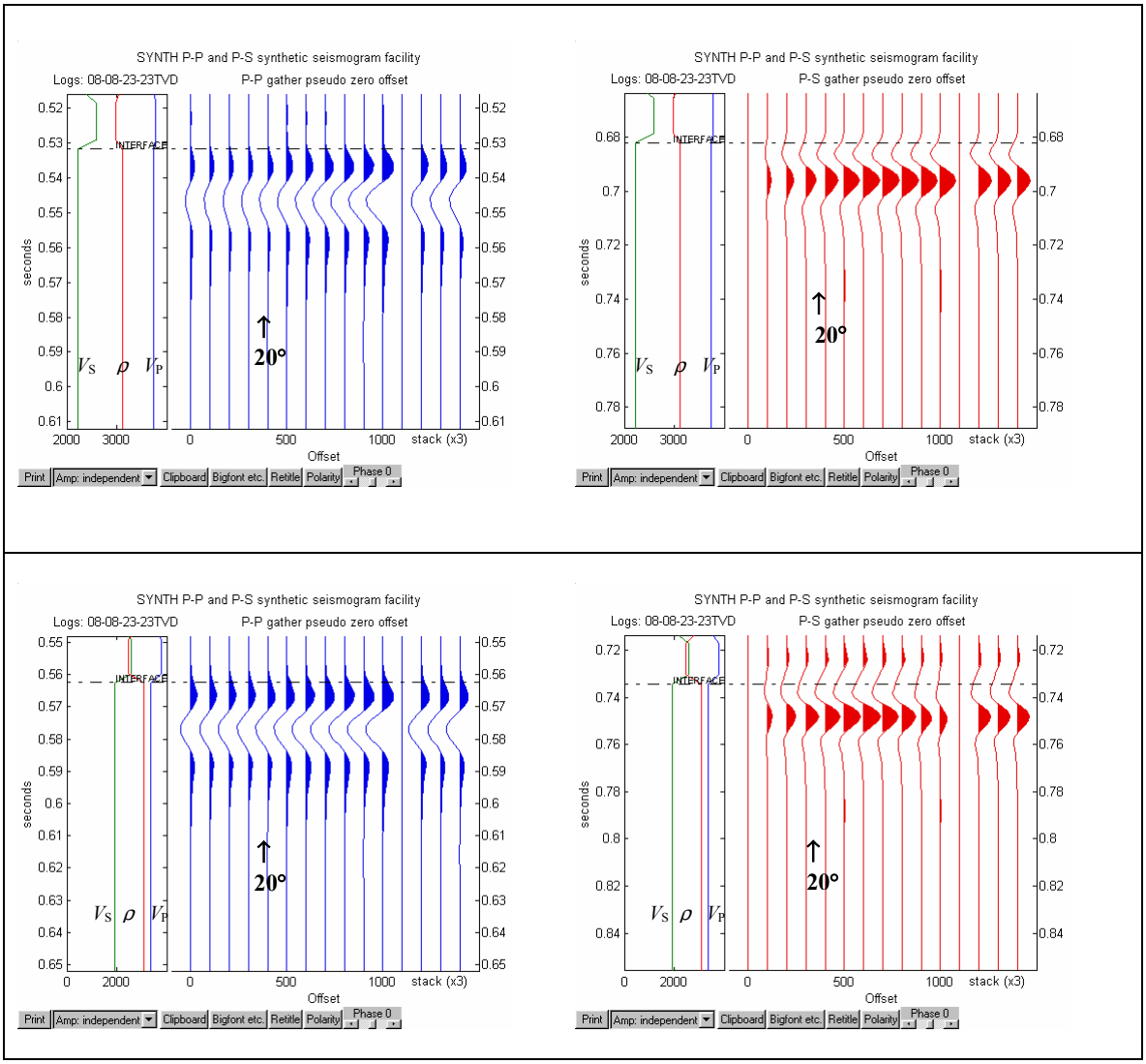

Figure 3. 9. AVO responses and synthetic stacks for two combinations of elastic parameters (Table 3.4) of the gas-sandstone over gas-limestone model buried at a depth of 1000 m. The model assumes a two-layer half-space.

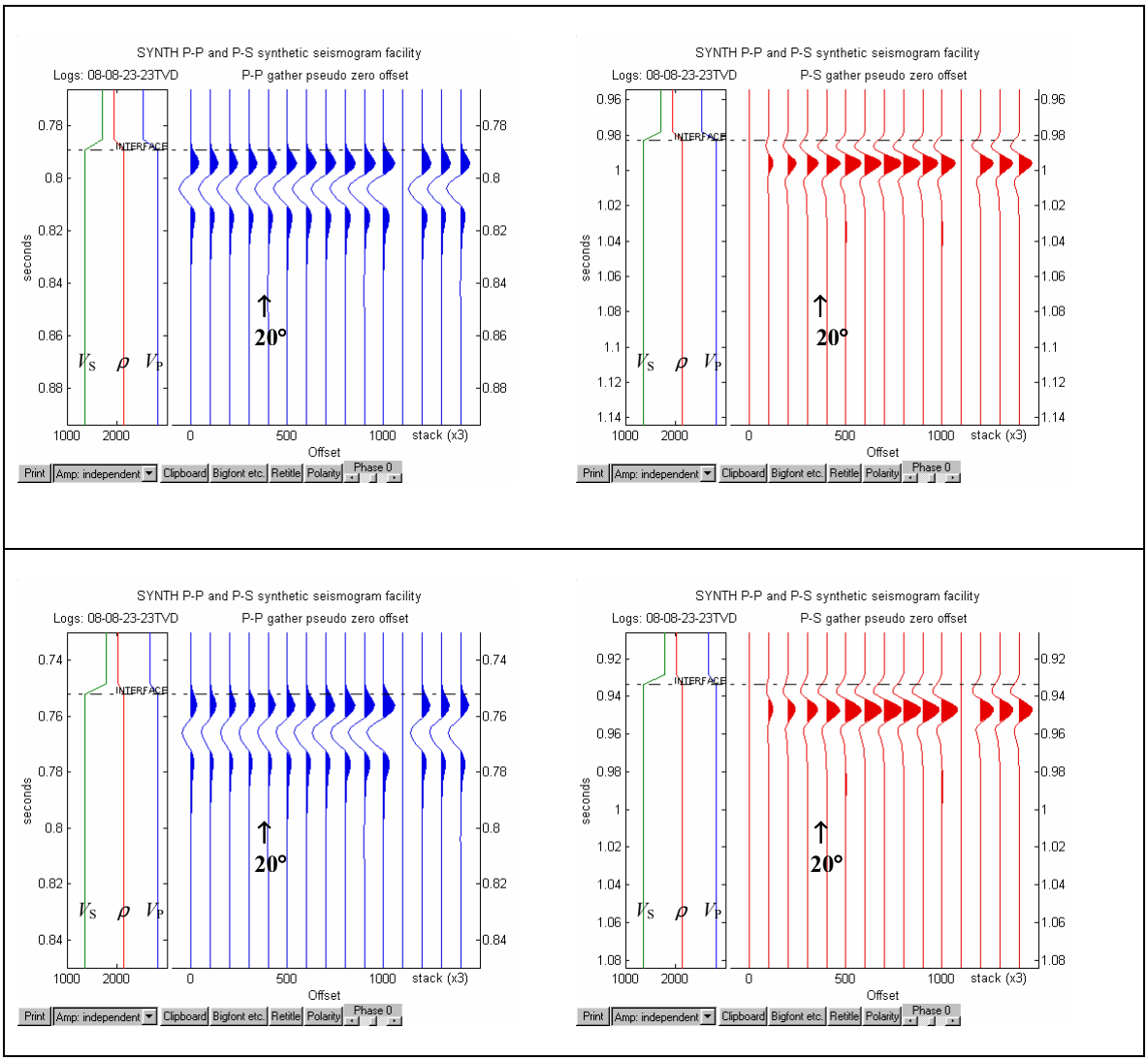

Figure 3.10. AVO responses and synthetic stacks for two combinations of elastic parameters (Table 3.4) of the gas-sand over gas-limestone model buried at a depth of 1000 m. The model assumes a two-layer half-space.

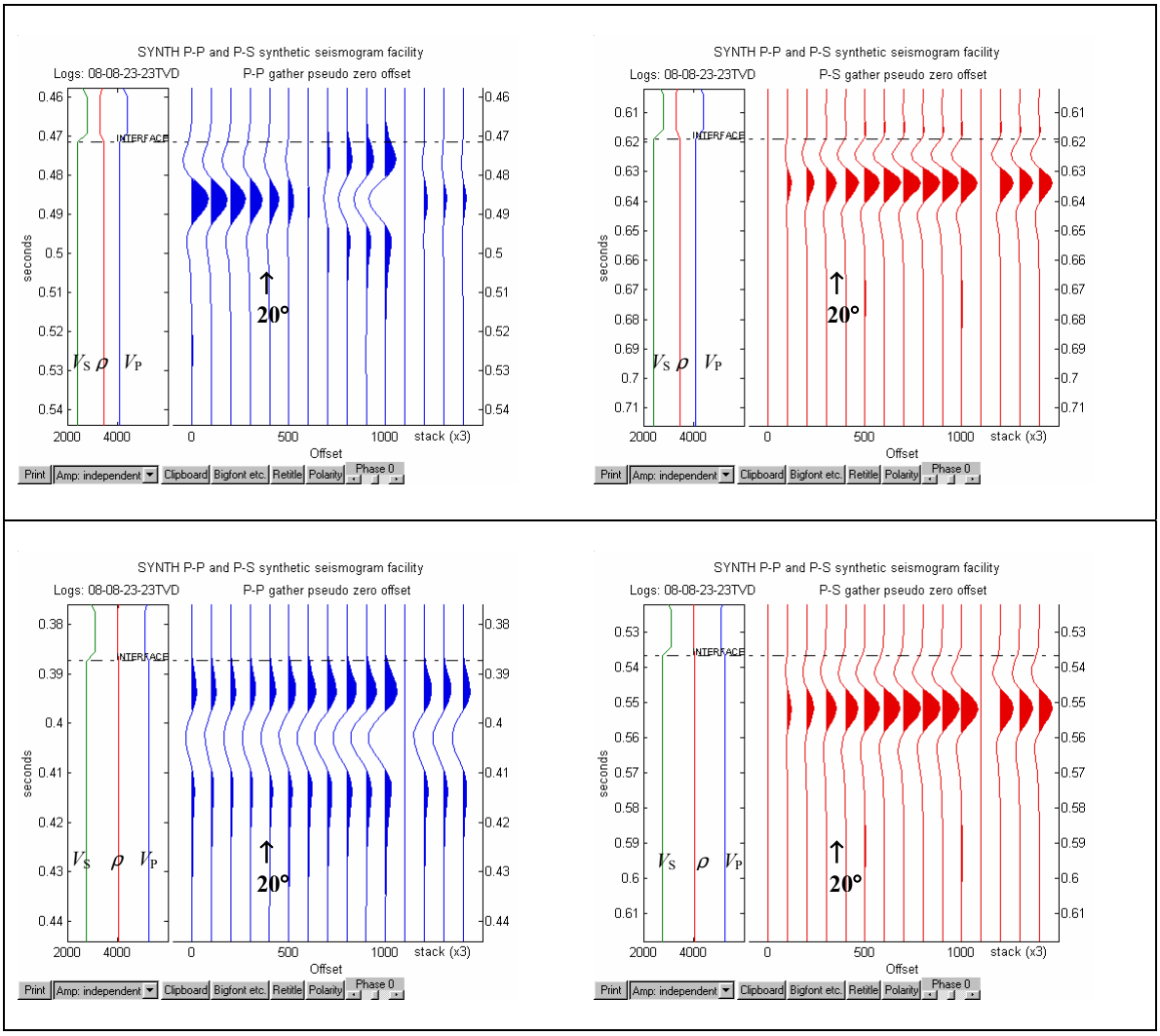

Figure 3.11. AVO responses and synthetic stacks for two combinations of elastic parameters (Table 3.4) of the water-saturated-sandstone over chalk model buried at a depth of 1000 m.

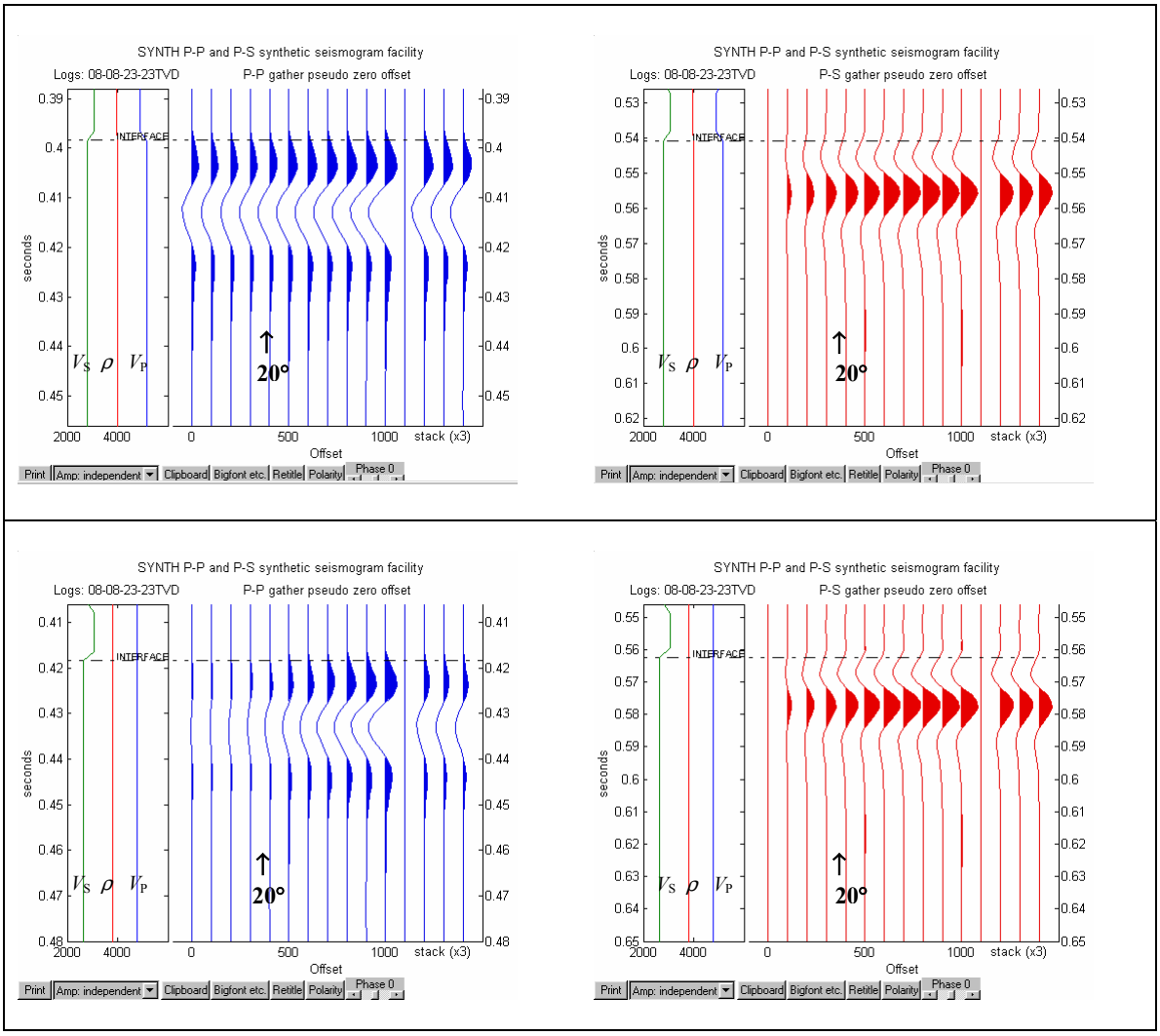

Figure 3.12. AVO responses and synthetic stacks for two combinations of elastic parameters (Table 3.4) of the water-saturated-sandstone over water-saturated-dolomite model buried at a depth of 1000 m.

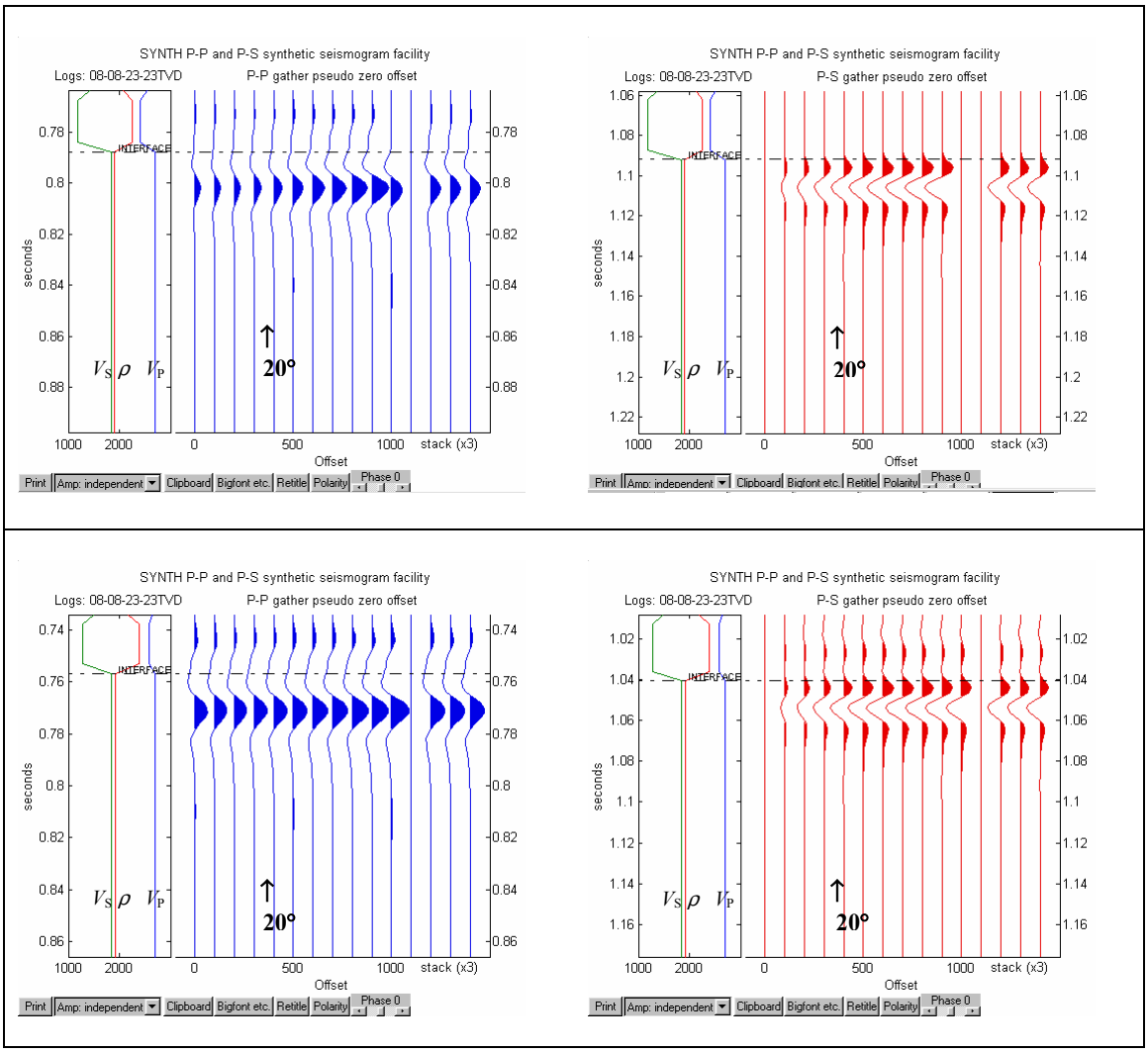

Figure 3.13. AVO responses and synthetic stacks for two combinations of elastic parameters (Table 3.4) of the water-saturated-sand over coal model buried at a depth of 1000 m.

Next I will concentrate on delineating a set of conditions for which the unusual polarity situation appears. To my knowledge, the first published analysis of the unusual polarity situation was made by Brown et al. (2002). They suggest that this exception is usually associated with parameter reversals across the interface, meaning that the three rock

parameters (the two velocities and the density) do not all change in the same direction across the interface; for example, when both velocities increase and the density decreases across the interface, etc.

In contrast, the normal situation would appear when all three parameters change in the same direction. Indeed, if we analyze the well logs that are plotted in the left part of each synthetic gather, we observe that the same rule applies to our interface examples.

Another pertinent observation is that in almost all situations from Appendix B (except for the gas-limestone over gas-dolomite and gas-sand over gas–limestone and gas–dolomite) if there are points in the quadrants III and I they appear in the vicinity of the origin and they don't deviate from the general trend of the plot. In these cases, both the P-P and P-S reflection coefficients are fairly small, not exceeding the maximum limit of 0.2. As we will show next, the small reflection coefficients are, as expected, associated with small changes in rock properties across the interface.

3.5.3 *Statistical analysis of the data used in modelling*

Since our examples only cover a part of the pool of situations presented in Appendix B, I tried to find out if the rules delineated by Brown et al. (2002) are truly universal. Thus, I picked all the situations where the plots have a significant number of points in quadrants I or III and I ran a statistical analysis of the reflection coefficients and the corresponding change in elastic properties.

Table 3.5 below presents the statistical analysis performed on 36 interface types that can produce a significant number of P-P and P-S reflection coefficients of the same sign.

As mentioned before, each point on the plots represents a unique combination of elastic parameters for the two rocks that form the interface. For each plot, I calculated the

maximum variation of V_P, V_S and ρ across the interface, only for the cases when $R_{PP}/R_{PS} > 0$ (the points that fall into quadrants I or III).

Except for the three interface cases mentioned above (for which some rock parameters produce complex R_{PP} values), the parameter variation across the interface is fairly small.

Here is a summary of the variation of the elastic parameters across the studied interface models:

- Max ΔV_P values range between 6.8 % and 25.8%, with an average of 11.3%
- Max ΔV_S values range between 1.5 % and 38.7%, with an average of 18.7%
- Max $\Delta\rho$ values range between 5.5 % and 31.9%, with an average of 12.4%

The numbers above show that the unusual polarity situation coincides with fairly small variations of the elastic parameter across the interface.

In order to prove the second condition (stated by Brown et al., 2002), for each case when $R_{PP}/R_{PS} > 0$ I investigated if the condition of elastic-parameter reversal across the interface is also met. They match perfectly: each unusual polarity point on the plots corresponds to a reversal of the elastic-parameter across the interface.

I also investigated if the elastic-parameter reversal also appears in cases when $R_{PP}/R_{PS} < 0$. It does. For most interface types there are a few situations in which the normal situation is associated with parameter reversals.

Table 3.5. Statistical analysis of the reflection coefficients and the variation of elastic properties across the interface, for all interface types that show cases of $R_{PP}/R_{PS} > 0$

Interface	SS-WS				SS-DR		S-DR		S-WS		SS-TG-WS		
	SH-WS	DO-WS	HALITE	CHALK	SH-DR	LS-DR	LS-DR	DO-DR	COAL	CHALK	SH-TG	SH-WS	HA
ΔV_P max. (%)	7.8	8.1	12.0	8.8	10.7	13.1	10.0	21.5	16.4	8.6	6.8	9.1	10.2
ΔV_S max. (%)	12.5	17.1	17.6	15.6	19.9	38.7	24.0	37.9	36.5	19.8	10.7	20.7	1.5
$\Delta\rho$ max. (%)	9.7	5.5	12.1	6.5	11.7	20.1	8.8	31.9	31.5	6.8	7.1	7.3	10.7
$R_{PP}/R_{PS}>0$	3	12	5	12	6	6	2	3	8	10	9	4	5
Parameter reversal count	3	12	5	12	6	6	2	3	8	10	9	3	5
$R_{PP}/R_{PS}<0$	27	38	25	128	18	30	34	45	46	74	31	20	19
Parameter reversal count	13	17	12	15	15	7	3	9	26	17	14	2	7

Interface	SH-TG	SH-WS			SH-DR		SH-OS	LS-DR				DO-DR	
	SS-TG	SS-WS	SS-TG	DO-WS	SS-DR	LS-DR	HALITE	SS-DR	S-DR	SH-DR	DO-DR	S-DR	LS-DR
ΔV_P max. (%)	6.8	7.8	9.1	11.7	10.7	9.0	16.8	11.6	10.0	9.0	25.9	21.5	65.5
ΔV_S max. (%)	9.9	12.5	20.7	5.0	19.9	14.6	11.7	26.2	24.0	14.6	18.3	37.9	64.9
$\Delta\rho$ max. (%)	7.1	9.7	7.3	7.8	11.7	11.4	13.5	20.1	8.8	11.4	25.4	31.9	25.4
$R_{PP}/R_{PS}>0$ - point count	8	3	5	2	6	2	3	5	2	2	5	4	6
Parameter reversal count	8	3	5	2	6	2	3	5	2	2	5	4	6
$R_{PP}/R_{PS}<0$- point count	32	27	19	13	18	22	3	31	34	22	43	44	42
Parameter reversal count	15	13	0	4	15	6	3	8	3	6	19	8	18

Interface	DO-WS		COAL		HALITE			CHALK		
	SS-WS	SH-WS	S-WS	CH-WS	SS-WS	SS-TG	SH-OS	SS-WS	S-WS	COAL
ΔV_P max. (%)	9.7	11.7	16.4	8.4	12.0	10.2	16.8	8.8	8.6	8.4
ΔV_S max. (%)	17.1	5.0	36.5	32.7	17.6	1.5	11.7	15.6	19.8	32.7
$\Delta\rho$ max. (%)	7.0	7.8	20.2	14.3	12.1	10.7	13.5	6.5	6.8	14.3
$R_{PP}/R_{PS}>0$ – point count	13	2	7	14	3	4	3	12	10	14
Parameter reversal count	13	2	7	14	3	4	3	12	10	14
$R_{PP}/R_{PS}<0$- point count	37	13	47	112	27	20	3	128	74	112
Parameter reversal count	16	4	27	18	14	8	3	15	17	18

Another observation can be made vis-à-vis the trend that is observed on all the plots. All the data tend to group diagonally across quadrants II and IV, with some of the points falling into quadrants III and I.

If we look now at the whole data in say, quadrants II and IV (Figure 3), we observe that their R_{PP} varies proportionally with R_{PS}. That is, an increase or decrease of R_{PP} corresponds to the same kind of R_{PS} variation. In contrast, the data in quadrants III and I presents an inverse variation of R_{PP} with R_{PS}.

In conclusion, it can be stated that there is a high probability that sedimentary interfaces across which the elastic parameters change in a small amount and not all in the same direction will produce events that display opposite polarity on the P-P and P-S stacked sections.

3.6 Related interpretation problems

As mentioned in the Introduction, one of the frequent interpretation problems that are associated with the unusual polarity problem is the matching of events on P-P and P-S sections.

Let's take the case of a seismic reflection acquired using the SEG normal polarity standard. If $R_{PP} > 0$ and $R_{PS} > 0$, it will display positive polarity on the P-P section and negative polarity on the P-S section. Provided that one has all the necessary well logs (sonic, shear-wave sonic and density), the calculated synthetic stacks should display an event having the same polarities as the ones on the seismic sections (Figure 3.14, upper part).

The problem arises when shear-wave or full-waveform sonic logs of the survey area are not available. In this case, based on the lithology information available, a constant V_P/V_S ratio is usually chosen. Afterwards, this ratio is modified until the events on the synthetic stack match the events on the section.

By assuming a fixed V_P/V_S ratio across an interface, we assume that both velocities vary in the same direction across the interface. Because in our example V_P increases and V_S decreases across the interface, our assumption leads to an erroneous shear-wave synthetic log. The computed P-S synthetic stack will display an incorrect polarity (Figure 3.14, lower part).

Then, by correlating this biased synthetic stack with the potential seismic section the events are mismatched by half a cycle. Further, it yields an incorrect V_P/V_S ratio for the medium below the interface, in this case an underestimate. This can propagate the polarity problem to the next interface by introducing errors in the elastic properties of its upper medium; also, the lithological interpretation can be biased by errors in velocity.

The same kind of problem can also be triggered by the lack of information on density. Sonic logs are run much more frequently than density logs and in many situations they only cover the target zone of the well. Thus, we face the need to generate a synthetic seismogram or stack without density information.

Although this is may be a less frequently encountered situation, it is worth studying its effects. When the density log is missing, an empirical formula developed by Gardner et al. (1974) and widely known as “Gardner’s rule” (equation 1) is usually used for determining it:

$$\rho = a\alpha^m \tag{3-1}$$

where ρ is the density and α is the velocity; the exponent m and the scalar a are constants determined by fitting a line to a plot of log ρ versus log α.

Gardner et al. recommended m = 0.25 as being a reasonable value which was also used in my study. For the scalar a, I chose to keep the default value of 310 suggested in the SYNTH package.

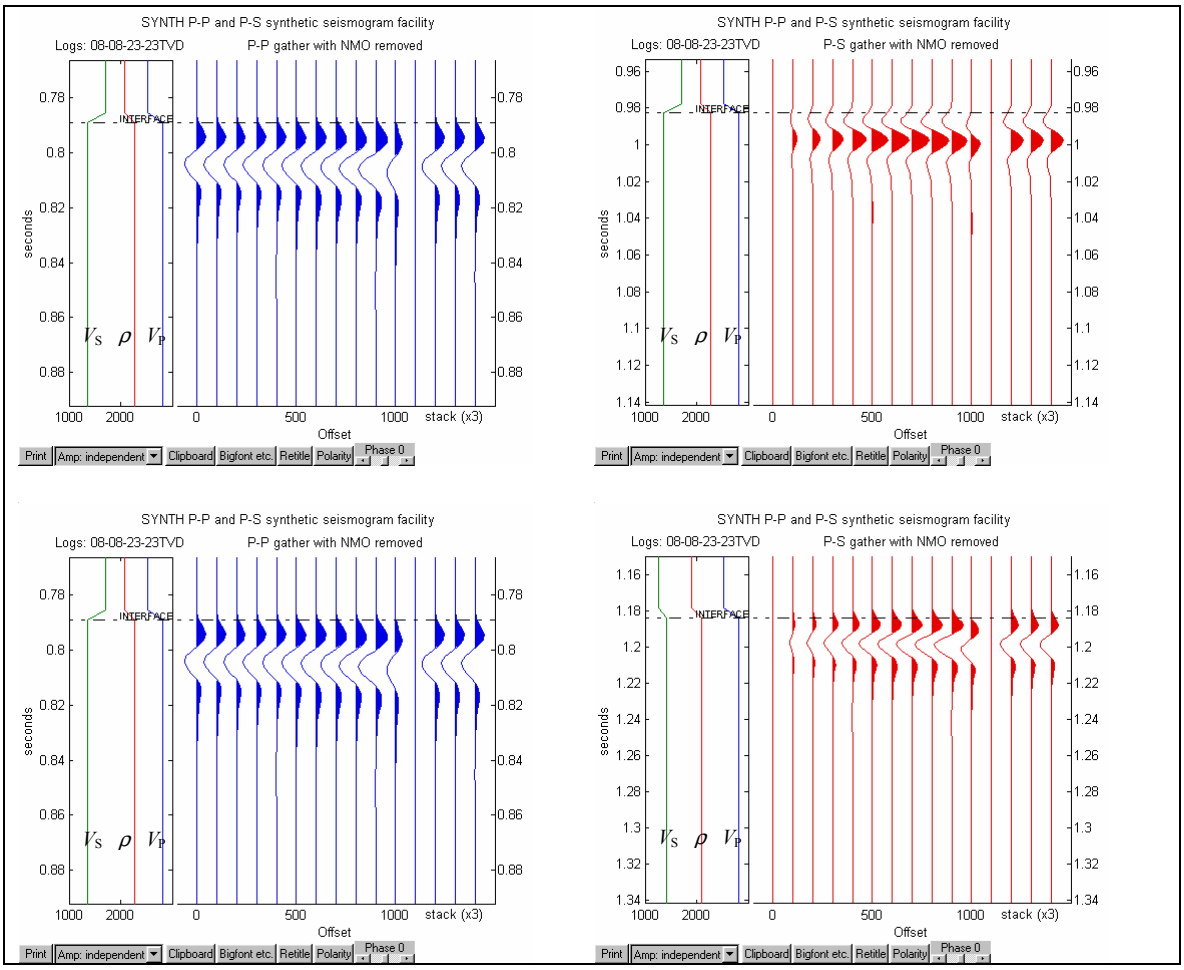

Figure 3.14. AVO responses and synthetic stacks for a water-saturated-sand over coal interface model. All logs were used to create the synthetic stack (above). The usual V_P/V_S ratio of 2 was used to construct a potentially missing shear-wave sonic log (below)

As an example, I chose another water-saturated sand over coal interface. The reason for choosing this interface is that for this rock combination, there is a decrease in both velocities combined with an increase in density across the interface.

The synthetic stacks generated by using all logs display opposite polarities (Figure 3.15, upper part), whereas the stacks obtained with Gardner's rule have the same polarity (Figure 3.15, lower part).

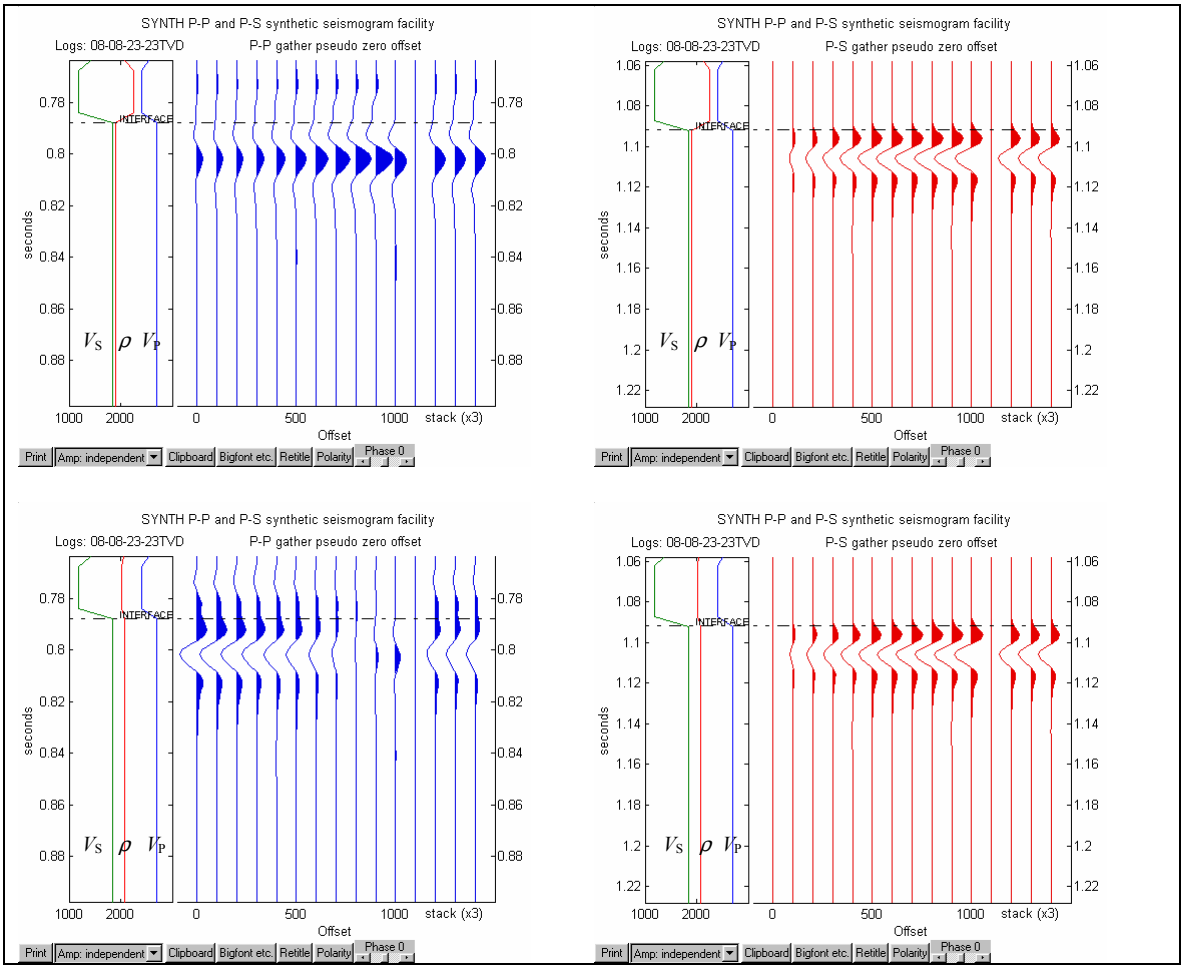

Figure 3.15. AVO responses and synthetic stacks for a water-saturated sand over coal interface model. All logs were used to create the synthetic seismogram (above). Gardner's rule was used for estimating a potentially missing density log (below)

In this example, the lack of density information affects the P-P synthetic stack whose polarity is reversed. The reason for this can be seen on the well log plotted in the left part of each stack image. Gardner's rule produces a density log (middle) that varies in the same way as the sonic log (right).

In this section I have shown in what way the lack of velocity and density information can produce miscorrelations. Errors caused by the lack of shear-wave sonic logs can affect the correlation by leading to the wrong polarity on the P-S synthetic stack and section. If the density information is not available, the correlation process can be erroneous for particular interface types due to the wrong polarity on the P-P synthetic stack.

3.7 The variation of reflection coefficients for shallow and deep interfaces

As mentioned earlier, when I chose the input data for the interface-modelling program, one selection criterion was that velocity measurements for a wide range of confining pressures were available. For the completeness of my analysis, I chose to investigate how the depth of burial affects the distribution of reflection coefficients generated by our interface models.

For each interface type, the depth of burial was simulated by using elastic parameters that were measured at confining pressures that correspond to the depths of 500, 1000 and 2000 m. The same 20º angle of incidence was used for all the models and depths studied.

All the models that were investigated show a small variation of the reflection coefficients with depth, the trend of the plots remaining the same. A few examples are shown in Figure 3.16. Although I only show here examples of water-saturated and gas-

saturated interfaces, the observation was also found to be true for all the interface types presented in Table 3.2.

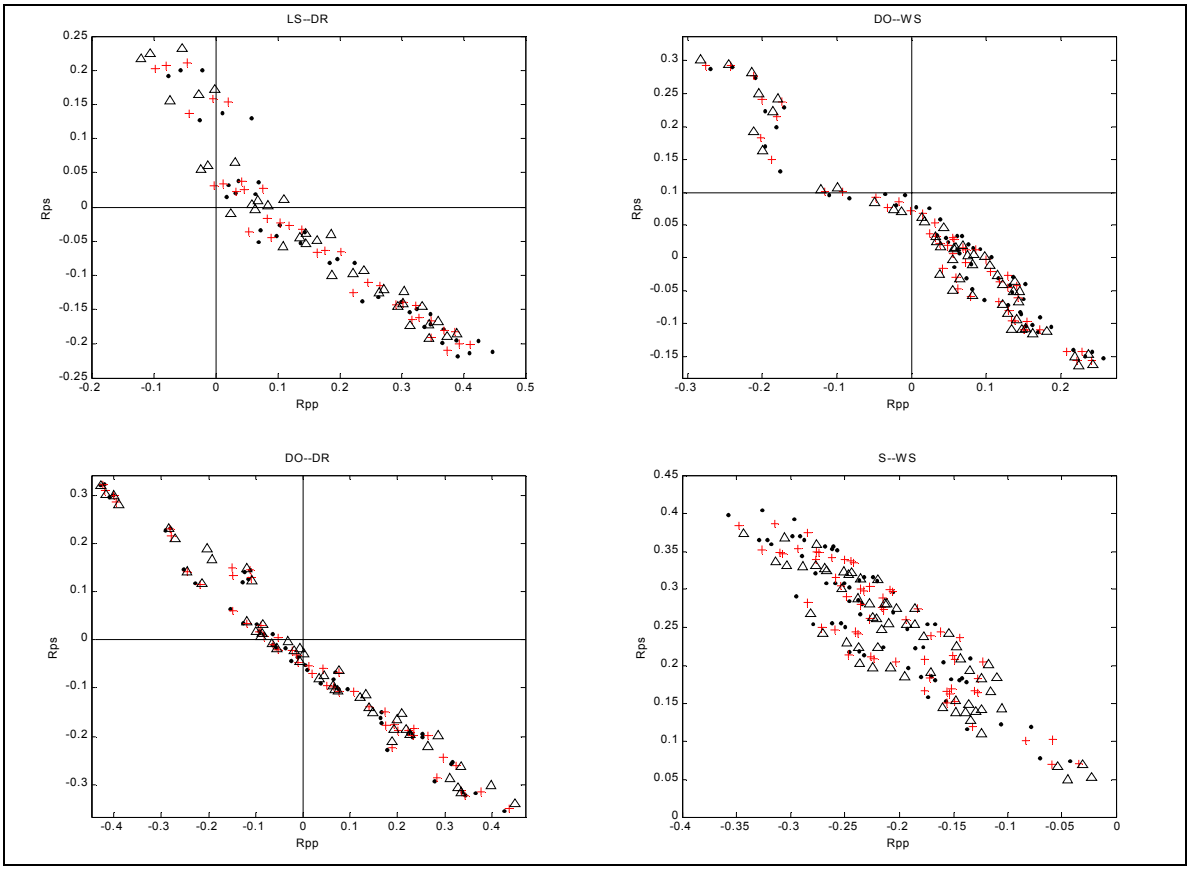

Figure 3.16. R_{PP} vs. R_{PS} plots for the following interfaces: gas sandstone over gas dolomite (upper left), gas limestone over gas dolomite (lower left), water-saturated sandstone over water-saturated dolomite (upper right) and water-saturated sandstone over water-saturated sand (lower right). Black dots represent a depth of 500 m; red plus signs, a depth of 1000 m; and black triangles, a depth of 2000 m.

The effect of interface depth on the reflection coefficients is variable, some showing a slight increase and others a slight decrease. The variation is not significant and we can conclude that although velocity and density values increase slightly with depth, the

conditions for which R_{PP}/R_{PS} >0 remain substantially the same over the depth range considered in our study.

3.8 Delineation of the exact conditions for which $R_{PP}/R_{PS} > 0$

In the Section 3.5 I set down by means of modelling the raw conditions that determine 'the unusual polarity situation'. Apart from this, another important observation was made: all cases when $R_{PP}/R_{PS} > 0$ are associated with small values of R_{PP} and R_{PS}. This remark will also help us extract a more exact set of conditions from the R_{PP} and R_{PS} approximations.

Therefore, we now go back to the approximation for R_{PS} (expression 2-30) derived in Chapter 2. That is:

$$R_{PS} = \frac{-2i_1(\alpha_2\beta_2\rho_2\Delta\rho + 2\rho_1\Delta\mu)}{(\rho_1\alpha_1 + \rho_2\alpha_2)(\rho_1\beta_1 + \rho_2\beta_2)}$$

Small values of R_{PS} can be obtained when, in the numerator of expression above, $\Delta\rho$ and $\Delta\mu$ have opposite signs. In this case, the numerator can become small or even zero, when $\alpha_2\beta_2\rho_2\Delta\rho = -2\rho_1\Delta\mu$; in this particular case $R_{PS} = 0$.

Taking this into consideration, we can write:

R_{PS} is a small quantity when:	$\Delta\rho > 0$ $\Delta\mu < 0$	or	$\Delta\rho < 0$ $\Delta\mu > 0$

We notice that the conditions for change in elastic parameters are the same for both small negative and small positive R_{PS}. These can be rewritten using the formula for $\Delta\mu$ as:

$\Delta\rho > 0$ $\Delta\mu < 0$	$\Rightarrow$	$\rho_2 > \rho_1$ $\rho_2\beta_2^2 < \rho_1\beta_1^2$	$\Rightarrow$	$\rho_2 > \rho_1$ $\beta_2 < \beta_1$
$\Delta\rho < 0$ $\Delta\mu > 0$	$\Rightarrow$	$\rho_2 < \rho_1$ $\rho_2\beta_2^2 > \rho_1\beta_1^2$	$\Rightarrow$	$\rho_2 < \rho_1$ $\beta_2 > \beta_1$

thus:

$R_{PS} > 0$ and R_{PS} small	when	$\alpha_2\beta_2\rho_2\Delta\rho < 2\rho_1\Delta\mu$	and	$\rho_2 > \rho_1,\ \beta_2 < \beta_1$ or $\rho_2 < \rho_1,\ \beta_2 > \beta_1$
$R_{PS} < 0$ and R_{PS} small	when	$\alpha_2\beta_2\rho_2\Delta\rho > 2\rho_1\Delta\mu$	and	$\rho_2 > \rho_1,\ \beta_2 < \beta_1$ or $\rho_2 < \rho_1,\ \beta_2 > \beta_1$

If we apply the same reasoning and assumptions used in the derivation of the R_{PS} approximation (Chapter 2), we can also derive an expression for R_{PP}. By doing so, we obtain the exact same formula as the zero-offset approximation for R_{PP}. That is:

$$R_{PP} = \frac{\rho_2\alpha_2 - \rho_1\alpha_1}{\rho_2\alpha_2 + \rho_1\alpha_1}.$$

This is no surprise, considering that R_{PP} has a very slow variation near zero-offset, when compared to R_{PS}. The conditions for the sign of R_{PP} can now be easily delineated by looking at the numerator of the expression above:

$R_{PP} > 0$ and R_{PP} small	when: $\rho_2\alpha_2 > \rho_1\alpha_1$	$\Rightarrow$	$\rho_2 > \rho_1$ $\alpha_2 < \alpha_1$ $\lvert\Delta\alpha\rvert < \lvert\Delta\rho\rvert$	or	$\rho_2 < \rho_1$ $\alpha_2 > \alpha_1$ $\lvert\Delta\alpha\rvert > \lvert\Delta\rho\rvert$	or	$\rho_2 > \rho_1$ $\alpha_2 > \alpha_1$ $\Delta\alpha, \Delta\rho$ small
$R_{PP} < 0$ and R_{PP} small	when: $\rho_2\alpha_2 < \rho_1\alpha_1$	$\Rightarrow$	$\rho_2 < \rho_1$ $\alpha_2 > \alpha_1$ $\lvert\Delta\alpha\rvert < \lvert\Delta\rho\rvert$	or	$\rho_2 > \rho_1$ $\alpha_2 < \alpha_1$ $\lvert\Delta\alpha\rvert > \lvert\Delta\rho\rvert$	or	$\rho_2 < \rho_1$ $\alpha_2 < \alpha_1$ $\Delta\alpha, \Delta\rho$ small

Then, by combining conditions for the sign of R_{PP} and R_{PS}, the following constraints are obtained for cases when $R_{PP}/R_{PS} > 0$:

$R_{PP} > 0$ and $R_{PS} > 0$	when: $\alpha_2\beta_2\rho_2\Delta\rho < 2\rho_1\Delta\mu$ and	$\rho_2 > \rho_1$ $\alpha_2 < \alpha_1$ $\beta_2 < \beta_1$ $\lvert\Delta\alpha\rvert < \lvert\Delta\rho\rvert$	or $\rho_2 < \rho_1$ $\alpha_2 > \alpha_1$ $\beta_2 > \beta_1$ $\lvert\Delta\alpha\rvert > \lvert\Delta\rho\rvert$	or $\rho_2 > \rho_1$ $\alpha_2 > \alpha_1$ $\beta_2 < \beta_1$ $\Delta\alpha, \Delta\rho$ small
$R_{PP} < 0$ and $R_{PS} < 0$	when: $\alpha_2\beta_2\rho_2\Delta\rho > 2\rho_1\Delta\mu$ and	$\rho_2 < \rho_1$ $\alpha_2 > \alpha_1$ $\beta_2 > \beta_1$ $\lvert\Delta\alpha\rvert < \lvert\Delta\rho\rvert$	or $\rho_2 > \rho_1$ $\alpha_2 < \alpha_1$ $\beta_2 < \beta_1$ $\lvert\Delta\alpha\rvert > \lvert\Delta\rho\rvert$	or $\rho_2 < \rho_1$ $\alpha_2 < \alpha_1$ $\beta_2 > \beta_1$ $\Delta\alpha, \Delta\rho$ small

Hence, the most complete set of conditions was obtained only by combining the outcome of the lithological modelling with the results obtained by approximating the P-P and P-S reflection coefficients. The final results do not differ in essence from the ones obtained through modelling. They merely contain more constraints that are specific only to the unusual polarity situation.

It is clear that, although they complicate the scenario, these extra conditions predict in a more exact manner the situations where polarities of P-P and P-S events don't match.

CHAPTER 4

CONVERTED-WAVE AVO

Amplitude-variations-with-offset (AVO) techniques are widely used as a direct indicator of oil and gas deposits and lithology identification when interpreting the seismic data. This is possible due to the fact that seismic reflection amplitude is directly influenced by the differences in elastic parameters in the media above and below the interface.

AVO can also be used to evaluate elastic rock properties from seismic data. This type of analysis is usually performed on P-wave reflections. Recent developments in ocean-bottom seismic surveying (OBS) made possible the acquisition of high-quality multicomponent data. The use of converted-wave (P-S) data for AVO analysis can give better estimates of S-wave velocities and density contrasts (Jin et al., 2000).

A handful of approximations to the Zoeppritz equations were developed for AVO. Approximations like the one developed by Shuey and published in 1985 for R_{PP} have the merit of expressing the reflection coefficient as a sum of products of trigonometric functions of the angle of incidence and terms that depend only on the elastic properties of the upper and lower medium [Appendix A, equation (A-2)]. Shuey's approximation is usually written as:

$$R_{PP} = A + B\sin^2 i + C\sin^2 i \tan^2 i \qquad (4\text{-}1)$$

where $A = R_0$, $B = \left[A_0 R_0 + \dfrac{\Delta\sigma}{(1-\sigma)^2} \right]$ and $C = \dfrac{1}{2}\dfrac{\Delta\alpha}{\alpha}$.

In Shuey's approximation, the first term is normal-incidence reflection coefficient, the second term characterizes R_{PP} at intermediate angles and the third term characterizes the approach to critical angles.

The coefficients of such an approximation, usually known as AVO attributes, form the basis of different weighted-stacking procedures. Through weighted stacking, the prestack information is reduced to AVO attribute traces versus time. This is carried out by using incidence angles computed for each time sample to perform a regression analysis and solve for the coefficients of an equation such as equation (4-1). The AVO attributes are then plotted on A (intercept) vs. B (gradient) crossplots. In this way we can separate lithologies or pore-fluids according to the position occupied on the crossplot.

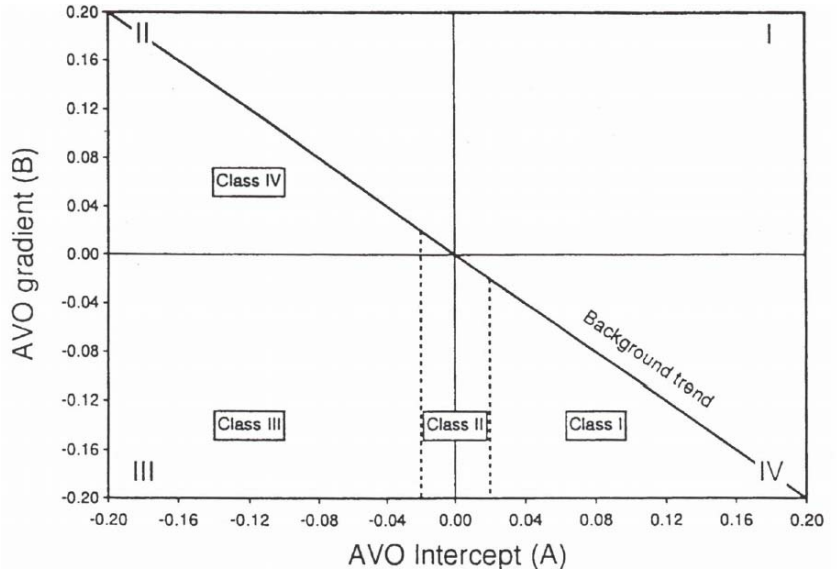

Figure 4.1. Classification of the P-P AVO anomalies: Class I (high impedance contrast sands), Class II (low impedance contrast sands), Class III and IV (low impedance contrast sands) (after Castagna and Swan, 1997).

Although the purpose of deriving the R_{PS} approximation in Chapter 2 was not its use for AVO analysis, its behaviour shown in Figures 2.6 and 2.7 is encouraging and I will show here that with only a minor modification, it becomes a suitable approximation for a wider offset range.

Usually, the AVO attributes obtained from the real data are compared on crossplots with theoretical attributes obtained through modelling for different types of interfaces. In the second part of this chapter I discuss a method that improves the determination of the theoretical AVO attributes. Because development of new AVO methods is not the major focus of this thesis, I will not further pursue more in-depth AVO studies.

4.1 Modifying the previously derived R_{PS} approximation

I begin by rewriting the approximation for R_{PS} obtained in Chapter 2, expression (2-28), as follows:

$$R_{PS} = i_1 \frac{-2(\alpha_2\beta_2\rho_2\Delta\rho + 2\rho_1\Delta\mu)}{(\rho_1\alpha_1 + \rho_2\alpha_2)(\rho_1\beta_1 + \rho_2\beta_2)} \tag{4-2}$$

If we examine the plots in Figure 2.6, we observe that the major drawback of this approximation, when it comes to offsets that are larger than 15º to 25º is that it continues to increase or decrease in a linear manner and does not follow the trend of the exact curve and the other approximations. If we now examine the approximation above, we notice that one of the reasons for this is the fact that it does not contain any trigonometric functions that can modulate its behaviour at larger offsets. Its dependence on the angle of incidence is obviously linear.

If we now, take expression (2-1), which is the exact formula for R_{PS}, we can rewrite it by using $p = \sin i_1 / \alpha_1$, it becomes:

$$R_{PS} = \frac{-2\dfrac{\cos i_1}{\alpha_1}\left(ab + cd\dfrac{\cos i_2}{\alpha_2}\dfrac{\cos j_2}{\beta_2}\right)\alpha_1\dfrac{\sin i_1}{\alpha_1}}{\beta_1 D} \tag{4-3}$$

or

$$R_{PS} = \cos i_1 \sin i_1 \frac{-\dfrac{2}{\alpha_1}\left(ab + cd\dfrac{\cos i_2}{\alpha_2}\dfrac{\cos j_2}{\beta_2}\right)}{\beta_1 D} \tag{4-4}$$

When comparing this exact expression with the approximation for R_{PS}, we notice that factor i_1 in the approximation was obtained by replacing $\sin i_1$ and $\cos i_1$ with their approximate values of i_1 and 1 respectively.

The next step is to try to keep the $\sin i_1$ and $\cos i_1$ factors, but simplify the rest of the formula. One way of doing this is to approach the whole problem differently. If we treat the exact R_{PS} formula as a multiplication of two factors, rather than as a whole, and apply the reasoning used in Chapter 2 only to its second factor, we obtain:

$$R_{PS} = \sin i_1 \cos i_1 \frac{-2(\alpha_2\beta_2\rho_2\Delta\rho + 2\rho_1\Delta\mu)}{(\rho_1\alpha_1 + \rho_2\alpha_2)(\rho_1\beta_1 + \rho_2\beta_2)} \tag{4-5}$$

To show that this new approximation works better than the one previously derived, we use the same three models from Chapter 2 and create plots similar to those from Figures 2.6 and 2.7. Here, only the exact Zoeppritz expression and the Aki-Richards approximation are used for comparison. As in most P-S AVO studies (e.g. Ramos and Castagna, 2001), I will only use incidence angles ranging from 0º to 40º. Plots showing the variation of R_{PS} and the absolute approximation error with the incidence angle are shown in Figure 4.2.

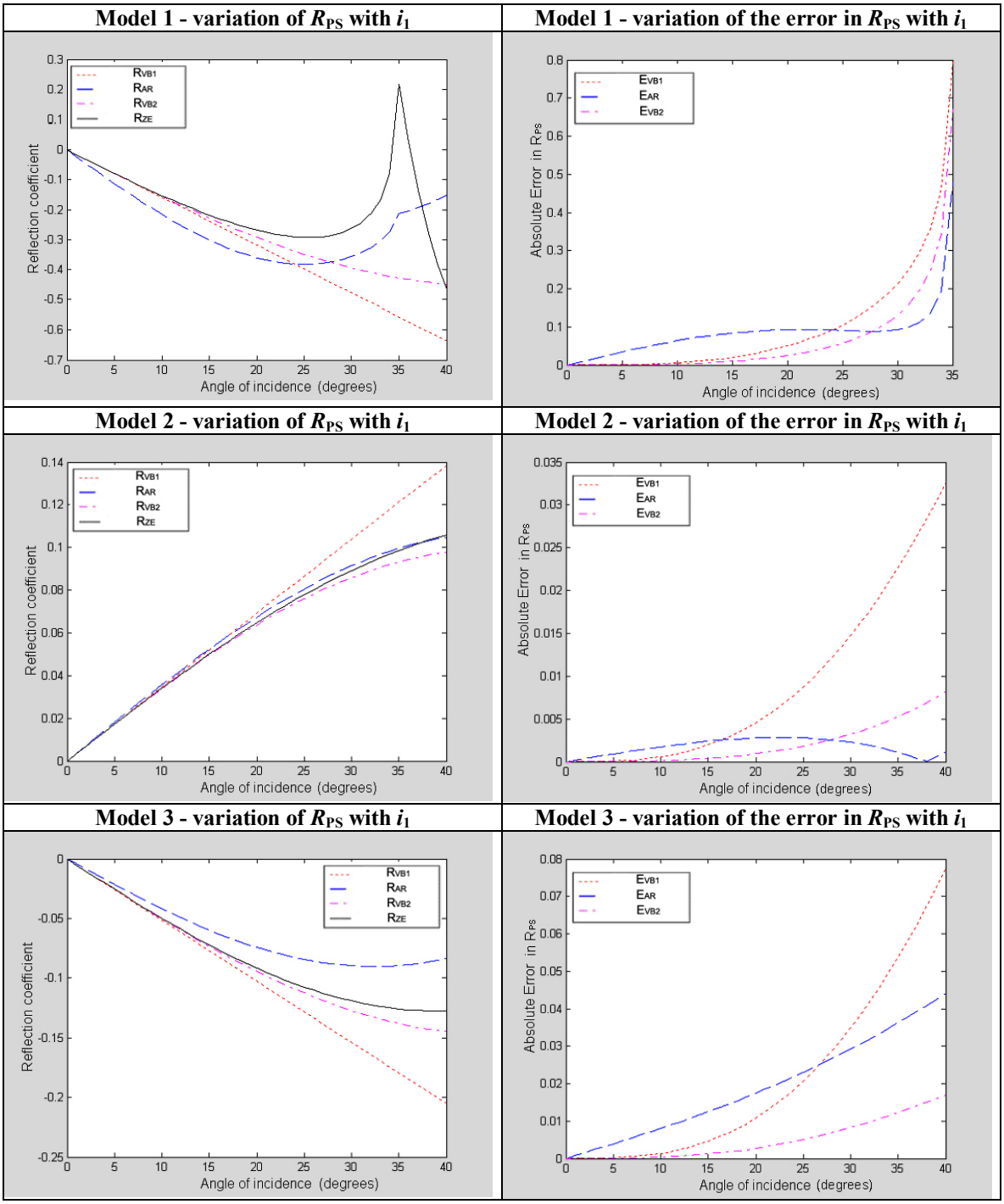

Figure 4.2. Variation of R_{PS} (left) and the absolute error in R_{PS} (right) with the incidence angle; the plotted curves were computed with three approximations: Aki and Richards (1980) (R_{AR}) and my two approximations (R_{VB1}, R_{VB2}). The curves were plotted for all three models from Table 2.1.

From the testing done so far, the new approximation has batter results at greater angles of incidence and seems suitable to be used for AVO, although, further testing may be needed. The plots show a very improved variation with offset of the P-S reflection coefficient. The new approximation works better than the Aki-Richards approximation on the models used here, at least for angles of incidence up to 30º to 40º.

The new formula developed here can be used for one-term converted-wave AVO when dealing with larger changes in elastic properties across an interface, case for which the Aki-Richards approximation was not designed.

4.2 A better determination of the theoretical AVO attributes

In this section, I will show that, by using approximations for the reflection coefficients together with the exact Zoeppritz equations, we can obtain improved theoretical values for the AVO attributes. For AVO, these coefficients are usually referred to as 'gradient' and 'intercept' in P-P AVO and 'gradient' and 'curvature' in P-S AVO.

As shown in Chapter 2, in the last twenty years, many approximations for both the P-P and P-S reflection coefficients have been developed. The most recent trend (Foster et al., 1997) is to express R_{PP} and R_{PS} as a series expansion of either the exact Zoeppritz formulae or of the Aki-Richards approximations and to keep only the first two or three terms of the expansion, depending on the required degree of accuracy; that is:

$$R_{PP} = A + B\sin^2 i + C\sin^4 i + \ldots \tag{4-6}$$

and

$$R_{PS} = \hat{A}\sin i + \hat{B}\sin^3 i + \hat{C}\sin^5 i \tag{4-7}$$

where *A, B, C,* $\hat{A}, \hat{B}, \hat{C}$ are terms that depend only on the elastic properties of the two media and *i* is the angle of incidence.

Because two-term approximations are the most widely used in industry, I will also stick to these. For computing the P-P AVO attributes *A* and *B*, I will use the expressions of Foster et al. (1997) and for their P-S counterparts, $\hat{A}$ and $\hat{B}$ the expressions of Ramos and Castagna (2001), from which:

$$A = \frac{\Delta\alpha}{2\alpha} + \frac{\Delta\rho}{2\rho} \qquad B = \frac{\Delta\alpha}{2\alpha} - 4\frac{\beta^2}{\alpha^2}\left(\frac{\Delta\rho}{2\rho} + \frac{\Delta\beta}{\beta}\right) \tag{4-8}$$

and

$$\hat{A} = \left(-2\frac{\beta}{\alpha}\frac{\Delta\beta}{\beta}\right) - \left[\left(\frac{1}{2} + \frac{\beta}{\alpha}\right)\frac{\Delta\rho}{\rho}\right]; \quad \hat{B} = \left[\left(\frac{2\beta^2}{\alpha^2} + \frac{\beta}{\alpha}\right)\frac{\Delta\beta}{\beta}\right] + \left[\left(\frac{3}{4}\frac{\beta^2}{\alpha^2} + \frac{\beta}{2\alpha}\right)\frac{\Delta\rho}{\rho}\right] \tag{4-9}$$

For any particular situation when the elastic parameters of the media that form an interface are known, we can use a system of equations to solve for *A* and *B* or $\hat{A}$ and $\hat{B}$:

$$\begin{bmatrix} A \\ B \end{bmatrix} = \begin{bmatrix} 1 & \sin^2 i_1 \\ 1 & \sin^2 i_2 \end{bmatrix}^{-1} \begin{bmatrix} R_{PP}(i_1) \\ R_{PP}(i_2) \end{bmatrix} \tag{4-10}$$

and

$$\begin{bmatrix} \hat{A} \\ \hat{B} \end{bmatrix} = \begin{bmatrix} \sin i_1 & \sin^3 i_1 \\ \sin i_2 & \sin^3 i_2 \end{bmatrix}^{-1} \begin{bmatrix} R_{PS}(i_1) \\ R_{PS}(i_2) \end{bmatrix} \tag{4-11}$$

where i_1 and i_2 are two angles of incidence within our range of interest and $R_{PP}(i_1)$ and $R_{PP}(i_2)$ are the corresponding reflection coefficients, computed using the Zoeppritz equations.

Using as an example the interface from model 2 defined in Chapter 2, Section 2.3, I now create plots that prove that this method improves the accuracy of the P-P intercept and gradient terms as well as the P-S gradient and curvature and thus, of the approximation. Plots in Figure 4.2 show that by using the improved values of A, B, $\hat{A}$ and $\hat{B}$ we obtain better approximations (R_{FK2} and R_{RC2}) to the exact reflection coefficient (R_{ZE}).

In order to compute the intercept, gradient and curvature terms from equations (4–10) and (4–11), I had to pick the two incidence angles for each model. For models 2 and 3, I used incidence angles of 10º and 40º. In the case of model 1, where the change in R_{PP} and R_{PS} with offset is very sudden, I used incidence angles of 10º and 25º for the P-P case and 10º and 30º for the P-S case. By choosing the two angles of incidence close to the margins of the range of angles we are interested in, we obtain a better fit between the exact curve and the approximation.

Crossplots of A vs. B and $\hat{A}$ vs. $\hat{B}$ were also produced and are shown in Figure 4.3. The shale-over-brine-sand and shale-over-gas-sand interface models used in the plots (Table 4.1) come from Castagna and Smith (1994), where were also used for AVO studies.

Table 4.1. Values of elastic parameters for 12 sets of shales, brine-sands and gas-sands (from Castagna and Smith, 1994)

	Shale			Brine sand			Gas sand		
Model	**V_P (m/s)**	**V_S (m/s)**	**ρ (kg/m^3)**	**V_P (m/s)**	**V_S (m/s)**	**ρ (kg/m^3)**	**V_P (m/s)**	**V_S (m/s)**	**ρ (kg/m^3)**
1	3270	1650	2200	3280	1680	2190	3040	1740	2050
2	4690	2610	2490	4060	2030	2400	3700	2060	2260
3	2770	1520	2290	3850	2240	2240	3080	2340	2140
4	4060	2180	2580	4060	2340	2300	3620	2580	2300
5	3050	1690	2340	3210	1790	2220	2910	1850	2010
6	3210	1600	2390	4550	2610	2440	3960	2800	2410
7	2770	1270	2450	3050	1560	2400	2690	1590	2250
8	2770	1450	2670	3420	1780	2530	3390	1790	2500
9	2310	850	2180	2520	900	2110	1580	940	1940
10	2750	1260	2430	3440	1940	2520	3190	1980	2450
11	3510	1850	2460	3550	1540	2380	3470	1750	2210
12	3600	1850	2630	5030	3320	2610	4910	3300	2590

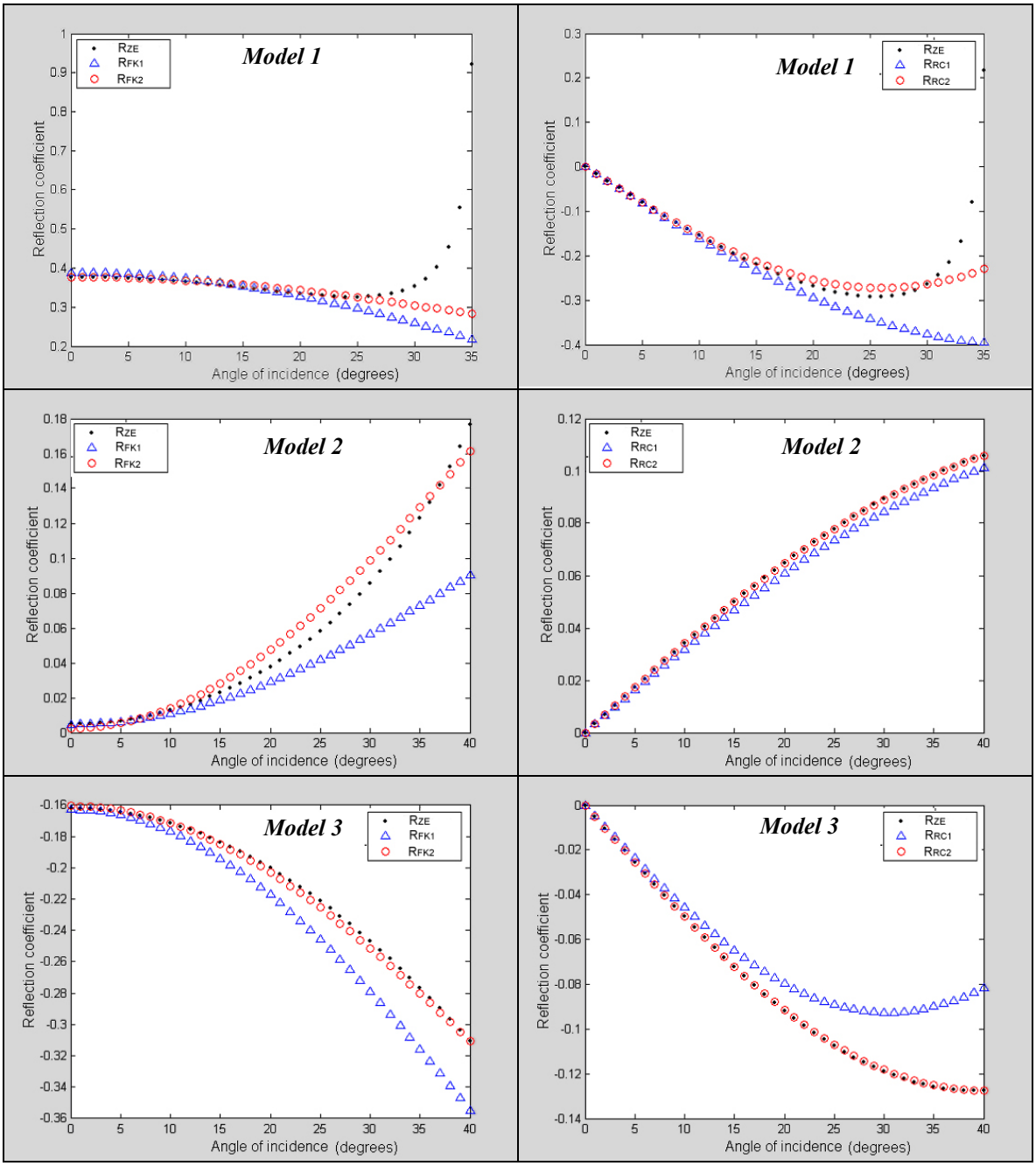

Figure 4.3. Variation of R_{PP} (left) and R_{PS} (right) with the incidence angle; the curves correspond to the exact Zoeppritz equations (R_{ZE}) and the approximations of Foster et al. (R_{FK}) and Ramos and Castagna (R_{RC}), respectively. The curve represented by circles denotes values of R_{PP} and R_{PS} obtained by using the newly calculated A, B, $\hat{A}$ and $\hat{B}$ coefficients. The graphs were plotted for all three models from Table 2.1

The plots in Figure 4.3 show that the new gradient and intercept and their corresponding trend lines differ slightly from the ones obtained by using the approximations. These new trend lines characterize more exactly the geological models used here and may be used in conjunction with real-data attributes to facilitate discrimination between different lithologies or pore fluids.

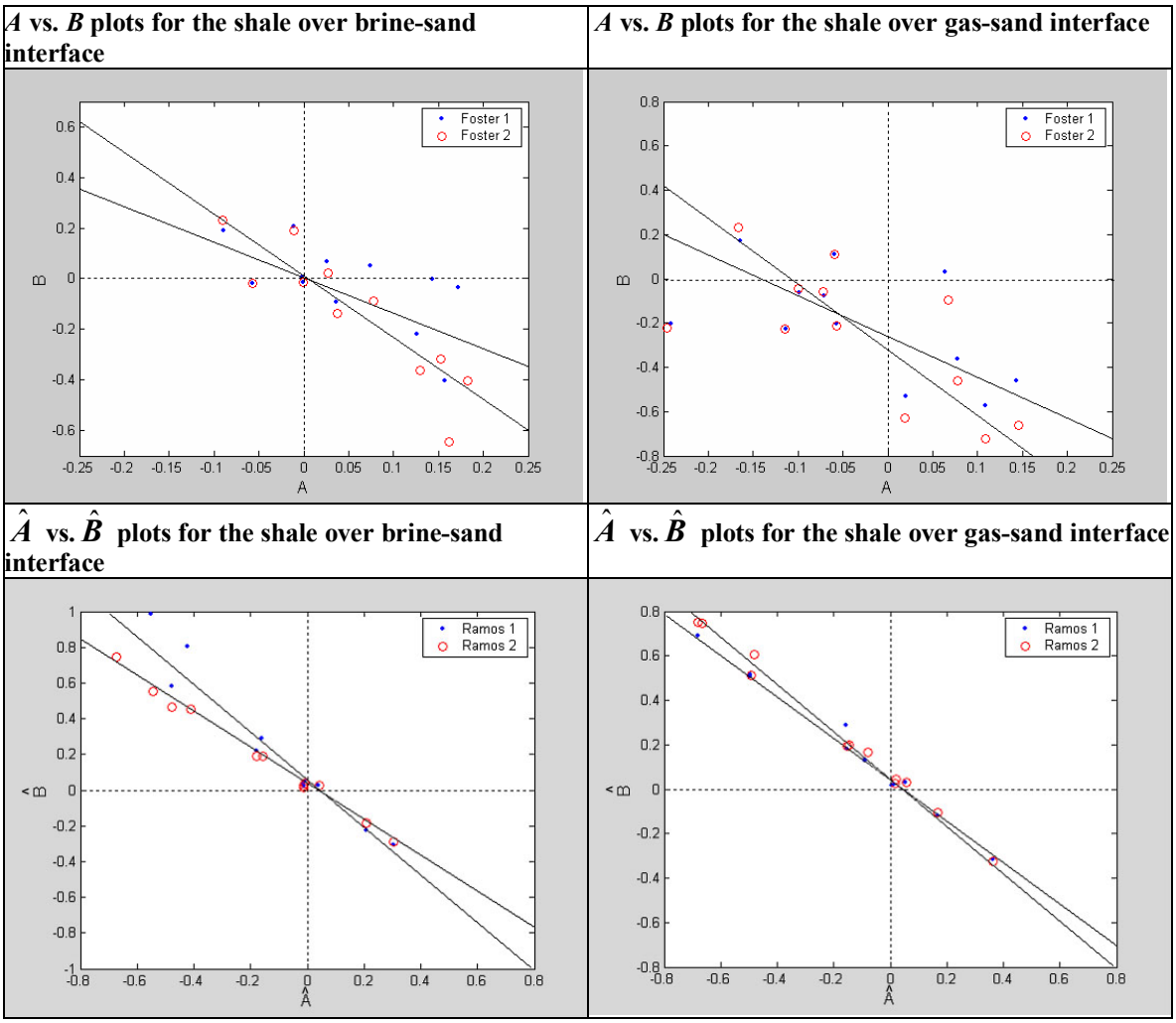

Figure 4.4. A vs. B and $\hat{A}$ vs. $\hat{B}$ plots for shale-over-brine-sand and shale-over-gas-sand interfaces presented in Table 2.1; dots represent values computed with approximations by Foster et al. (1997) and Ramos and Castagna (2001); circles represent the improved values, computed with the same approximations via the method proposed here; trend lines for each set of AVO coefficients are also shown.

In the shale-over-gas-sand plot we observe that the trend lines do not pass through the origin. This is due to the sparse sampling of the interface.

I can conclude that the method presented here produces values of the P-P gradient and intercept and P-S gradient and curvature that represent more accurately the interface models that are used.

The new method can be used in conjunction with any expression that approximates R_{PP} and R_{PS} by a sum of products of trigonometric functions of the incidence angle and terms that depend only on the elastic parameters α, β, and ρ. Some examples are approximations developed by Shuey (1985) and by me [expression (4-4)].

For more exact solutions, over-determined systems of equations can be formed by using more than two angles of incidence. The same method can also be used in conjunction with three-term approximations of the reflection coefficients.

More in-depth studies on this subject will be the subject of my future research.

CHAPTER 5

CONCLUSIONS

The new expression for R_{PS} developed in Chapter 2 was tested for three interface models and was proven to be a very accurate approximation for small angles of incidence (near-zero offsets). Therefore, I am confident that the conditions derived from it are sufficiently accurate for most purposes.

The interface modelling using real velocity and density data carried out throughout Chapter 3 has led me to the following conclusions:

- At least for the geological situations covered by the models, the unusual polarity situation was found to be associated with cases in which not all the rock parameters change in the same direction (i.e. P and S velocities change in opposite direction or density changes in the opposite direction than both velocities) across the interface.
- In these cases, the changes in elastic parameters are relatively small across the interface and the reflection coefficients are also relatively small when compared to their theoretical range.
- Because changes in parameters are small, the use of a Shuey-type approximation to the Zoeppritz equations can also be used to create the synthetic stacks used in interpretation.
- Although there are exceptions, for most of the models, the pseudo-zero-offset gathers show that apparent event polarity is generally uniform with offset for an offset-to-depth ratio up to 1 at a depth of 1000 m.

- Variation of the elastic parameters with depth does not impact significantly on the reflection coefficients and, although they show a slight variation with depth, the conditions delineated above remain valid.
- By combining the results obtained through modelling with conditions obtained from the R_{PS} and R_{PP} approximations, I have defined a more precise set of conditions that characterize the unusual polarity situation

To avoid miscorrelations between events on the P-P and P-S sections due to the 'unusual polarity situation', I propose the following approach:

If sonic, shear-wave and density logs are available, it may still be difficult to visually identify events with opposite polarities on the P-P and P-S synthetic seismograms or stacks, due to the abundance of events that often interfere. I propose that, in addition to generating synthetic seismograms, we should also verify the conditions delineated in Chapter 3 using the three well logs and flag the depth intervals where opposite polarities are likely.

If one of the well-logs is not available, extra attention should be paid in the correlation process to the possibility of negative polarity correlation.

In Chapter 4, I have shown that, with only a slight modification, the R_{PS} approximation derived in Chapter 2 becomes more accurate at larger offsets and is suitable for one-term P-S AVO, especially in cases where elastic parameters have a large variation. In the same chapter I also proposed a method of obtaining better theoretical values for the P-P intercept and gradient and the P-S gradient and curvature terms used in AVO. This method can be useful when comparing theoretical models and crossplots to real data.

REFERENCES

Aki, K. and Richards, P.G., 1980, Quantitative seismology: Theory and Methods: W.H. Freeman and Co.

Bale, R. A., 2003, Personal communication.

Blangy, J.D., 1992, Integrated seismic lithologic interpretation: the petrophysical basis: Ph.D. thesis, Stanford University.

Bonner, B. P. and Schock, R. N., 1989, Seismic wave velocity, *in* Touloukian, Y. S., Judd, W. R. and Roy, R. F., Eds., Physical properties of rocks and minerals: McGraw-Hill Book Co.

Bortfeld, R., 1961, Approximation to the reflection and transmission coefficients of plane longitudinal and transverse waves: Geophys. Prosp., **9**, 485-503.

Brown, R. J., Stewart, R. R. and Lawton, D. C., 2002, A proposed polarity standard for multicomponent seismic data: Geophysics, **67**, 1028-1037.

Brevik, I. (Statoil), 2002, Personal communication.

Castagna, J. P., Batzle, M. L., and Eastwood, R. L., 1985, Relationships between compressional-wave and shear-wave velocities in clastic silicate rocks: Geophysics, **50**, 571-581.

Castagna, J. P., Swan, H. W., 1997, Principles of AVO crossplotting: The Leading Edge, **16**, 337-342.

Colorado School of Mines, 2003, The common ground internet database: http://commonground.mines.edu/

Foster, D. J., Keys, R.G. and Schmitt, D. P., 1997, Detecting subsurface hydrocarbons with elastic wavefields, *in* Inverse problems in wave propagation, Volume 90 of The IMA Volumes in Mathematics and its Applications: Springer

Gardner, G. H. F., Gardner, L.W. and Gregory, A. R., 1974, Formation velocity and density: The diagnostic basis of stratigraphic traps: Geophysics, **39**, 770-780.

Han, D., 1986, Effects of porosity and clay content on acoustic properties of sandstones and unconsolidated sediments: Ph.D. thesis, Stanford University.

Jin, S., Cambois G. and Vuillermoz, C., 2000, Shear wave velocity and density estimations from PS-wave AVO analysis: Application to an OBS dataset from the North Sea: Geophysics, **65**, 1446-1454.

Jizba, D. L., 1991, Mechanical and acoustical properties of sandstones and shales: Ph.D. thesis, Stanford University.

Knott. C. G., 1899, Reflexion and refraction of elastic waves with seismological applications: Phil. Mag., 48, 64-97.

Landrum, R. A., Brook, R. A., and Sallas, J. J., 1994, Polarity convention for vibratory source/recording systems: Geophysics, **59**, 315-322.

Lawton, D. C. and Howell, C. E., 1992, P-SV and P-P synthetic stacks: 62nd Ann. Internat. Mtg., Soc. Expl. Geophys., Expanded Abstracts, 1344-1347.

Margrave, G. F., Stewart, R. R. and Larsen, J. A., 2001, Joint PP and PS seismic inversion: The Leading Edge, **20**, 1048-1052.

Mavko, G., Mukerji, T. and Dvorkin, J., 1998, The rock physics handbook: Tools for seismic analysis in porous media: Cambridge Univ. Press.

Miller, S. L. M., 1996 Multicomponent seismic data interpretation: M.Sc. thesis, Univ. of Calgary.

Pickett, G. R., 1963, Acoustic character logs and their applications in formation evaluation: J. Petr. Tech., **15**, 650-667

Prasad, M., 2002, Acoustic measurements in unconsolidated sands at low effective pressure and overpressure detection: Geophysics, **67**, 405-412.

Ramos, A. C. B. and Castagna, J. P., 2001, Useful approximations for converted-wave AVO: Geophysics, **66**, 1721-1734

Sheriff, R.E., 2002, Encyclopedic dictionary of exploration geophysics, 4th ed.: Geophysical References Series, **13**, Soc. Expl. Geophysics.

Shuey, R.T., 1985, A simplification of the Zoeppritz equations: Geophysics, **50**, 609-614.

Thigpen, B.B., Dalby, A.E. and Landrum, R., 1975, Special report of the subcommittee on polarity standards: Geophysics, **40**, 694-699.

Zheng, X., 1991, Approximations to P-P, P-SV, SV-SV and SV-P reflections and transmissions: 61st Ann. internat. Mtg., Soc. Expl. Geophysics, Expanded Abstracts, 1102-1105.

Wang, Y., 1999, Approximations to the Zoeppritz equations and their use in AVO analysis: Geophysics, **64**, 1920-1927.

Zoeppritz, K., 1919, Erdbebenwellen VIIIB, On the reflection and propagation of the seismic waves: Göttinger Nachrichten, I, 66-84.

APPENDIX A

APPROXIMATIONS TO THE ZOEPPRITZ EQUATIONS

The Aki – Richards (1980) approximation of the P-S reflection coefficient

Assumptions and approximations:

$\frac{\Delta\alpha}{\alpha}, \frac{\Delta\beta}{\beta}, \frac{\Delta\rho}{\rho} << 1$;	$\Delta i = i_2 - i_1 \approx \tan i \left(\frac{\Delta\alpha}{\alpha} \right)$	$\Delta j = j_2 - j_1 \approx \tan j \left(\frac{\Delta\beta}{\beta} \right)$

where:

$\Delta\alpha = \alpha_2 - \alpha_1$ $\Delta\beta = \beta_2 - \beta_1$ $\Delta\rho = \rho_2 - \rho_1$	$\alpha = (\alpha_2 + \alpha_1)/2$ $\beta = (\beta_2 + \beta_1)/2$ $\rho = (\rho_2 + \rho_1)/2$	$i = (i_2 + i_1)/2$ $j = (j_2 + j_1)/2$

The Aki-Richards (1980) approximation for R_{PS}:

$$R_{PS} = \frac{-p\alpha}{2\cos j}\left[\left(1 - 2\beta^2 p^2 + 2\beta^2 \frac{\cos i}{\alpha}\frac{\cos j}{\beta}\right)\frac{\Delta\rho}{\rho} - \left(4\beta^2 p^2 - 4\beta^2 \frac{\cos i}{\alpha}\frac{\cos j}{\beta}\right)\frac{\Delta\beta}{\beta}\right] \quad \text{(A-1)}$$

Shuey's approximation for the PP reflection coefficient

Assumptions: The same as in Aki and Richards (1980)

The approximation for R_{PP} (Shuey, 1985)

$$R_{PP} = R_0 + \left[A_0 R_0 + \frac{\Delta\sigma}{(1-\sigma)^2}\right]\sin^2 i + \frac{1}{2}\frac{\Delta\alpha}{\alpha}\left(\tan^2 i - \sin^2 i\right). \quad \text{(A-2)}$$

where:

R_0 is the normal-incidence reflection coefficient

$\sigma = (\sigma_1+\sigma_2)/2$; $\Delta\sigma = (\sigma_1-\sigma_2)$, where σ_1 and σ_2 are Poisson's ratios in the two media

The approximations of Wang (1999) for the P-P and P-S reflection coefficients

The starting formula for R_{PP}: the exact R_{PP} formula:

$$R_{PP}(p) = \frac{E + Fp^2 + Gp^4 - Dp^6}{A + Bp^2 + Cp^4 + Dp^6} \qquad \text{(A-3)}$$

where:

$$A = (p_2 q_{\alpha 1} + p_1 q_{\alpha 2})(p_2 q_{\beta 1} + p_1 q_{\beta 2}),$$
$$B = -4\Delta\mu(p_2 q_{\alpha 1} q_{\beta 1} - p_1 q_{\alpha 2} q_{\beta 1}) + (\Delta\rho)^2 + 4(\Delta\mu)^2 q_{\alpha 1} q_{\alpha 2} q_{\beta 1} q_{\beta 2},$$
$$C = 4(\Delta\mu)^2 (q_{\alpha 1} q_{\beta 1} + q_{\alpha 2} q_{\beta 2}) - 4\Delta\mu\Delta\rho,$$
$$D = 4(\Delta\mu)^2,$$
$$E = (\rho_2 q_{\alpha 1} - \rho_1 q_{\alpha 2})(\rho_2 q_{\beta 1} + \rho_1 q_{\beta 2}),$$
$$F = -4\Delta\mu(\rho_2 q_{\alpha 1} q_{\beta 1} + p_1 q_{\alpha 2} q_{\beta 2}) - (\Delta\rho)^2 + 4(\Delta\mu)^2 q_{\alpha 1} q_{\alpha 2} q_{\beta 1} q_{\beta 2},$$
$$G = 4(\Delta\mu)^2 (q_{\alpha 1} q_{\beta 1} - q_{\alpha 2} q_{\beta 2}) + 4\Delta\mu\Delta\rho,$$
$$H = 2(\rho_2 q_{\beta 1} - \rho_1 q_{\beta 2})\rho_1 q_{\alpha 2}(\alpha_1 / \alpha_2),$$
$$I = -4\Delta\mu(q_{\beta 1} - q_{\beta 2})\rho_1 q_{\alpha 1}(\alpha_1 / \alpha_2).$$

Other notation:

p is the horizontal slowness and q is the vertical slowness
$\sigma = (\sigma_1+\sigma_2)/2$; σ_1 and σ_2 are Poisson's ratios in the two media
$\Delta\mu = \rho_2\beta_2^2 - \rho_1\beta_1^2$ is the contrast in shear modulus

Wang's pseudoquartic approximation for R_{PP}

Main steps of derivation:

$$(A+Bp^2+Cp^4+Dp^6)^{-1} \approx \frac{1}{A}-\frac{B}{A^2}p^2-\left(\frac{C}{A^2}-\frac{B^2}{A^3}\right)p^4 \quad \Rightarrow$$

$$R_{PP}(p) \approx \frac{E}{A}+\left(\frac{F}{A}-\frac{BE}{A^2}\right)p^2-\left(\frac{G}{A}-\frac{BF}{A^2}-\frac{CE}{A^2}+\frac{B^2E}{A^3}\right)p^4. \tag{A-4}$$

Assumption:

$$\left(\frac{\Delta\rho}{\rho}\right)^2 \approx 0; \quad \frac{\rho_2 q_{\alpha 1} q_{\beta 1}-\rho_1 q_{\alpha 2} q_{\beta 2}}{(\rho_2 q_{\alpha 1}+\rho_1 q_{\alpha 2})(\rho_2 q_{\beta 1}+\rho_1 q_{\beta 2})} \Rightarrow \quad \frac{F}{A}-\frac{BE}{A^2} \approx -2\frac{\Delta\mu}{\rho}+(1-R_f)\left(\frac{\Delta\mu}{\rho}\right)^2 q_\alpha \rho_\beta.$$

$$R_{PP} \approx R_f-\left[2\frac{\Delta\mu}{\rho}-(1-R_f)q_\alpha q_\beta\left(\frac{\Delta\mu}{\rho}\right)^2\right]p^2-\left[2R_f\left(\frac{\Delta\mu}{\rho}\right)^2-2q_\alpha q_\beta\left(\frac{\Delta\mu}{\rho}\right)^3+(1-R_f)q_\alpha^2 q_\beta^2\left(\frac{\Delta\mu}{\rho}\right)^4\right]p^4 \tag{A-5}$$

where:

$$R_f=\frac{(\rho_2 q_{\alpha 1}-\rho_1 q_{\alpha 2})}{(\rho_2 q_{\alpha 1}+\rho_1 q_{\alpha 2})}.$$

The other notation is the same as that from the Aki-Richards approximation presented earlier.

Wang's quadratic approximation for R_{PP}

Assumptions and approximations:

$$\tan\frac{\Delta\theta}{2} \approx \frac{1}{2}\frac{\Delta\alpha}{\alpha}\tan\theta, \qquad \frac{q_{\alpha_1}\alpha_1}{q_{\alpha_2}\alpha_2} \approx 1+\alpha\Delta\alpha\, p^2. \qquad R_f \approx \frac{1}{2}\left(\frac{\Delta\rho}{\rho}+\sec^2\theta\frac{\Delta\alpha}{\alpha}\right),$$

$$\Delta\mu=\beta^2\Delta\rho+2\rho\beta\Delta\beta+\frac{1}{4}\Delta\rho(\Delta\beta)^2$$

$$R_{PP} \approx \left[\frac{1}{2}-2\left(\frac{\beta}{\alpha}\right)^2\sin^2\theta\right]\frac{\Delta\rho}{\rho}+\frac{1}{2}\sec^2\theta\frac{\Delta\alpha}{\alpha}-4\left(\frac{\beta}{\alpha}\right)^2\sin^2\theta\frac{\Delta\beta}{\beta}+\left(\frac{\beta}{\alpha}\right)^3\cos\theta\sin^2\theta\left(\frac{\Delta\rho}{\rho}+2\frac{\Delta\beta}{\beta}\right)^2 \tag{A-6}$$

where θ is the mean incidence angle.

The linearized approximation for R_{PP}

Assumptions:

In the quadratic approximation, we ignore the terms that contain $\left(\frac{\Delta\rho}{\rho}+2\frac{\Delta\beta}{\beta}\right)^2$

$$R_{PP}\approx\left[\frac{1}{2}-2\left(\frac{\beta}{\alpha}\right)^2\sin^2\theta\right]\frac{\Delta\rho}{\rho}+\frac{1}{2}\sec^2\theta\frac{\Delta\alpha}{\alpha}-4\left(\frac{\beta}{\alpha}\right)^2\sin^2\theta\frac{\Delta\beta}{\beta} \tag{A-7}$$

This expression is equivalent to the ones developed by Bortfeld (1961), Aki and Richards (1980), and Shuey (1985).

The starting formula for R_{PS}

$$R_{PS}(p)=\left(2q_{\alpha_1}\frac{\alpha_1}{\beta_1}p\right)\frac{J+Kp^2-Dp^4}{A+Bp^2+Cp^4+Dp^6} \tag{A-8}$$

where

A, B, C and *D* are the same as in the R_{PP} formula above, and

$J=-\rho_2\Delta\rho-2\rho_1 q_{\alpha_2} q_{\beta_2}\Delta\mu$	$K=2(\rho_2+\Delta\rho)\Delta\mu-4q_{\alpha_2}q_{\beta_2}(\Delta\mu)^2$	$L=\rho_2\Delta\rho-2\rho_1 q_{\alpha_2} q_{\beta_1}\Delta\mu$ $M=-2\rho_1\Delta\mu$

After Taylor series expansion of the denominator, we obtain the pseudoquartic approximation for R_{PS}:

$$R_{PS}(p)\approx\left(2q_{\alpha_1}\frac{\alpha_1}{\beta_1}p\right)\left[\frac{J}{A}+\left(\frac{K}{A}-\frac{BJ}{A^2}\right)p^2-\left(\frac{D}{A}+\frac{BK}{A^2}+\frac{CJ}{A^2}+\frac{B^2J}{A^3}\right)p^4\right] \tag{A-9}$$

or

$$R_{PS}(p)\approx\frac{\alpha_1}{\beta_1}\frac{\Delta\mu}{\rho}q_\alpha p\left\{1-\left[\frac{1}{q_\alpha q_\beta}-2\frac{\Delta\mu}{\rho}+q_\alpha q_\beta\left(\frac{\Delta\mu}{\rho}\right)^2\right]p^2\right.$$
$$\left.+\left[\frac{2}{q_\alpha q_\beta}\frac{\Delta\mu}{\rho}-\left(\frac{\Delta\mu}{\rho}\right)^2-2q_\alpha q_\beta\left(\frac{\Delta\mu}{\rho}\right)^3+q_\alpha^2 q_\beta^2\left(\frac{\Delta\mu}{\rho}\right)^4\right]p^4\right\} \tag{A-10}$$

APPENDIX B

INTERFACE MODELLING: A LIST OF ELASTIC PARAMETERS AND PLOTS

B.1 Velocities and densities used in modelling

Table B.1. Velocities and densities used for modelling in Chapter 3. Pore fluid, density and the velocities corresponding to depths of 500, 1000 and 2000 m are listed for each sample.

Rock Type	Pore Fluid	ρ (g/cm^3)	500 m (11.27 MPa)		1000 m (22.54 MPa)		2000 m (45.08 MPa)	
			V_P (m/s)	V_S (m/s)	V_S (m/s)	V_S (m/s)	V_P (m/s)	V_S (m/s)
sandstone	water	2.330	4458	2709	4590	2849	4680	2928
sandstone	water	2.310	4279	2555	4350	2668	4440	2735
sandstone	water	2.390	4716	3016	4766	3065	4823	3110
sandstone	water	2.320	4330	2740	4408	2815	4475	2860
sandstone	water	2.180	3638	2015	3696	2054	3753	2088
sandstone	water	2.530	5003	3029	5104	3100	5228	3190
sandstone	water	2.410	3808	2045	3947	2161	4093	2263
sandstone	water	2.250	3351	1919	3438	1985	3505	2030
sandstone	water	2.500	4836	3045	4884	3083	4918	3105
sandstone	water	2.470	3974	2223	4083	2318	4195	2385
sandstone	dry/gas	2.082	3164	2072	3358	2248	3575	2360
sandstone	dry/gas	2.075	2934	2026	3240	2225	3484	2405
sandstone	dry/gas	2.094	3548	2449	3786	2591	4022	2817
sandstone	dry/gas	2.268	3520	2231	3733	2359	4015	2538
sandstone	dry/gas	2.268	3453	2269	3659	2381	3967	2581
sandstone	dry/gas	2.144	3217	1961	3380	2066	3692	2251
sandstone	oil	2.395	3955	2382	4179	2549	4335	2699
sandstone	oil	2.066	3051	1650	3089	1766	3136	1860
sandstone	oil	2.084	3136	1902	3373	2030	3518	2078
sand	dry/gas	1.774	1889	1314	2200	1469	2506	1571
sand	dry/gas	1.629	1744	1162	1946	1289	2226	1404
sand	dry/gas	1.767	2006	1334	2252	1468	2506	1574
sand	dry/gas	2.004	2445	1671	2660	1796	2948	1911
sand	dry/gas	1.943	2244	1535	2534	1701	2746	1803
sand	dry/gas	1.743	2127	1362	2392	1480	2764	1688
sand	water	2.104	2381	1167	2460	1274	2620	1398

(continued from last page of Table B.1)

Rock Type	Pore Fluid	ρ (g/cm^3)	500 m (11.27 MPa)		1000 m (22.54 MPa)		2000 m (45.08 MPa)	
			V_P (m/s)	V_S (m/s)	V_S (m/s)	V_S (m/s)	V_P (m/s)	V_S (m/s)
sand	water	1.999	2282	1072	2399	1176	2505	1284
sand	water	2.097	2459	1183	2589	1283	2701	1425
sand	water	2.234	2961	1547	3081	1616	3259	1751
sand	water	2.193	2738	1365	2938	1489	3226	1689
sand	water	2.053	2482	1186	2627	1302	2853	1441
tight-gas sandst.	water	2.584	4753	3233	5070	3422	5439	3645
tight-gas sandst.	water	2.383	4150	2714	4408	2887	4733	3101
tight-gas sandst	water	2.412	3832	2429	4193	2680	4428	2809
tight-gas sandst	water	2.478	4252	2921	4655	3140	5050	3348
tight-gas sandst	water	2.587	4433	3012	4887	3184	5283	3314
tight-gas sandst	water	2.402	3864	2550	4057	2658	4371	2832
tight-gas sandst	water	2.498	4580	2989	4826	3145	5031	3274
tight-gas sandst	water	2.627	4117	2822	4373	2951	4679	3129
tight-gas shale	water	2.614	4603	2904	4694	2956	4800	3017
tight-gas shale	water	2.667	4500	2809	4575	2833	4692	2873
tight-gas shale	water	2.596	4249	2846	4370	2890	4537	2954
tight-gas shale	water	2.605	4547	3166	4838	3305	5131	3450
tight-gas shale	water	2.627	4726	3036	4813	3056	4915	3095
shale	water	2.570	4133	2401	4233	2491	4345	2593
shale	water	2.340	3050	1750	3150	1800	3250	1830
shale	water	2.350	3150	1750	3250	1800	3310	1820
shale	oil	2.340	3050	1900	3150	1920	3300	1950
shale	oil	2.480	3650	2190	3760	2340	3810	2360
shale	dry/gas	2.350	2800	1750	3000	1800	3080	1820
shale	dry/gas	2.480	3100	2100	3400	2240	3550	2350
shale	dry/gas	2.150	3746	2190	3751	2190	3763	2193
shale	dry/gas	2.340	2920	2000	3080	2070	3250	2090
limestone	dry/gas	2.660	6042	3161	6056	3173	6084	3195
limestone	dry/gas	2.620	3071	1767	3345	1913	3822	2168
limestone	dry/gas	2.710	6354	3370	6392	3374	6454	3380
limestone	dry/gas	2.130	2788	1329	2816	1365	2873	1410
limestone	dry/gas	2.390	4974	2721	5003	2731	5025	2743
limestone	dry/gas	2.197	3708	2217	3736	2233	3793	2255
limestone	water	2.659	5987	3287	5987	3311	5987	3333
dolomite	dry/gas	2.860	6420	3849	6596	3932	6876	4065
dolomite	dry/gas	2.850	5339	3108	5504	3169	5809	3248
dolomite	dry/gas	2.813	2075	1160	2154	1200	2207	1232
dolomite	dry/gas	2.854	2085	1109	2088	1115	2095	1120

(continued from last page of Table B.1)

Rock Type	Pore Fluid	ρ (g/cm^3)	500 m (11.27 MPa)		1000 m (22.54 MPa)		2000 m (45.08 MPa)	
			V_P (m/s)	V_S (m/s)	V_S (m/s)	V_S (m/s)	V_P (m/s)	V_S (m/s)
dolomite	dry/gas	2.420	5172	3141	5252	3154	5681	3369
dolomite	dry/gas	2.600	5664	3400	5709	3445	5709	3445
dolomite	dry/gas	2.520	5742	3445	5741	3445	5741	3445
dolomite	dry/gas	2.140	4569	2765	4663	2792	4717	2792
dolomite	water	2.862	2120	1152	2120	1157	2125	1164
dolomite	water	2.570	5115	2780	5276	2863	5431	2984
dolomite	water	2.530	5061	2732	5169	2780	5383	2902
dolomite	water	2.390	4662	2540	4796	2624	4994	2725
dolomite	water	2.370	4536	2433	4644	2541	4775	2680
dolomite	oil	2.860	2078	1120	2081	1132	2088	1148
dolomite	oil	2.822	2243	1186	2244	1207	2255	1225
coal	water	1.377	2471	1166	2508	1184	2558	1203
coal	water	1.300	2569	1232	2597	1245	2680	1257
coal	water	1.396	2492	1172	2536	1186	2583	1208
coal	water	1.321	2567	1234	2605	1244	2689	1256
coal	water	1.316	2612	1204	2644	1223	2704	1252
coal	water	1.391	2473	1170	2524	1190	2575	1211
coal	water	1.360	2523	1170	2582	1180	2618	1193
coal	water	1.380	2523	1150	2582	1170	2618	1185
coal	water	1.390	2622	1240	2681	1260	2718	1273
coal	water	1.380	2671	1190	2695	1211	2714	1236
coal	water	1.800	Well-log values for a depth of 1000 m:				2941	1786
coal	water	1.680					2703	1852
coal	water	1.370					2564	1739
salt	--	2.146	4476	2607	4487	2623	4502	2635
salt	--	2.187	4514	2615	4514	2641	4514	2645
salt	--	2.172	4518	2633	4519	2651	4532	2645
chalk	water	2.430	Well-log values for a depth of 3000 m :				4204	2412
chalk	water	2.436					4081	2426
chalk	water	2.336					3782	2253
chalk	water	2.325					3694	2170
chalk	water	2.133					3093	1818
chalk	water	2.104					3006	1770
chalk	water	1.993					2693	1589
chalk	water	1.961					2655	1577
chalk	water	2.557					5225	2746
chalk	water	2.473					4598	2586
gypsum	--	2.350	Lab measurements at room conditions:				5865	3352
anhydrite	--	2.980					5643	3125

Table B.2. The sources of the velocity and density values used for modelling

Rock Type	Reference
Sandstone	Han (1986) Colorado School of Mines (2003) Colorado School of Mines (2003)
Shale	Colorado School of Mines (2003)
Sand	Blangy (1992)
Tight-gas sandstone	Jizba (1991)
Tight-gas shale	Jizba (1991)
Limestone	Bonner and Schock (1989)
Dolomite	Bonner and Schock (1989) Colorado School of Mines (2003) Pickett (1963)
Coal	Colorado School of Mines (2003) Margrave (2001)
Salt	Colorado School of Mines (2003)
Gypsum/Anhydrite	Bonner and Schock (1989)
Chalk	Brevik (2002)

B.2 R_{PP} versus R_{PS} plots obtained from all interface models at a depth of 1000 m

The following plots of R_{PP} vs. R_{PS} repeated for all possible rock interfaces are presented in Table 1. An incidence angle of 20° was used in all models. The overlying rock is at the beginning of each set of plots and the abbreviation for the underlying rock is printed above each plot.

Water-saturated sandstone

S - WS	SH - WS	LS – WS
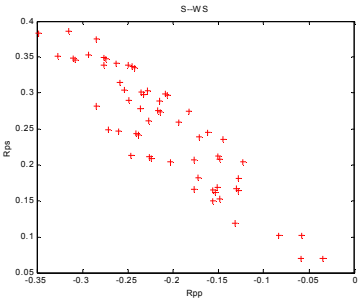	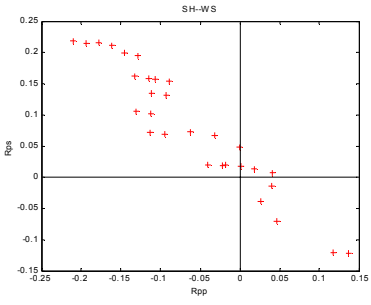	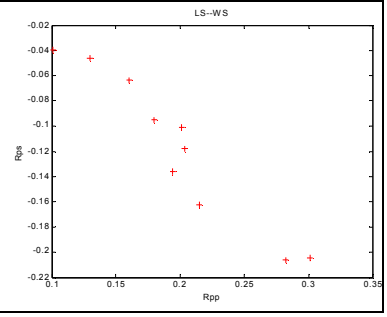

DO - WS	CO	HA
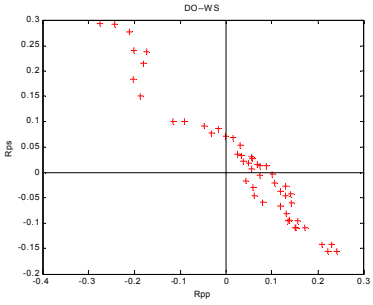	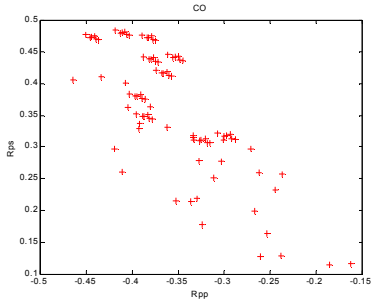	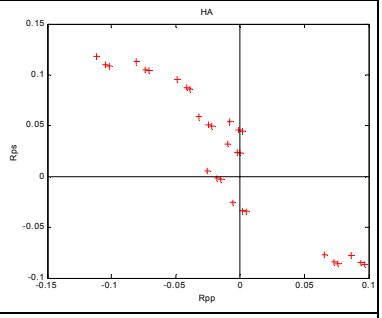
CH	**GY/AN**	
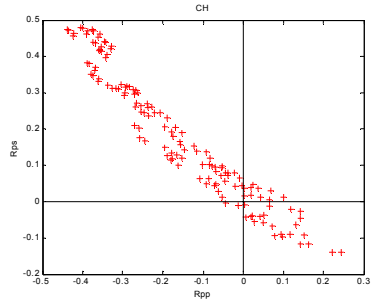	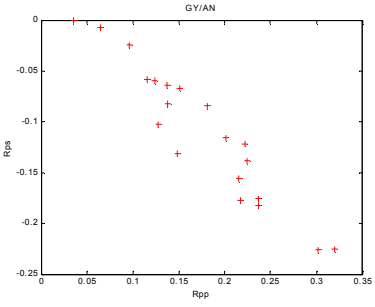	

Dry/gas sandstone

S - DR	SH - DR	LS – DR
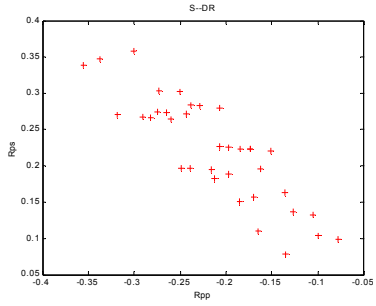	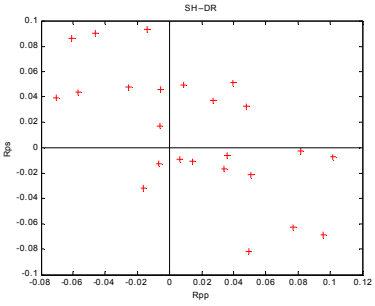	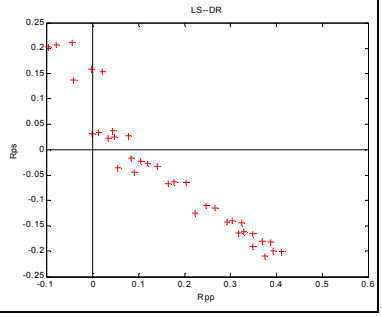
DO - DR	**HA**	
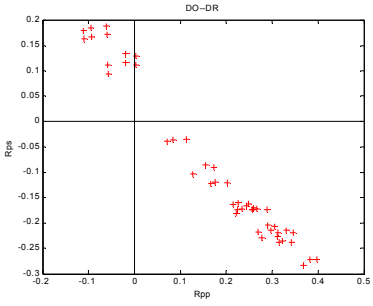	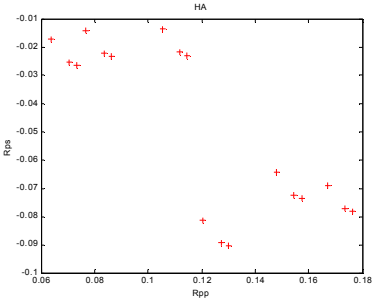	

Oil-saturated sandstone

SH - OS	DO - OS	HA
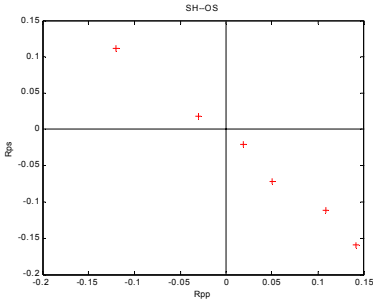	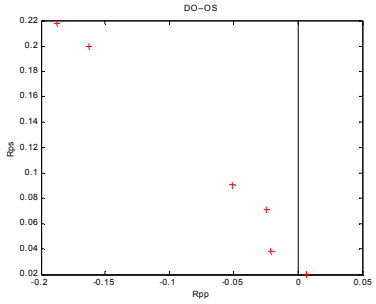	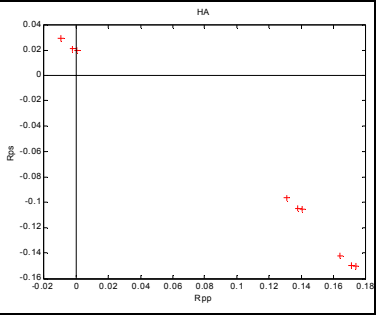

Dry/gas sand

SS - DR	SH - DR	LS - DR
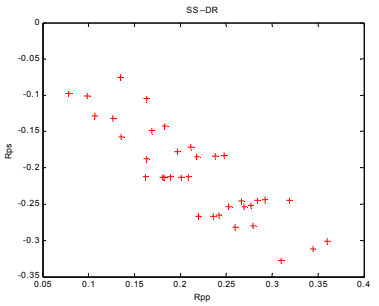	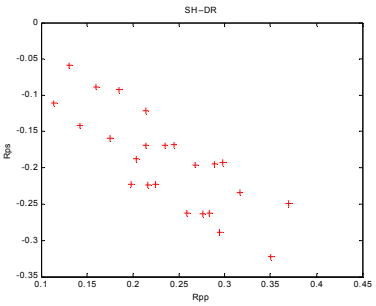	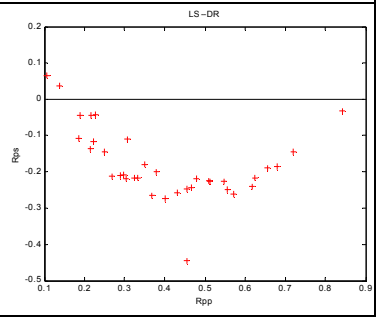

DO - DR	HA
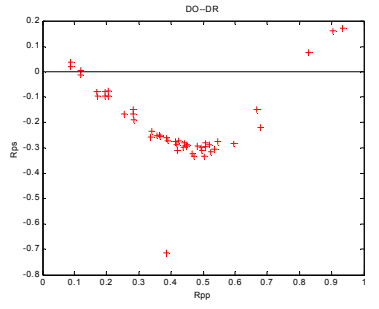	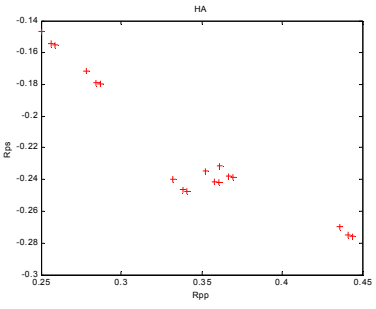

Water-saturated sand

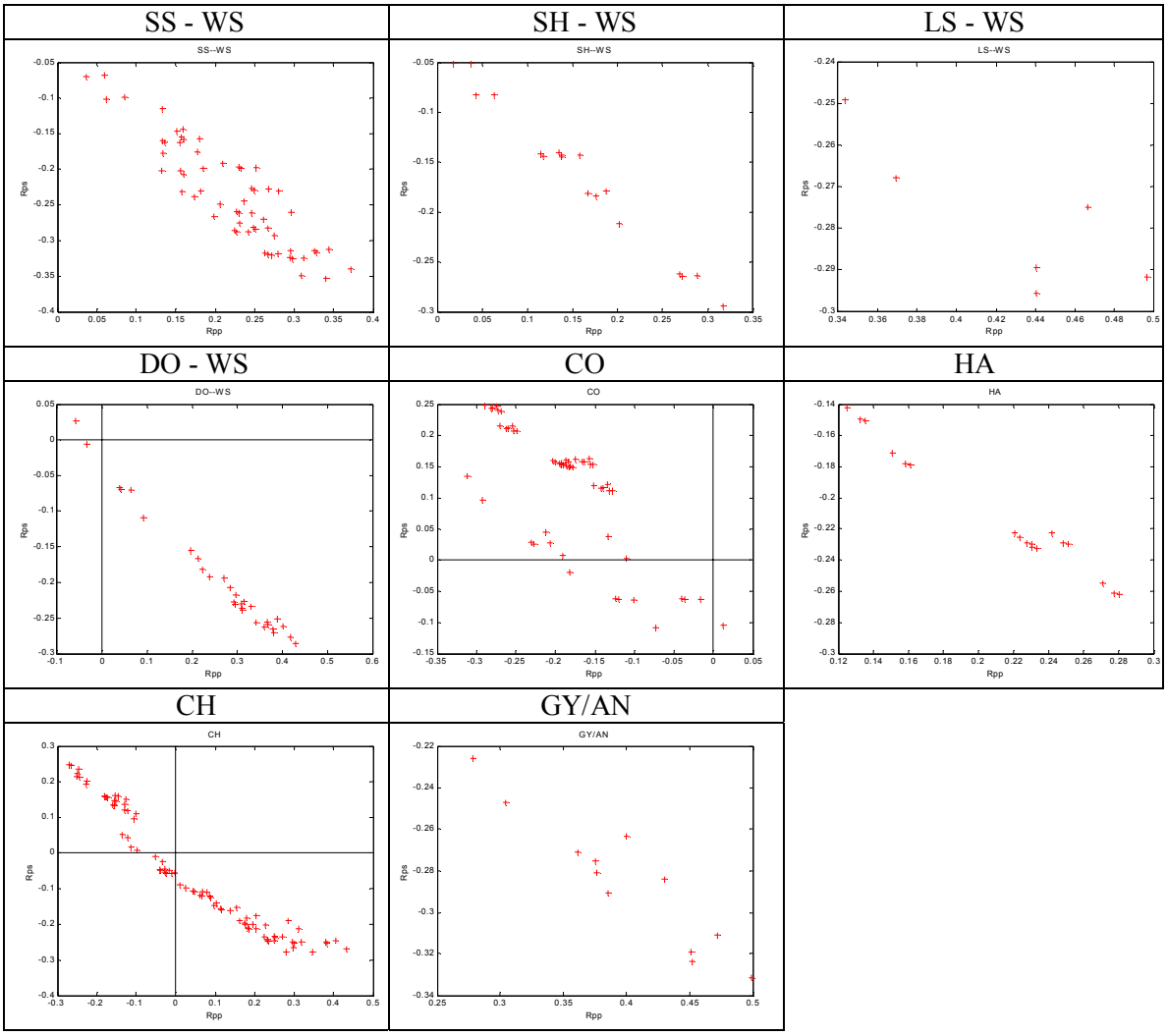

Tight-gas sandstone

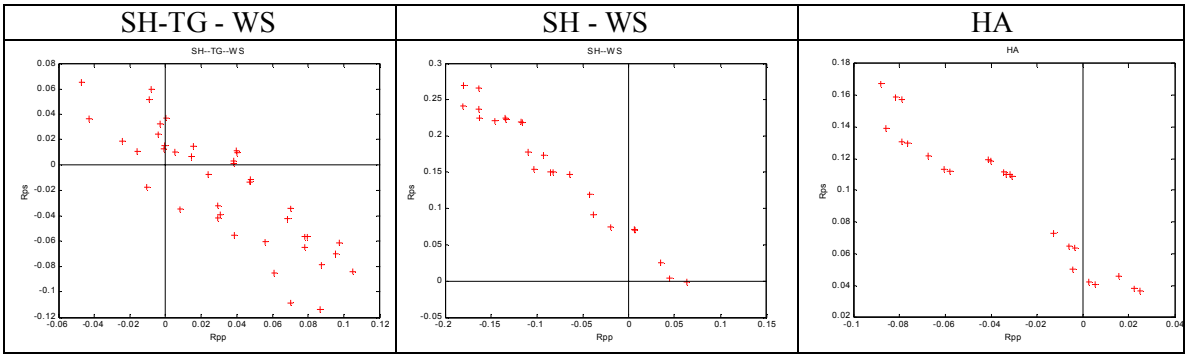

Tight gas shale

SS-TG - WS	SH - WS	HA
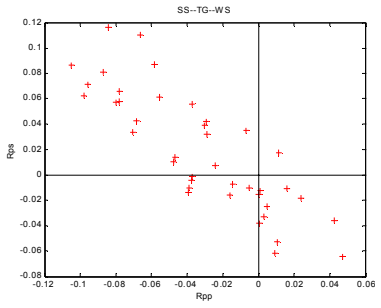	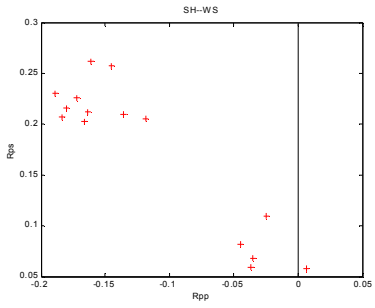	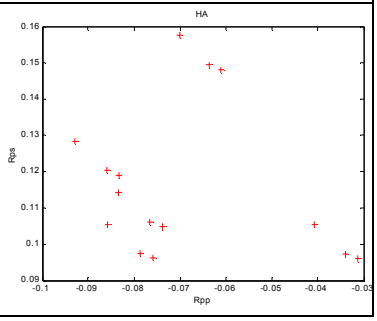

Water-saturated shale

SS - WS	S - WS	SS-TG – WS
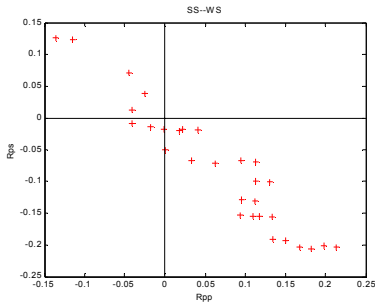	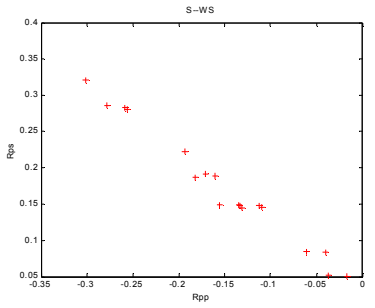	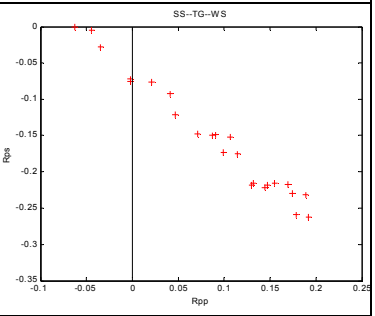
SH-TG - WS	**LS - WS**	**DO – WS**
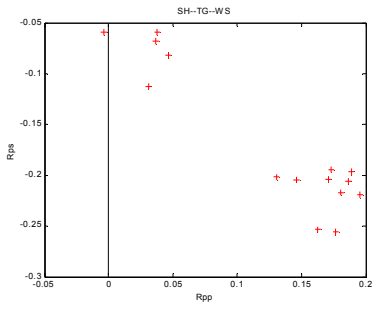	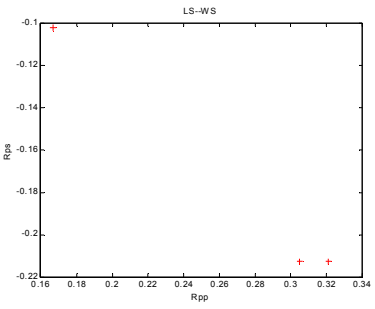	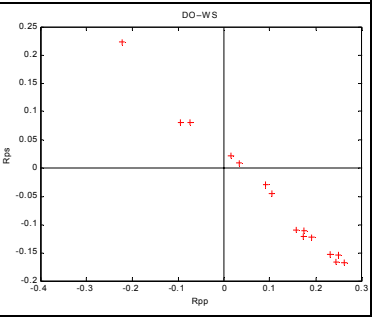
CO	**HA**	**CH**
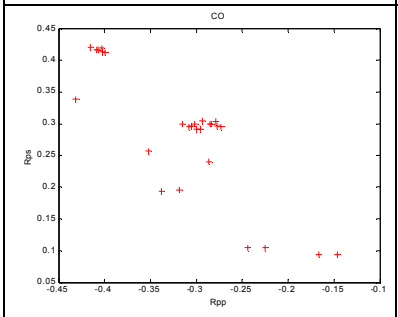	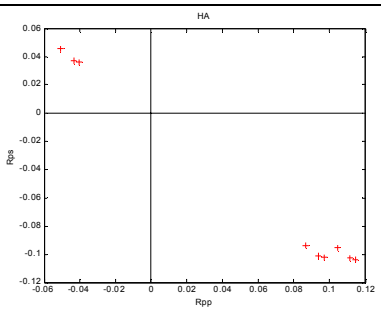	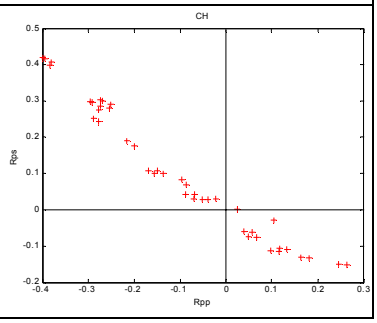

GY/AN

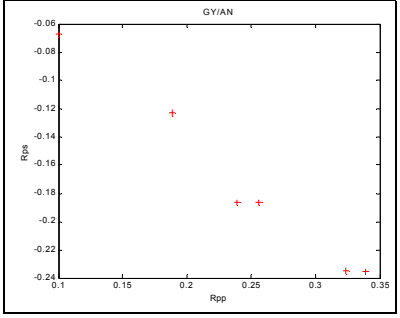

Dry/gas shale

SS – DR

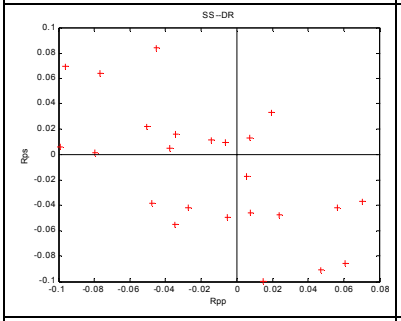

S - DR

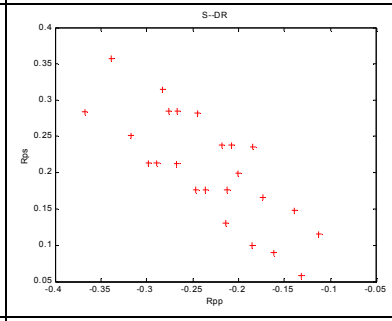

LS - DR

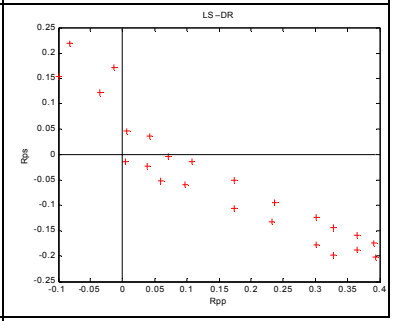

DO – DR

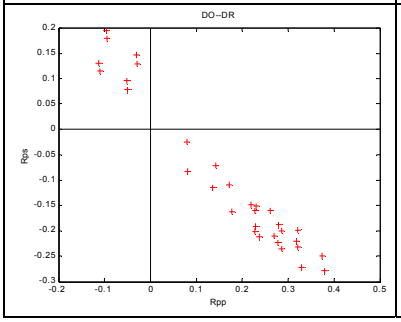

HA

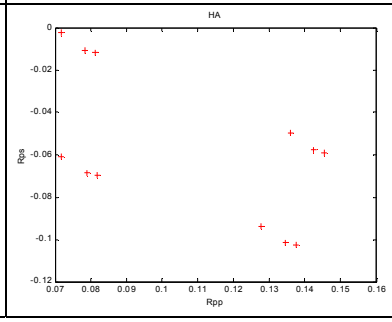

Oil-saturated shale

SS – OS

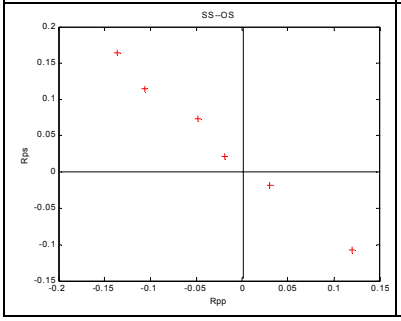

DO - OS

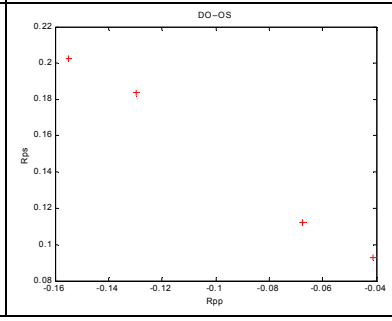

HA

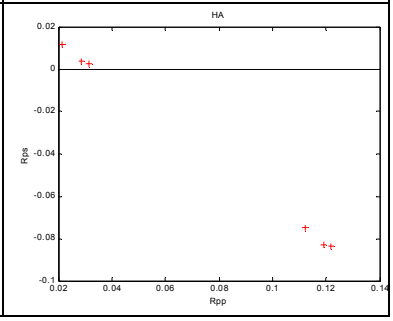

Dry/gas limestone

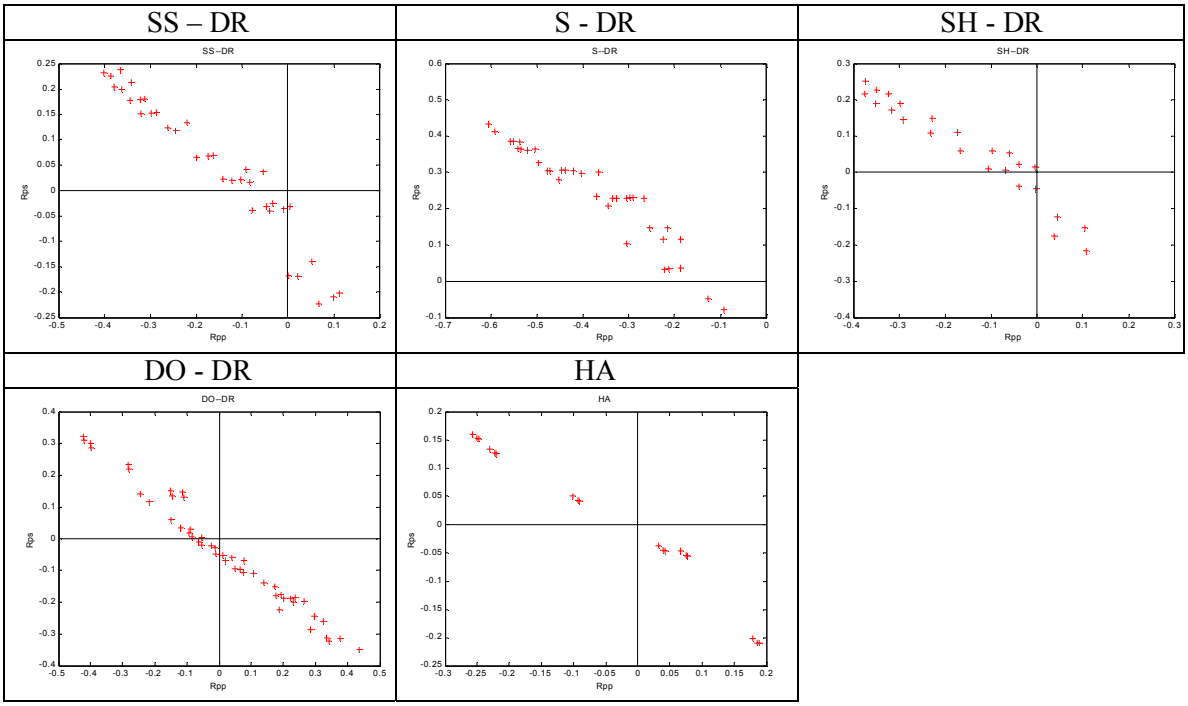

Water-saturated limestone

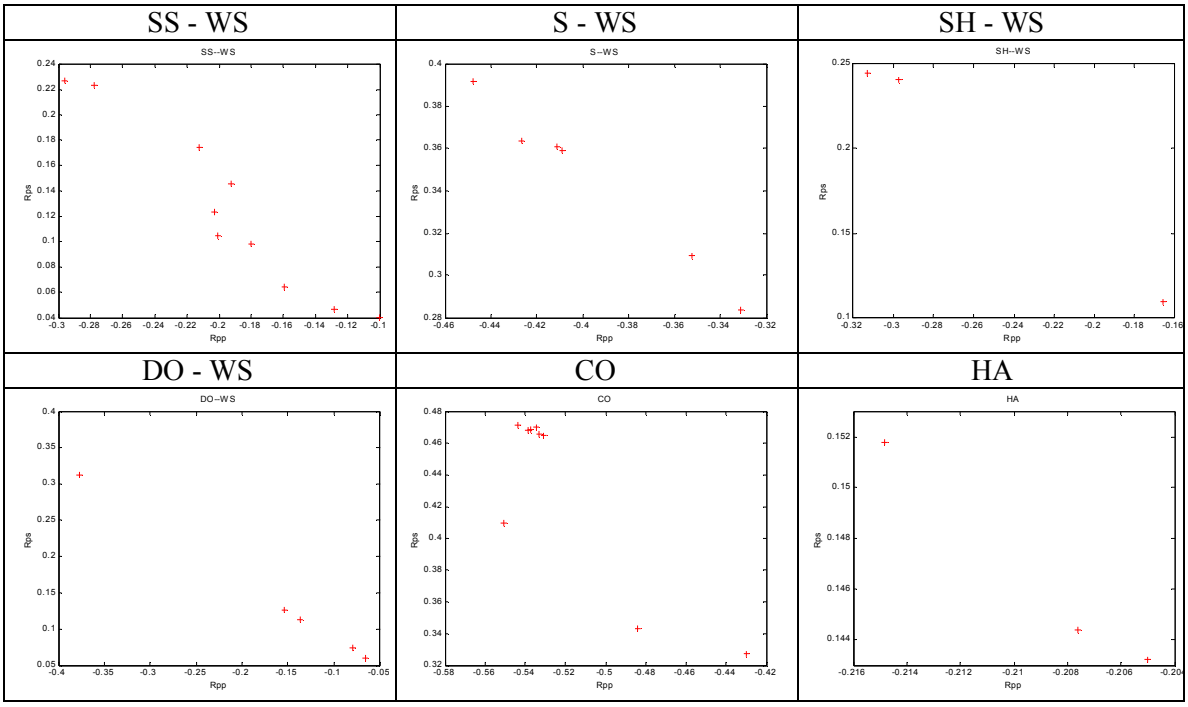

CH	GY/AN
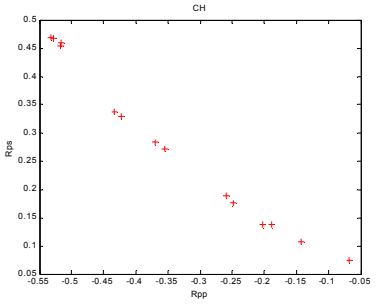	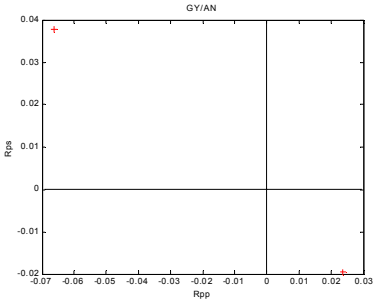

Dry/gas dolomite

SS - DR	S - DR	SH - DR
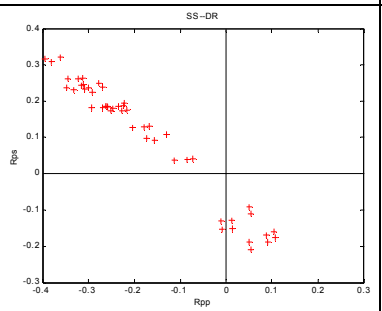	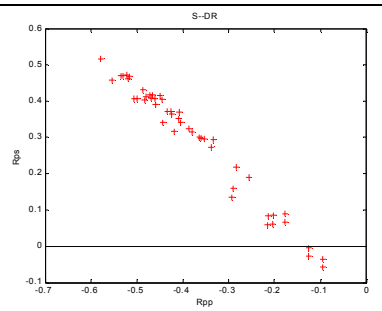	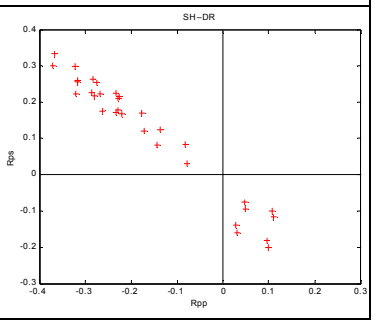
LS - DR	**HA**	
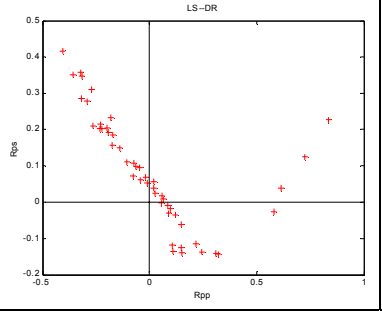	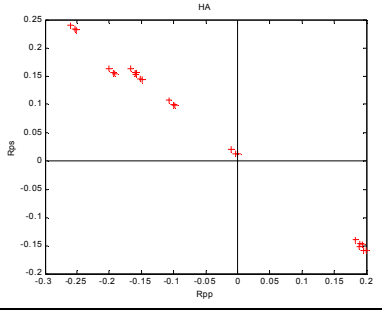	

Water-saturated dolomite

SS - WS	S - WS	SH - WS
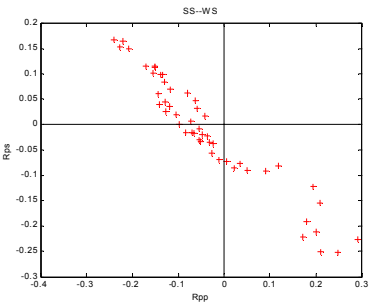	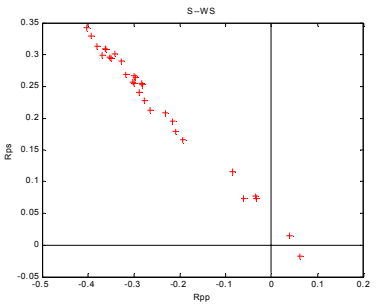	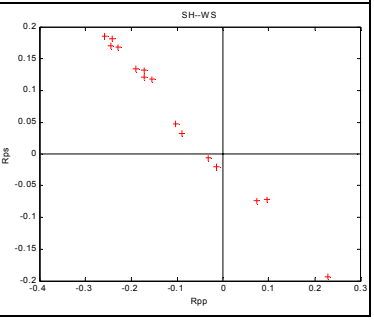

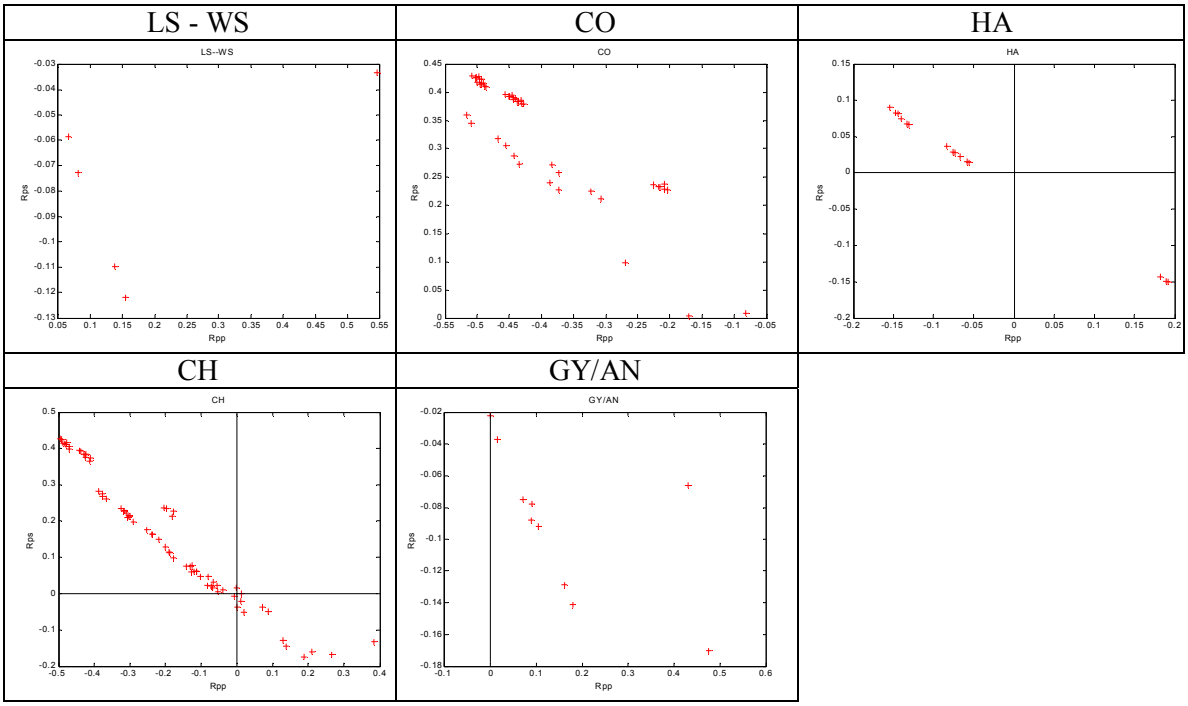

Oil-saturated dolomite

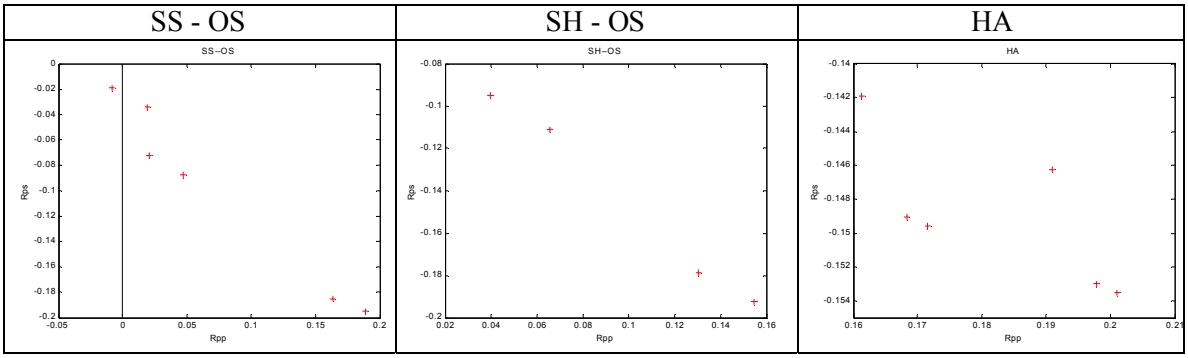

Coal

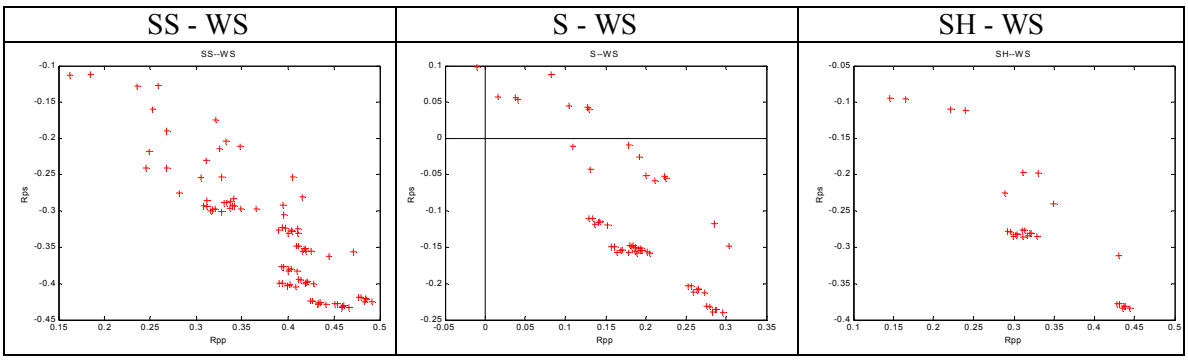

LS - WS

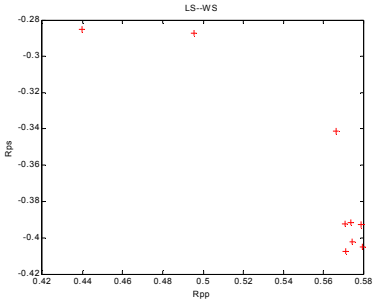

DO - WS

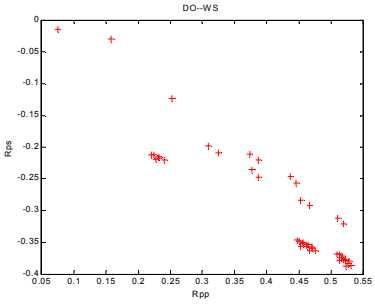

CH

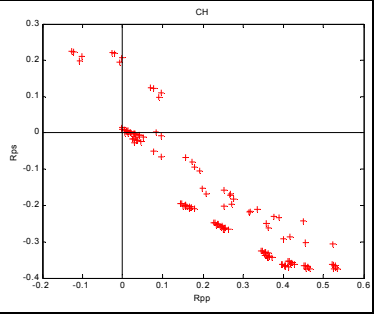

GY/AN

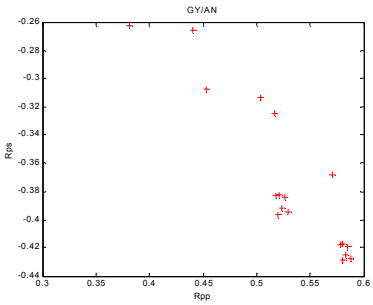

Halite

SS - WS

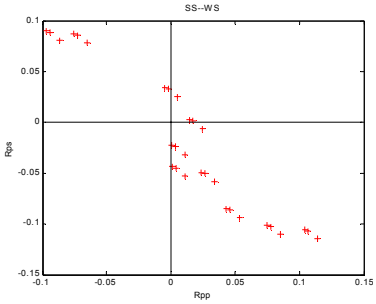

SS - DR

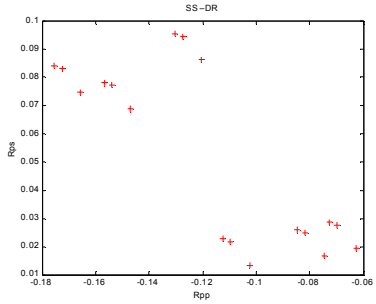

SS - OS

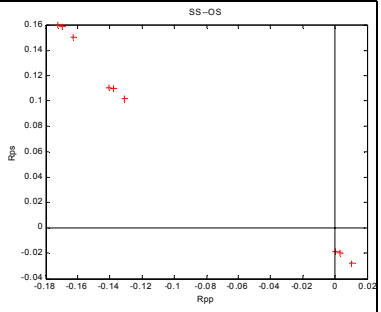

S - DR

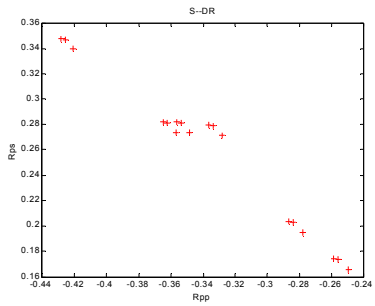

S - WS

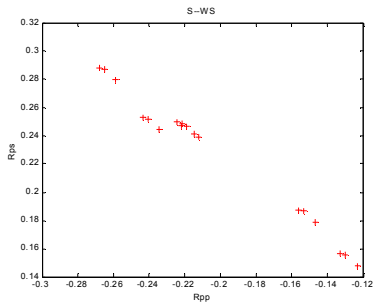

SS-TG - WS

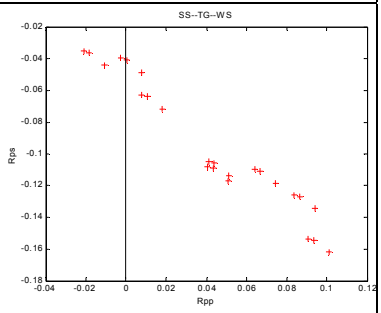

SH-TG - WS	SH - WS	SH - DR
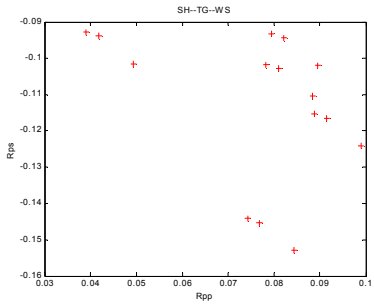	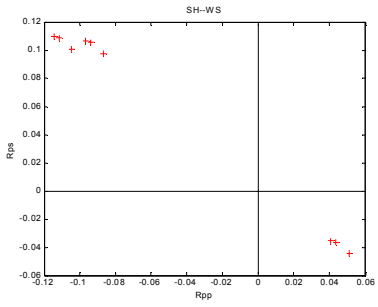	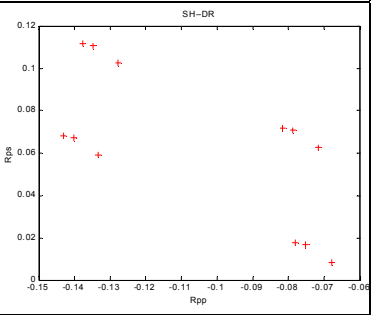
SH - OS	**LS - DR**	**LS - WS**
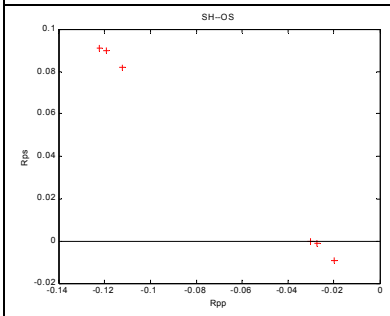	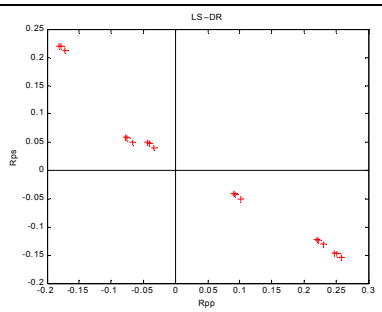	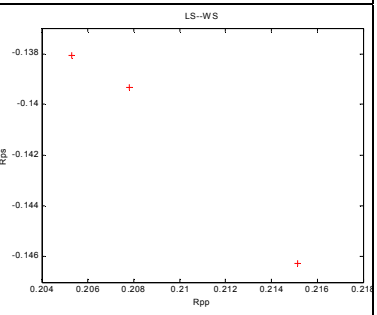
DO - DR	**DO - WS**	**DO - OS**
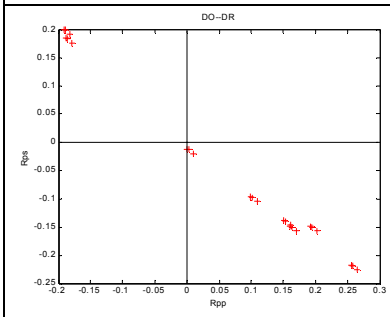	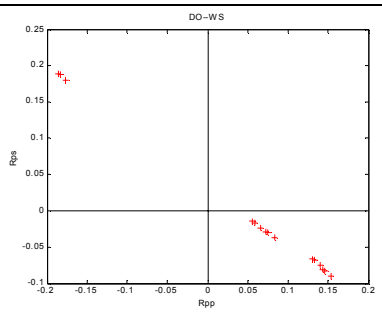	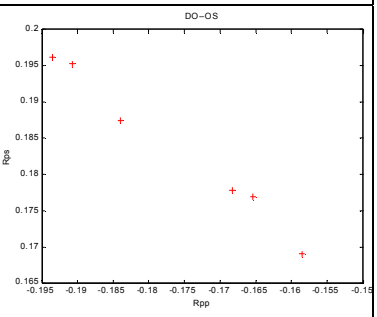
CO	**CH**	**GY/AN**
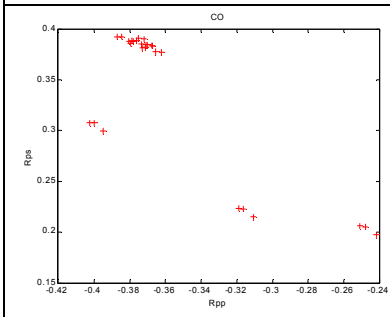	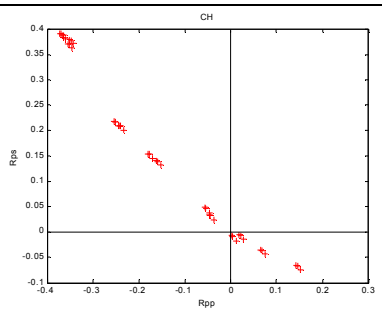	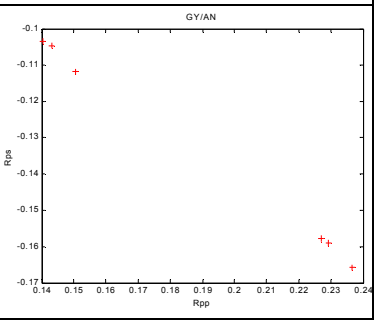

Chalk

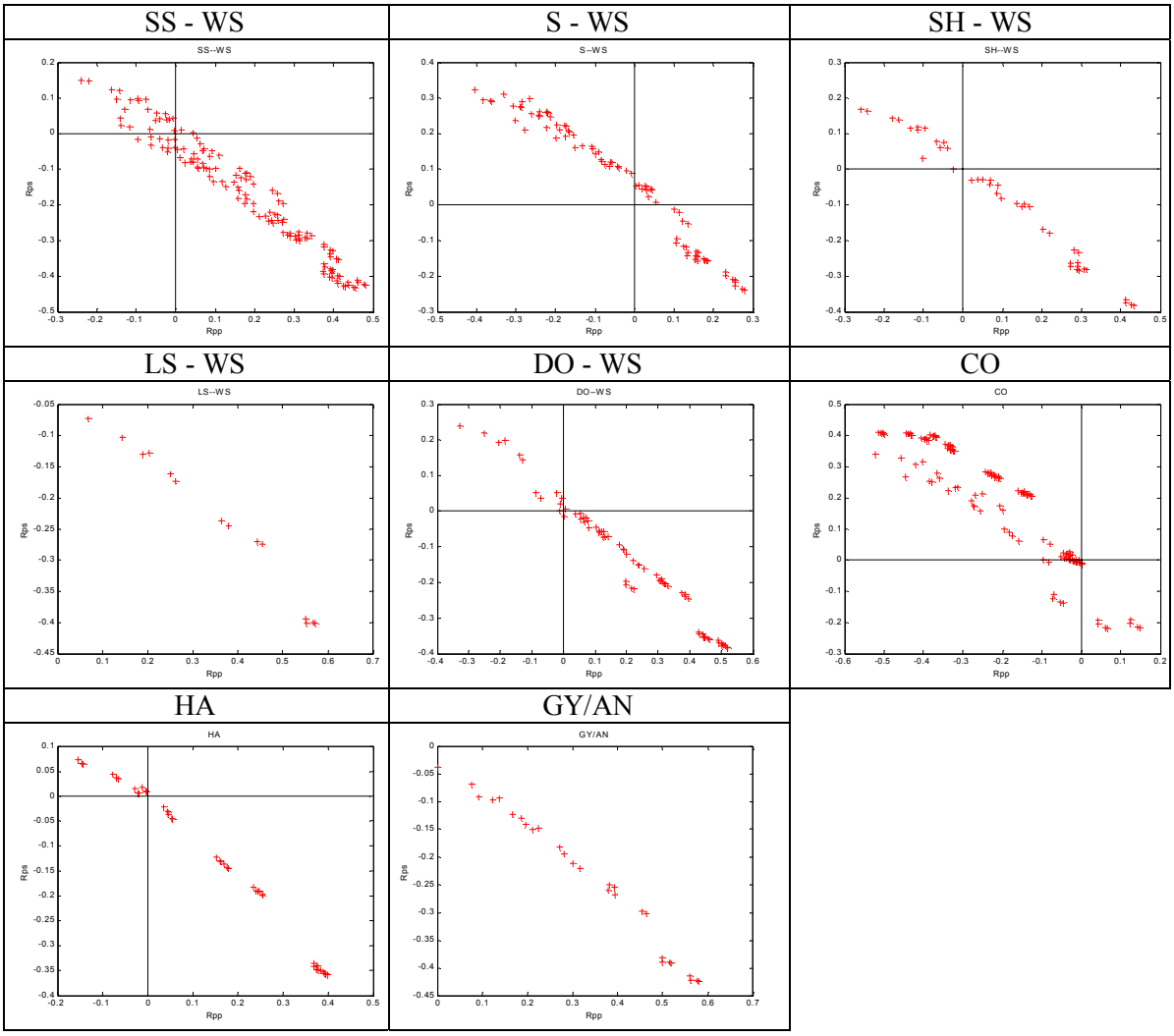

Gypsum/Anhydrite

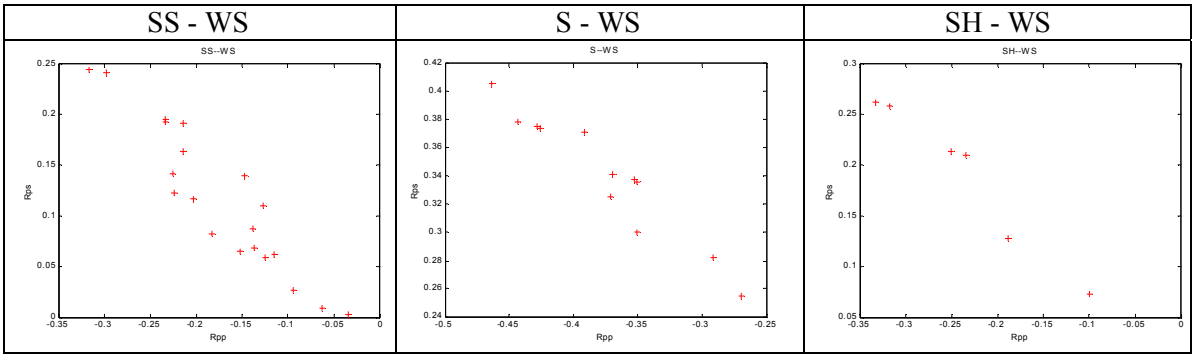

LS - WS	DO - WS	CO
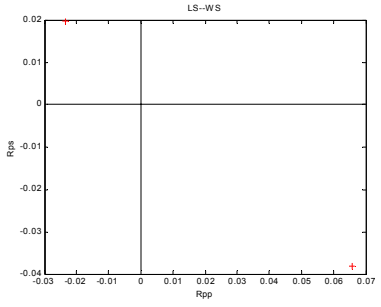	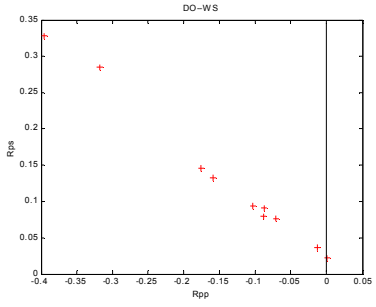	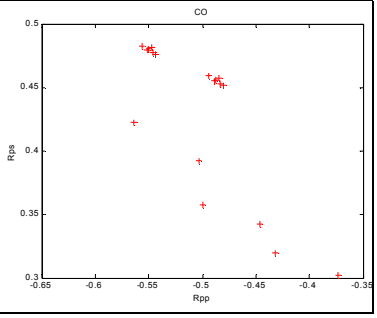
HA	**CH**